

STRUCTURE-PROPERTY RELATIONSHIP AND THERMAL STABILITY OF ORGANIC PHOTOVOLTAIC CELLS

DAVID EDMOND MOTAUNG

A thesis submitted in a partial fulfillment
of the requirements for the degree of

Doctor of Philosophy

in the

UNIVERSITY of the

DEPARTMENT OF PHYSICS

UNIVERSITY OF THE WESTERN CAPE

**Supervisors: Dr. G. F Malgas, Council for Scientific and Industrial Research
: Prof. C. J. Arendse, University of the Western Cape**

OCTOBER 2010

KEYWORDS

“STRUCTURE-PROPERTY RELATIONSHIP AND THERMAL STABILITY OF ORGANIC PHOTOVOLTAIC CELLS”



Poly(3-hexylthiophene)

Fullerene

Polymer solar cells

Morphology

Quenching

Crystallinity

Annealing

Thermal transition

Phase separation

Stability

Thermal degradation

ABSTRACT

“STRUCTURE-PROPERTY RELATIONSHIP AND THERMAL STABILITY OF ORGANIC PHOTOVOLTAIC CELLS”

DAVID. E. MOTAUNG

Organic solar cells have attracted considerable attention in the past few years owing to their potential of providing environmentally safe, flexible, lightweight, inexpensive, efficient solar cells. Especially, bulk-heterojunction solar cells consisting of a mixture of a conjugated donor polymer with a methanofullerene acceptor are considered as a promising approach. In this thesis, regioregular-poly(3-hexylthiophene) (rr-P3HT) polymer was used as a light absorption and electron donating material, while the C₆₀ fullerene and its derivative [6,6]-phenyl C₆₁-butyric acid methyl ester (PCBM) were used as electron acceptor materials. The effect of solvent to control the degree of mixing of the polymer and fullerene components, as well as the domain size and charge transport properties of the blends were investigated in detail using P3HT:C₆₀ films. The photo-physical, structural and electrical transport properties of the polymer blends were carried out according to their ratios. A distinctive photoluminescence (PL) quenching effect was observed indicating a photo-induced electron transfer. A complete reduction of PL of P3HT after mixing with C₆₀ in a 1:1 weight ratio indicates an

effective charge transfer from P3HT to C₆₀, while a 1:4 weight ratio revealed a blue shift and an incomplete quenching. Such changes on the photoluminescence intensity originate from a phase separation and thus changes in the morphology of the active layer as confirmed by electron spin resonance (ESR). The substrate annealing prior to deposition of an active layer demonstrated self-assembled fibrillar structures on the microscopic morphology due to the suppressed growth of fullerenes clusters induced by the controlled evaporation rate of the solvent. It is proposed that pre-substrate annealing controls the crystallization of P3HT, the phase separation and diffusion of the acceptor material (C₆₀ or PCBM), and therefore, improved device performance can be anticipated.

The thermal annealing on the photovoltaic parameters of these cells was investigated at different annealing temperatures under the air mass (AM) 1.5 illumination (100 mWcm⁻²). It was found that the performance of a P3HT:C₆₀ (1:1 wt. ratio) device was dramatically improved by annealing at 150 °C. Finally, changes in the nanoscale morphology, including the conjugation length, size and population of P3HT crystallites, of the blended films induced by a diffusion of C₆₀ molecules and degradation during longer thermal treatment above glass transition temperature (130 °C) were observed resulting in a degradation of power conversion efficiency of P3HT:C₆₀ solar cells. These findings signify that the stability of P3HT:C₆₀ solar cells cannot be secured for longer annealing periods owing to the unsettled morphology.

DECLARATION

I declare that

**“STRUCTURE-PROPERTY RELATIONSHIP AND
THERMAL STABILITY OF ORGANIC PHOTOVOLTAIC
CELLS”**

is my own work, that it has not been submitted for any degree or examination in any other university and that all the resources I have used or quoted have been indicated and acknowledged by means of complete references.

Signed:  _____

OCTOBER 2010

David E. Motaung

ACKNOWLEDGEMENTS

“Put the creature of all mankind, GOD ALMIGHTY, in the centre and everything will come together”. To Him I give all the GLORY and thanks for making all things possible!

My heartfelt gratefulness should be extended to my supervisors, Dr. Gerald Malgas and Prof. Christopher Arendse for their eternal supervision, patience, support, commitment, and their belief have been extraordinary in my academic work and I thank them for all the constructive criticism, which benefitted me immensely both during the experimental part and the compilation of this thesis.

To my Grandmother (Mamaburu), Mother (Ntswaki) I cannot express my gratitude for your constant love, support, encouragement, and of course persuasion to continue to study and understand the true value of education and the rewards of perseverance.

I am profoundly grateful to my Grand-grandmother (Mambeko), my late Grand-Fathers (Ntate Titiya John and Nthea Jonas), my uncles (Machine and Jimmy), brothers (Sello, Tankiso and Lucky) and sisters (Mpho, Dikomo and Lindiwe) thank you for your love, encouragement and moral support.

I am overwhelmingly thankful to my school teacher, friend, brother; Mr. T. D Motsoeneng for support me throughout my studies and by introducing me to the UWC.

I am also grateful to my brother in law (Hlony) and his Fiancé (Nokuthula) for always accommodating during my research visits in Cape Town.

My special thanks go to Ms Angela Adams secretary of Physics Department at UWC for always helping me with the registration issues.

Last, and most of all, I wish to express my deepest gratitude to my in-laws (Ntate Nduna, Mme Manduna) for all their support and compassion.

I am indebted to my fellow students and friends at CSIR, UWC and at home for their continuous support.

I am grateful to Jayita Bandyopadhyay, Thomas Malwela and Clive Oliphant for POM, DSC, AFM, and SEM analysis.

My sincere gratitude goes to the Staff of NCNSMs (CSIR) and Physics Department (UWC) for their support.

Finally, I acknowledge the financial support of the CSIR (Project: HGERA7S) and National Research Foundation (NRF).



“I have a dream that one day every valley shall be exalted, and every hill and mountain shall be made low, the rough places will be made plain, and the crooked places will be made straight; **"and the glory of the Lord shall be revealed and all flesh shall see it together."**”

MARTIN LUTHER KING, JR



Dedicated to my wife (Mpho Motaung), son (Omolemo Motaung), my late grandmother (Mamaburu Motaung-Tshabalala) and my mother (Ntswaki Motaung)

CONTENTS


CHAPTER ONE	1
BACKGROUND OF THE STUDY	1
1.1. ENERGY SENARIO	1
1.1.1. Inorganic Solar Cells.....	2
1.1.2. Organic Solar Cells.....	3
1.2. ORGANIC PHOTOVOLTAIC DEVICE OPERATION AND CHARACTERIZATION.....	5
1.2.1. Incoupling of the Photon and Absorption	5
1.2.2. Exciton Formation and Migration	5
1.2.3. Exciton Dissociation or Charge Pair Separation	6
1.2.4. Charge Transport and Collection	6
1.2.5. Recombination Processes in Solar Cells	7
1.2.6. Photovoltaic Parameters.....	9
1.3. ORGANIC PHOTOVOLTAIC STRUCTURES	12
1.3.1. Bi-layer Structure	12
1.3.2. Bulk Heterojunction Structure	13
1.4. STABILITY OF THE POLYMER SOLAR CELLS	14
1.5. AIMS AND OUTLINE	17
1.6. REFERENCES.....	20

CHAPTER TWO	24
COMPARATIVE STUDY: THE EFFECTS OF SOLVENT ON THE MORPHOLOGY, OPTICAL AND STRUCTURAL FEATURES OF REGIOREGULAR POLY(3-HEXYLTHIOPHENE): FULLERENE THIN FILMS ..	24
2.1. INTRODUCTION.....	25
2.2. EXPERIMENT DETAILS	26
2.2.1. Sample preparation	26
2.2.2. Characterization.....	27
2.3. RESULTS AND DISCUSSION.....	29
2.3.1. Morphology	29
2.3.2. Structural properties.....	32
2.3.3. Optical properties.....	41
2.4. CONCLUSION	45
2.5. REFERENCES.....	46
 CHAPTER THREE	 51
STRUCTURAL AND PHOTO-PHYSICAL PROPERTIES OF SPIN-COATED POLY(3-HEXYLTHIOPHENE) THIN FILMS	51
3.1. INTRODUCTION.....	52
3.2. EXPERIMENTAL DETAILS.....	53
3.3. RESULTS AND DISCUSSION.....	55
3.4. CONCLUSION	66
3.5. REFERENCES.....	68

CHAPTER FOUR	71
CORRELATION BETWEEN THE MORPHOLOGY AND PHOTO-PHYSICAL	
PROPERTIES OF P3HT: FULLERENE BLENDS	
4.1. INTRODUCTION.....	73
4.2. EXPERIMENT DETAILS	74
4.2.1. Materials and solutions	74
4.2.2. Sample preparation	75
4.2.3. Characterization.....	76
4.3. RESULTS AND DISCUSSION.....	77
4.4. CONCLUSION	89
4.5. REFERENCES.....	91
CHAPTER FIVE.....	96
INVESTIGATION OF THE EFFECTS OF SUBSTRATE ANNEALING ON THE	
PROPERTIES OF POLYMER BLENDS	
5.1. INTRODUCTION.....	97
5.2. EXPERIMENT DETAILS	98
5.3. RESULTS AND DISCUSSION.....	100
5.3.1. Structural properties.....	100
5.3.2. Surface Morphology.....	108
5.3.3. Photo-physical properties	114
5.4. CONCLUSION	116
5.5. REFERENCES.....	118



CHAPTER SIX.....	122
THE INFLUENCE OF THERMAL ANNEALING ON THE MORPHOLOGY AND STRUCTURAL PROPERTIES OF A CONJUGATED POLYMER IN BLENDS WITH AN ORGANIC ACCEPTOR MATERIAL	122
6.1. INTRODUCTION.....	123
6.2. EXPERIMENT DETAILS	124
6.2.1. Sample preparation	124
6.2.2. Characterization.....	125
6.3. RESULTS AND DISCUSSION.....	126
6.3.1. Atomic force microscopy measurements	126
6.3.2. Transmission electron microscopy measurements	128
6.3.3. Optical microscopy measurements	129
6.3.4. X-ray diffraction measurements	131
6.4. CONCLUSION	136
6.5. REFERENCES.....	138
 CHAPTER SEVEN	 141
THERMAL INDUCED CHANGES ON THE PROPERTIES OF SPIN-COATED P3HT:C ₆₀ THIN FILMS FOR SOLAR CELL APPLICATIONS	141
7.1. INTRODUCTION.....	142
7.2. EXPERIMENT DETAILS	144
7.2.1. Sample preparation	144
7.2.2. Characterization.....	145

7.3.	RESULTS AND DISCUSSION.....	146
7.3.1.	Differential scanning calorimetry (DSC).....	146
7.3.2.	Thermo-gravimetric analysis (TGA).....	148
7.3.3.	Ultraviolet-Visible Spectroscopy (UV-Vis).....	151
7.3.4.	Photoluminescence (PL).....	152
7.3.5.	Fourier Transform Infrared Spectroscopy (FT-IR).....	155
7.3.6.	Raman Spectroscopy.....	157
7.3.7.	Photovoltaic measurements.....	158
7.4.	CONCLUSION.....	161
7.5.	REFERENCES.....	163
CHAPTER EIGHT		167
		
UNIVERSITY of the WESTERN CAPE		
	INSIGHTS INTO THE STABILITY AND THERMAL-DEGRADATION OF P3HT:C ₆₀ BLENDED FILMS FOR SOLAR CELLS.....	167
8.1.	INTRODUCTION.....	169
8.2.	EXPERIMENTAL DETAILS.....	171
8.2.1.	Sample preparation.....	171
8.2.2.	Characterization.....	172
8.3.	RESULTS AND DISCUSSION.....	174
8.4.	CONCLUSION.....	192
8.5.	REFERENCES.....	194
SUMMARY		199

LIST OF ARTICLES INCLUDED IN THIS THESIS202
ARTICLES TO WHICH I HAVE CONTRIBUTED BUT NOT INCLUDED IN THE
THESIS.....203



CHAPTER ONE

BACKGROUND OF THE STUDY

1.1. ENERGY SENARIO

The continuous increase in the energy demand each year, the limiting supply of fossil fuel resources and their detrimental long term environmental effects, underline the urgency of developing renewable energy sources. Over 86 % of our energy demands are met by the combustion of fossil fuels [1.1]. However, since carbon dioxide (CO₂) is one of the by-products of this combustion [1.2]; it is estimated that the CO₂ emissions from the use of fossil fuels is growing at the rate of 1.9% annually. As a result, the CO₂ concentration in the atmosphere continues to considerably add to the green-house effect. Therefore, to reduce the CO₂ concentration; alternative ways should be considered to generate electricity that will meet the needs of the society. These alternative energy sources should also be environmentally friendly and capable of competing with the current renewable energy by either decreasing the cost or increasing the efficiency or a combination of both.

There are several types of renewable energy sources, such as wind power, hydroelectric generation, geothermal sources and solar power. Solar power, however, is one of the brightest prospects for future energy generation.

Harvesting energy directly from the sunlight using photovoltaic (PV) technology is being widely recognized as an essential component of future global energy production.

1.1.1. Inorganic Solar Cells

In 1839, Edmond Becquerel a French physicist discovered the photovoltaic effect [1.3]. Becquerel found that when electrodes made with certain materials were inserted into an electrolytic cell and illuminated with white light a small current was produced. Later, in 1887, Day and Adams confirmed the existence of the same effect in solids. In 1954, one of the first inorganic PVs was made in Bell Laboratories [1.4]. It was based on silicon (Si) and had power conversion efficiency (PCE) of about 6%. Since then, the efficiency has reached 24% for crystalline Si solar cells [1.5], which is already close to the theoretical predicted upper limit of 30% [1.6]. Practically all conventional inorganic solar cells incorporate a semiconductor that is doped to form a *p-n* junction across which the photo-voltage is generated. Currently, about 85% of the PV market is shared by crystalline solar cells.

Despite of large PV market expansion and many research achievements made over the last couple of decades, only about 0.1% of total electricity generated in the world is supplied from PV installations. This is mainly due to the high costs of raw materials, high temperature processing (400-1400 °C), high vacuum conditions requirements, difficulty in fabrication of Si solar cells and installations [1.7]. In addition, they cannot produce energy at the low cost like

conventional fossil fuel power plants. Therefore, organic materials could be a possible alternative to replace and/or compliment the class of inorganic materials due to several drawbacks mentioned above.

1.1.2. Organic Solar Cells

The first investigation of organic solar cells came as early as 1959, with the use of crystals and organic molecules. The cell exhibited a photo-voltage of 200 mV with an extremely low efficiency of ~ 0.1% [1.8]. This gave the first indications that organic systems could rival established inorganic systems for electronic applications. A major breakthrough in the performance of organic solar cells came in 1985 when Tang *et al.* [1.9] developed a two layer solar cell which consist of copper phthalocyanine and perylene tetracarboxylic derivatives as the organic materials with an efficiency of ~1 %. This work of Tang *et al.* [1.9] which is commonly cited as the groundbreaking discovery sparked the current interest in the field of solar cells. In 1977, Heeger *et al.* [1.10] discovered the semi-conducting properties of polyacetylene polymer material. After that, polymer materials attracted researchers by showing that their electrical properties can range from insulating to semi-conducting to conducting. This led to the discovery of electroluminescence in a poly (p-phenylene vinylene) (PPV) by Burroughes *et al.* [1.11, 1.12] in 1990.

In 1992, Sariciftci *et al.* [1.13] introduced a major breakthrough in a charge separation in polymer/fullerene systems. A charge separation polymer/fullerene system is achieved by ultrafast transfer of photo-excited electrons from a polymer

to a fullerene. An upper limit for electrons transfer time was found to be 300 femtoseconds (fs) in this system versus a photoluminescence life time of picoseconds (ps) in a pristine polymer. This discovery initiated an enormous research into fullerene/polymer based solar cells. Aernouts *et al.* [1.14] showed that excitons can be rapidly split by electron transfer before the recombination of electron and hole if C₆₀ derivatives, phenyl-C₆₁-butyric acid methyl ester (PCBM) are blended into the polymer, and they reported a PCE of over 3% via a network of internal donor-acceptor heterojunction (HJ).

However, due to wide band gaps, 2.1~2.4 eV, of PPV polymer which seem to be insufficient for efficient light harvesting from solar spectrum, the focus shifted to poly(3-hexylthiophene) (P3HT) as an electron donor material due to its low band gap (~ 1.9 eV) [15], high mobility (0.1 cm²V⁻¹s⁻¹) [1.16], good chemical stability. Recently, PCE of 5% was reported for HJ cells [1.17, 1.18] and 6.5% for tandem cells [1.19], while theoretical predictions suggest that it should be possible to obtain 10% [1.20, 1.21]. Therefore, this progress in PCEs makes them more competitive to amorphous Si solar cells. In spite of the low PCE, organic solar cells have novel features that make them more attractive, such as their light weight, mechanical flexibility, easy processing at low temperatures (20-200°C) through spin-coating [1.22], doctor blade method, screen printing [1.23] and no vacuum system requirements.

1.2. ORGANIC PHOTOVOLTAIC DEVICE OPERATION AND CHARACTERIZATION

1.2.1. Incoupling of the Photon and Absorption

Illustrated in Fig. 1.1 is the basic operation of an organic solar cell. The incoming photons encounter the first interface, i.e. glass or plastics, when they reach the device. The reflection losses at the air/substrate interface as well as at each subsequent interface, which depend on the difference between optical refractive indices of the two materials, have to be reduced. The incoming photons are then absorbed in the active layer, whose absorption spectrum should match the solar irradiation for maximum absorption. As a result, low band-gap polymers are highly desired. For instance, crystalline Si has a band gap of 1.1 eV; it can harvest more than 90% of the photons. While P3HT with a band gap ~1.9 eV and high absorption coefficient that is close to the maximum photon flux in the solar spectrum (1.8 eV), is capable of absorbing only ~ 46% of the available solar photons [1.24]. The limitation in the absorption however is primarily due to limited spectral breadth rather than the absorption coefficient.

1.2.2. Exciton Formation and Migration

After a photon has been absorbed in the polymer, an exciton is formed. The excitons then diffuse in the material with a characteristic exciton diffusion length (L_D) typically of the order of 5–10 nm [1.25], which depends on the structure of

the material and the dielectric properties. The excitons have a finite lifetime and during the diffusion they decay or dissociate through several mechanism. In order to achieve efficient photovoltaic conversion, the excitons have to be dissociated into free electrons and holes, before they decay radiatively, thermally or vibronically.

1.2.3. Exciton Dissociation or Charge Pair Separation

The most common way to achieve exciton dissociation into free electrons and holes is through a photoinduced charge transfer process (Fig. 1.1). The processes that act as counterforces to exciton dissociation are geminate recombination, where separated electrons and holes recombine to form an exciton, and non-geminate bimolecular recombination, where an electron and a hole from different excitons recombine.

1.2.4. Charge Transport and Collection

The free charges must then travel through the active layer to reach the electrodes where they can be collected to produce photocurrent (Fig. 1.1). The charge carrier mobilities for both the electron and hole therefore play an important role in determining device efficiency. The charge carrier mobility in conjugated polymers is usually very low, [1.26, 1.27] which makes it essential to have a thin active layer, which on the other hand unfortunately reduces the optical absorption. Finally, the free electrons that reach the electrodes are collected and passed into the outer circuit to generate device photocurrent. The

charge collection efficiency depends on the energy level matching at the metal/polymer interface, interfacial defects, etc. A detailed descriptions of the steps used for physical processes in polymer solar cell are found elsewhere [1.28, 1.29].

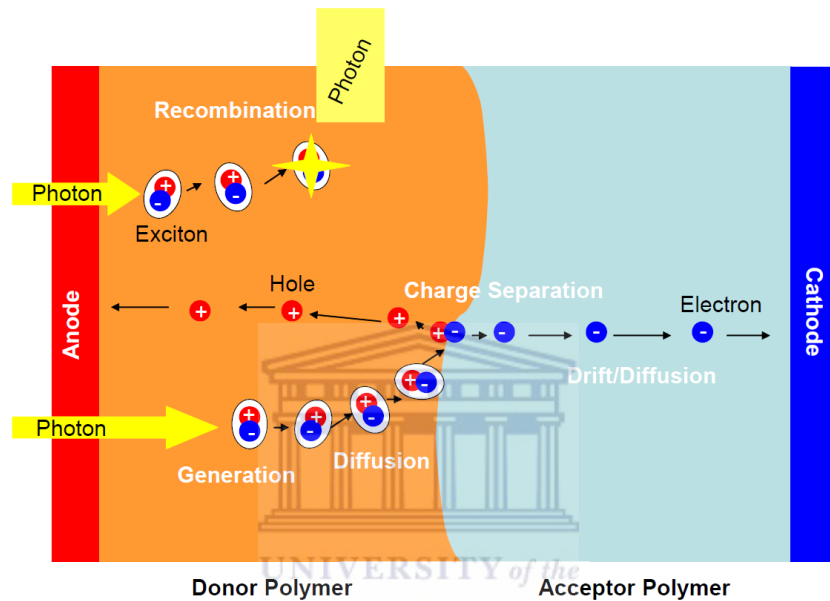


Figure 1. 1: Schematic drawing of an organic solar cell device Principle of charge separation in an organic solar cell.

1.2.5. Recombination Processes in Solar Cells

After the charge transfer process, the charges may either escape their mutual Coulombic attraction and can be collected, or they can recombine with a charge carrier of opposite sign to the ground state at the donor–acceptor interface. At the interface, the charges can either recombine geminately or non-geminately. In case of geminate recombination, the charge carriers within a single photogenerated charge pair recombine. In this case, the recombination

rate is expected to be independent on excitation density, and the concentration of the generated charge pairs depends linearly on excitation density (monomolecular decay). However, in case of non-geminate recombination, the charge carriers from multiple charge pairs recombine and the recombination kinetics is therefore strongly dependent on excitation density. Non-geminate recombination is expected at high excitation densities. In the absence of trap sites, non-geminate recombination is a bimolecular reaction and it occurs at a single reaction rate (non-dispersive).

In the presence of trap sites, non-geminate recombination does not necessarily show bimolecular type kinetics. Relaxation of the photogenerated charge carriers to trap sites in the disordered potential landscape leads to dispersive recombination kinetics [1.30]. In disordered materials, a power-law type decay of the charge carriers has been observed and related to dispersive recombination kinetics [1.31]. If the recombination is limited by the de-trapping rate of the charge carriers, it may show decay rates, which are independent of intensity in a certain time range. In such a case, it is difficult to distinguish the non-geminate bimolecular decay from a monomolecular decay process. Furthermore, numerical simulations of bimolecular recombination kinetics of excitations in a system in which the excitations are allowed to hop within a Gaussian density of states, show that, with time exceeding the energetic relaxation time of the excitations, at thermodynamic equilibrium a transition from dispersive ($dn/dt \sim t^{-1}$) to non-dispersive ($dn/dt \sim t^{-2}$) recombination may be observed [1.32]. To identify the processes governing the recombination

dynamics, the decay of the charge-separated state is usually studied by temperature dependent, excitation density dependent and time-resolved measurements.

1.2.6. Photovoltaic Parameters

In order to study the PV performance of a solar cell, as well as its electric behaviour, the current density -voltage (I - V) characteristics in the dark and under illumination are measured. The (I - V) characteristics are obtained by applying a variable voltage and measuring the current density obtained. Fig. 1.2 depicts an I - V curve of a PV device in the dark, where the cell displays regular diode-like characteristics with the curve passing through the origin; and under illumination, where the I - V curve is shifted down by the amount of photocurrent generated.

The intersection of the curve with the y-axis at zero applied voltage is referred to as the short circuit current density (I_{SC}). The intersection of the curve with the x-axis where current under illumination is zero is referred to as an open circuit voltage (V_{OC}). At any point, the power output of this device is given by the product of the current and voltage at that point. The I_{max} and V_{max} are the measured current and voltage values at which the device has the maximum power output (P_{max}). P_{max} is then given by the product of these two values. This is depicted in the diagram as the area of the smaller shaded rectangle. Ideally, when a forward bias is applied, until the voltage crosses the V_{OC} value, there would be no reduction in the photocurrent, and after it is crossed, the forward

bias current should immediately become exponentially large. Therefore, using these quantities the fill factor (FF) can be calculated as:

$$FF = \frac{P_{\max}}{I_{sc} \times V_{oc}} = \frac{I_{\max} \times V_{\max}}{I_{sc} \times V_{oc}} \quad (1.4)$$

The FF has no units; it is generally represented in percentage and it is a measure of the quality of the I - V characteristics of a solar cell. It is determined by charge carriers reaching the electrodes when the built-in field is lowered toward the open circuit voltage.

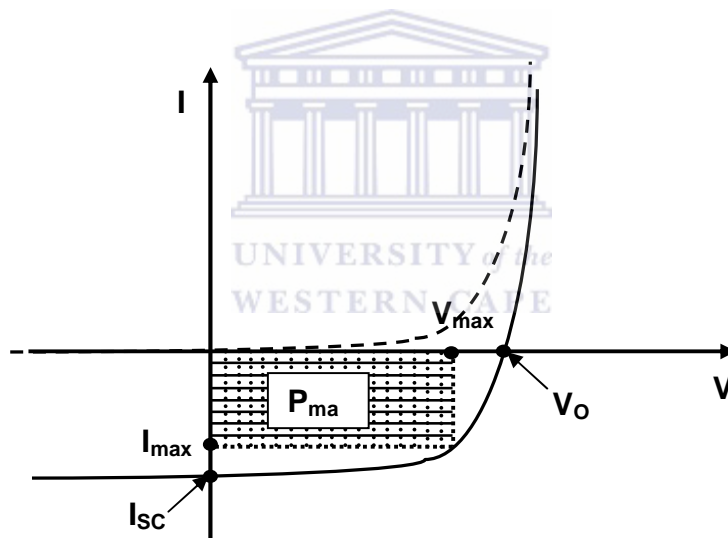


Figure 1. 2: Typical J - V characteristics of an organic PV cell in the dark (dashed line) and illumination (solid line) conditions. A shaded area is the P_{\max} output of the measured device.

The power conversion efficiency (PCE) which indicates the overall efficiency, the quality of device fabrication, etc. is the ratio between the P_{\max} and the P_{source} :

$$PCE = \frac{P_{\max}}{P_{\text{source}}} = \frac{V_{\max} \times I_{\max}}{P_{\text{source}}} = \frac{FF \times V_{oc} \times I_{sc}}{P_{\text{source}}} \quad (1.5)$$

However, it should be noted that the PCE has no units as well; it is generally quoted as a percentage. Since it is dependent on the wavelength and intensity of P_{\max} , the PCE should be measured under standard test conditions. These conditions include the temperature of the PV cells (25 °C), the intensity of radiation (1000 Wm⁻²), and the spectral distribution of the light (air mass 1.5 or AM1.5, which is the spectrum of sunlight that has been filtered by passing through 1.5 thicknesses of the earth's atmosphere. Mostly in the lab, the solar simulator that consists of a white source and a set of filters is used to simulate the solar illumination. Hence, in this thesis the solar simulator will be used. For organic solar cells based on polymer: fullerene BHJs, the magnitude of I_{sc} , V_{oc} , and FF depends on several parameters such as: light intensity, temperature, composition of the components, thickness of the active layer, the choice of electrodes used, as well as the solid state morphology of the film [1.23, 1.33]. Their optimization and maximization require a proper understanding of the device operation and photocurrent generation and its limitations in these devices. The relation between the experimental photocurrent and material parameters (i.e. charge-carrier mobility, band-gap, molecular energy levels, or relative dielectric constant) needs to be understood and controlled in order to allow for further design of new materials that can improve the efficiency of this type of solar cells.

1.3. ORGANIC PHOTOVOLTAIC STRUCTURES

1.3.1. Bi-layer Structure

A revolutionary development on the donor-acceptor (D/A) hetero-junction (HJ) has brought a significant improvement in the performance of organic solar cells [1.9]. The concept behind a HJ is to employ two materials with different electron affinities and ionization potentials in order to create an electric field. Hence, if both resulted ionization potentials and electron affinity are strong at the interface and may favour exciton dissociation; the electron will be accepted by the material with a larger electron affinity and the hole by the material with lower ionization potential. This is only true if the differences in a potential energy are larger than the exciton binding energy. Thus, in a planar HJ or a bi-layer device the organic D/A interface separates the excitons more proficiently than the organic-metal interface in the single layer device. However, in a bi-layer only excitons created within a distance of about 10-20 nm from the interface can reach the HJ interface. This leads to the loss of absorbed photons further away from the interface and results to low quantum efficiencies (QE) [1.34]. The PCE of bilayer (Fig. 1.3a) solar cells is limited by the charge generation 10-20 nm around the donor-acceptor interface.

In this device several processes occur for conversion of energy: (1) absorption of light and creation of excitons, (2) diffusion of the excitons within the donor phase, (3) dissociation of excitons when they encounter an interface with a generation of charge and (4) separation of charge (5) separated free electrons

(holes) are transported by the internal field created by electrodes with different work functions towards the cathode and anode where (6) they are collected by the electrodes and transported into the external circuit [1.13, 1.35].

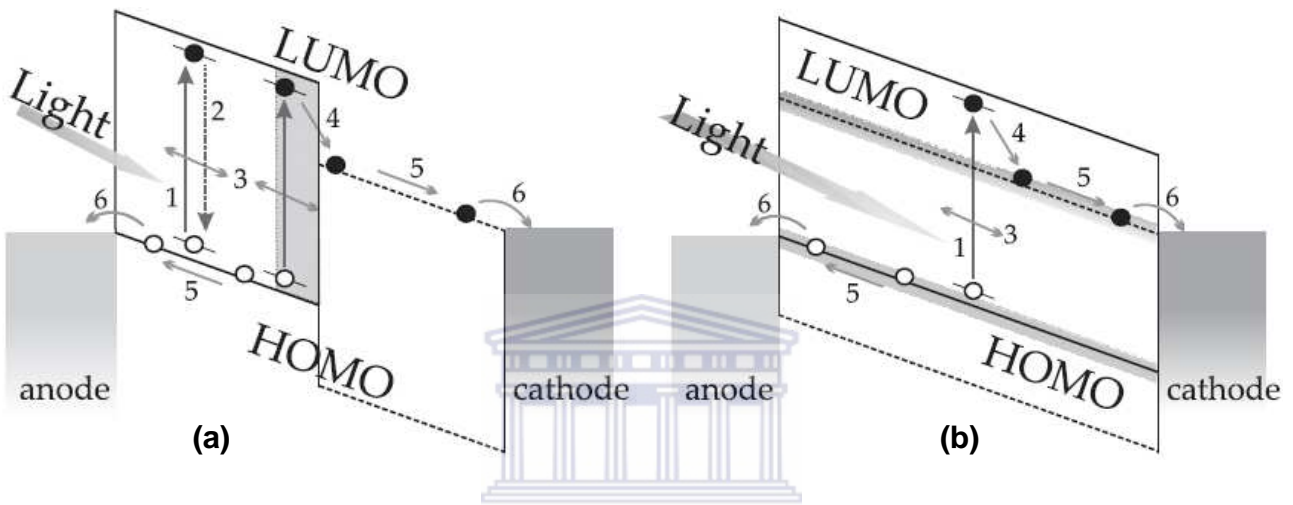


Figure 1. 3: Schematic band drawing of (a) a bi-layer and (b) a BHJ devices. The numbers refer to the operation processes explained in the text. The dashed line represents the energy levels of the acceptor, while the full lines indicate the energy level of the donor in the PV cell. HOMO: highest occupied molecular orbital; LUMO: lowest unoccupied molecular orbital [1.36].

1.3.2. Bulk Heterojunction Structure

The concept of bulk heterojunction (BHJ) introduced by Yu *et al.* [1.36, 1.37] in 1995 marked a new era in organic solar cells. This concept of hetero-junction is the heart of all three currently existing types of organic PV cells: dye-sensitized

solar cells [1.38, 1.39]; planar organic semiconductor cells [1.40]; and high surface area, or BHJ cells [1.36, 1.37]. In general, a BHJ is a blend of the donor and acceptor in a bulk volume. It exhibits a D/A phase separation in about 1-20 nm length scale. The BHJ concept has remarkably increased (orders of magnitude) the interfacial area between the D and A phases and consequently improves the efficiency of PVCs. Fig. 1.3b depicts a schematic representation of a bulk (or dispersed) HJ. It illustrates the components involved in the mechanistic steps where the donor and acceptor materials are blended together. In this case, if the length scale of the blend is quite similar to the exciton diffusion length; then the decay processes (2) is dramatically reduced since in the proximity of every generated exciton there is an interface with an acceptor where fast dissociation takes place (4). In general, charge generation occurs everywhere in the active layer. Provided that continuous pathways exist in each material from the interface to the respective electrodes, the photon-to-electron conversion efficiency and, hence, the photosensitivity is dramatically increased. In brief, the details of these mechanistic steps in BHJ have been described intensively in the literature [1.41, 1.42].

1.4. STABILITY OF THE POLYMER SOLAR CELLS

To date, improvement on organic PCE has been considered as the most vital research goal; while the stability of the organic material which is equally important as efficiency has been ignored. As a result, the stability still remains as

one of the universal bottlenecks in organic PV technologies. Significant improvement of stability and increase of lifetimes up to scales that could comply with industrial standards are essential requirements for further progress and commercialization of organic solar cell devices [1.43-1.48]. To date, some of these criteria have been achieved individually, but they have not all been combined for the same material or material technology. Jørgensen *et al.* [1.48] investigated the mechanism of the degradation of OPVs through different pathways (Fig. 1.4). The organic materials and metal used as the electrodes react with oxygen and water, which are diffused from both electrodes or lateral of the device are believed to be the major reason causing short lifetime of OPVs.

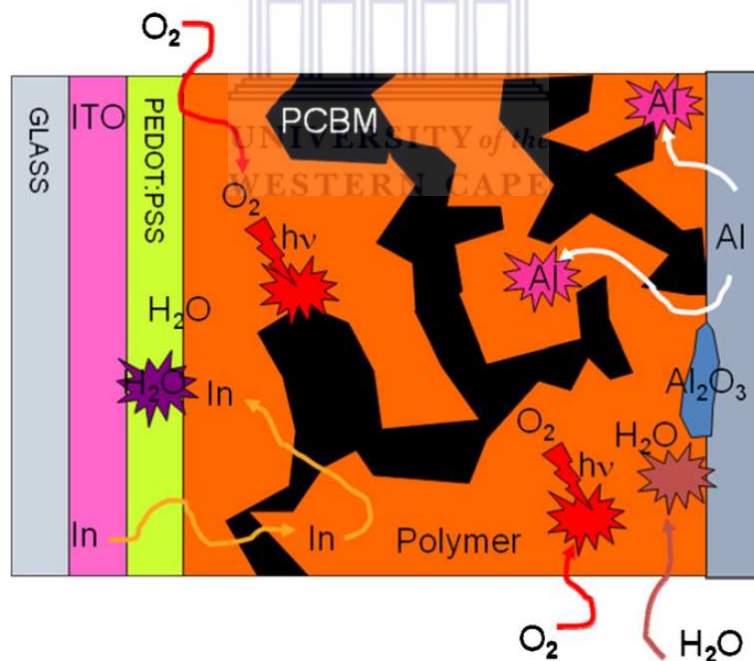


Figure 1. 4: A graphical overview of the field of stability and degradation of polymer solar cells. [1.48].

Krebs *et al.* [1.44] demonstrated that the oxygen diffused into the Al electrode through Al grains and microscopic holes on the Al film by using time-of-flight secondary ion mass spectrometry (TOF-SIMS) methodologies. They also observed that indium was diffused in the layer in an OPV with a structure of Al/C₆₀/P3CT/ITO, where P3CT is poly(3-carboxythio-phenylene-co-thiophene). Based on that, Krebs *et al.* [1.44, 1.45] demonstrated a solar cell with a lifetime of up to 10000 h with the careful exclusion of water and oxygen. Moreover, they also predicted an operational lifetime in excess of 20 000 h by using a thermal acceleration factor of 4 between 25 and 72 °C and an indoor illumination intensities of 50–100Wm⁻². Kawano *et al.* [1.49] also found that the resistance of ITO was increased due to the hygroscopic poly(3,4-ethylenedioxythiophene):poly(styrenesulfonate) (PEDOT:PSS) layer absorbed the moisture from the ambient atmosphere.

It has been reported that ITO/ZnO/ZnO:P3CT/PEDOT:PSS/Ag inverted type solar cells without sealing maintained 80% of the initial performance for continuous illumination for 100 h in an ambient atmosphere [1.47]. Hauch *et al.* [1.50] have investigated the performance of a flexible P3HT:PCBM based modules in outdoor atmosphere with operational stability of a lifetime up to a year. Surprisingly the total efficiency of the modules have not decreased, but increased by 3.3%. This increase was due to a relative increase in FF by 10.8%, with a drop in V_{OC} by 6.8%. There was no noticeable change in I_{SC} . These studies on the stability/degradation [1.43-1.48] issues showed that the topic is rather complicated and not fully understood.

1.5. AIMS AND OUTLINE

The use of polymeric materials in the fabrication of low cost photovoltaic devices or plastic electronics has been extensively studied due to its low-cost synthesis and easy manufacture of thin film devices by vacuum evaporation/sublimation or solution cast or printing technologies. It has been shown that the electronic band gap of organic semiconductors can be engineered by chemical synthesis for simple colour changing of light emitting diodes (LEDs). In spite of the good properties pointed above great progress in both power conversion efficiency and stability is needed for practical device applications

The aim of this thesis is to study the effect of solvent in order to control the degree of mixing of the polymer and fullerene components, as well as the domain size and charge transport properties of the blends. Additionally, it also focuses on the optimization on the morphology through various methods such as substrate annealing prior to deposition of active materials and post annealing on blended films in order to improve the efficiency of solar cells. Furthermore, the thermal ageing of P3HT:C₆₀ blended films and correlated with the chemical structure, morphological, opto-electronic properties and photovoltaic device changes induced during the long annealing time are also carried out.

This thesis will begin in chapter one by detailing the background of and physical theory involved in organic materials intended for use in photovoltaic devices. It will detail the theory of device operation and describe the different organic device configurations. The operation principle is also discussed in details

and includes light absorption processes, charge generation and transport and stability of the solar cells.

Chapter two will focus on the effect of solvent to control the degree of mixing of the polymer and fullerene components, as well as the domain size and charge transport properties of the blends using P3HT:C₆₀ films with different weight ratios.

Chapter three will report on the structural and photo-physical properties of spin-coated P3HT:C₆₀ thin films. Specific emphasis will be on the photo-induced charge generation in photo-excited P3HT films and its blends with fullerene as an electron acceptor material. Changes induced in the optical properties of rr-P3HT by the loading of C₆₀ with different weight ratios will also be discussed.

The photo-induced charge transfer and optoelectronic properties of photovoltaic cells correlated to the morphology and the structure of P3HT:C₆₀ blend are carried out in chapter four.

The investigation on the effect of substrate annealing prior to the deposition of the active layer on the morphological, structural and opto-electrical properties of two variations of organic polymer blends of poly(3-hexylthiophene):C₆₀ fullerene and poly(3-hexylthiophene):[6,6]-phenyl C₆₁ butyric acid methyl ester films is reported in chapter five.

Chapter six reports the influence of thermal annealing on the morphology and structural properties of a conjugated polymer in blends with an organic acceptor material. The morphological changes of the active layers were monitored using various techniques.

Chapter seven will continue this trend and present data on the thermal transition behaviour, structural, optical and photovoltaic properties (open-circuit voltage V_{oc} , short circuit current density I_{sc} , fill factor, FF and power conversion efficiency, PCE) of P3HT:C₆₀ films with different blends annealed at different temperatures. The current density–voltage (I – V) characteristics of the polymer based organic solar cells were measured both in the dark and under illumination using a Keithley 2420. The devices were irradiated at 100 mW cm^{-2} using a xenon lamp-based Sciencetech SF150 150W solar simulator equipped with an AM1.5 filter as the white light source. The optical power at the sample was 100 mW cm^{-2} , detected using a daystar meter. All the photovoltaic properties were evaluated in ambient air conditions at room temperature.

Chapter eight demonstrates the changes in the nanoscale morphology, opto-electronic and photovoltaic properties of the blended films induced by a diffusion of C₆₀ molecules and degradation/ageing of polymer-based active materials during longer thermal treatment above glass transition temperature.

Chapter nine gives a summary of the work presented in this thesis

1.6. REFERENCES

- [1.1] R. A. Messenger, J. Ventre, Photovoltaic Systems Engineering 2nd Edition (2006); A. Jäger-Waldau, PV Status Report, European Commission, EUR 20850 EN. (2003).
- [1.2] Intergovernmental Panel on Climate Change (IPCC), " Third Assessment Report of Working Group I - Summary for Policy makers" (2001) and Report Working Group III (2007); Web page: <http://www.ipcc.ch/>
- [1.3] T. Markvart, Ed., Solar Electricity, John Wiley & Sons, Chichester, U.K., (1994).
- [1.4] D. M. Chapin, C. S. Fuller, G. L. Pearson, J. App. Phys. 25 (1954) 676.
- [1.5] A. M. Green, K. Emery, Y. Hishikawa, W. Warta, Prog. Photovolt: Res. Appl. 16 (2008) 61
- [1.6] W. Shockley, H. J. Queisser, J. Appl. Phys. 32 (1961) 510
- [1.7] H. J. Lewerenz, H. Jungblut, Springer, Berlin, Heidelberg, New York (1995).
- [1.8] H. Kallmann, M. Pope, Journal of Chemical Physics **30** (1959), 585
- [1.9] C. W. Tang, Appl. Phys. Lett. 48 (1986) 183.
- [1.10] C. K. Chiang, C. R. Fincher, Y.W. Park, A. J. Heeger, H. Shirakawa, E. J. Louis, S. C. Gau, A. G. MacDiarmid, Phys. Rev. Lett. 39 (1977) 1098.
- [1.11] R. H. Friend, R. W. Gymer, A. B. Holmes, J. H. Burroughes, R. N. Marks, C. Taliani, D. D. C. Bradley, D.A. Dos Santos, J.L. Brédas, M. Löglund, W.R. Salaneck, Nature 397 (1999) 121.

- [1.12] J. H. Burroughes, D. D. C. Bradley, A. R. Brown, R. N. Marks, K. Mackay, R. H. Friend, P. L. Burns, A. B. Holmes, *Nature* 347 (1990) 539.
- [1.13] N.S. Sariciftci, L. Smilowitz, A.J. Heeger, F. Wudl, *Science* 258 (1992) 1474.
- [1.14] T. Aernouts, W. Geens, J. Poortmans, P. Heremans, S. Borghs, R. Mertens. *Thin Solid Films* 403–404 (2002) 297.
- [1.15] Y. Shao, G. Yuan, P. Reche and M. Lecerc, *Polymer* 36 (1995) 2211.
- [1.16] P. J. Brown, H. Sirringhaus, M. Harrison, M. Shkunov and R. H. Friend, *Phys. Rev. B* 63 (2001) 125204.
- [1.17] Li, V. Shrotriya, J. Huang, Y. Yao, T. Moriarty, K. Emery, Y. Yang, *Nat. Mater.* 4 (2005) 864.
- [1.18] W. Ma, C. Yang, X. Gong, K. Lee, A.J. Heeger, *Adv. Funct. Mater.* 15 (2005) 1617.
- [1.19] J.Y. Kim, K. Lee, N.E. Coates, D. Moses, T.–Q. Nguyen, M. Dante, A.J. Heeger, *Science* 317 (2007) 222.
- [1.20] L. J. A. Koster, V. D. Mihailetschi, P. W. M. Blom, *Appl. Phys. Lett.* 88 (2006) 093511.
- [1.21] M. C. Scharber, D. Muhlbacher, M. Koppe, P. Denk, C. Waldauf, A.J. Heeger, C.J. Brabec, *Adv. Mater.* 18 (2006) 789.
- [1.22] L. Chen, D. Godovsky, O. Inganäs, J. C. Hummelen, R. A. J. Janssens, M. Svensson, M. R. Andersson, *Adv. Mat.* 12(18) (2000) 1367.
- [1.23] C. J. Brabec, A. Cravino, D. Meissner, N. S. Sariciftci, M. T. Rispens, L. Sanchez, J. C. Hummelen, T. Fromherz, *T. S. Films* 403-404 (2002) 372.

- [1.24] C. Soci, I.-W. Hwang, D. Moses, Z. Zhu, D. Waller, R. Guadiana, C. J. Brabec, A. J. Heeger, *Adv. Funct. Mater* 17 (2007) 632.
- [1.25] C.J. Brabec, A. Cravino, D. Meissner, N.S. Sariciftci, T. Fromherz, M.T. Rispens, L. Sanchez, J.C. Hummelen, *Adv. Funct. Mater.*, 11 (2001) 374.
- [1.26] M. Pope, C. E. Swenberg, *Electronic processes in organic crystals*, Clarendon Press, Oxford, (1982).
- [1.27] H. S. Nalwa, *Handbook of organic conductive molecules and polymers*, (Wiley, New York vol. 1–4 (1997).
- [1.28] P. W. M. Blom, V. D. Mihailetschi, L. J. A. Koster, D. E. Markov, *Adv. Mater.* 19 (2007) 1551.
- [1.29] H. Hoppe, N. S. Sariciftci, *J. Mater. Res.* 19 (2004) 1924
- [1.30] H. Bässler, *Physica Status Solidi B: Basic Research* 175 (1993) 15.
- [1.31] I. Montanari, A. F. Nogueira, J. Nelson, J. R. Durrant, C. Winder, M. A. Loi, N. S. Sariciftci, C. Brabec, *App. Phys. Lett.* 81 (2002) 3001.
- [1.32] M. Scheidler, B. Cleve, H. Bässler, P. Thomas, *Chem. Phys. Lett.* 225 (1994) 431.
- [1.33] S. E. Shaheen, C. J. Brabec, N. S. Sariciftci, F. Padinger, T. Fromherz, J. C. Hummelen, *App. Phys. Lett.* 78 (2001) 841.
- [1.34] C. Winder, N. S. Sariciftci, *Mater. Chem.* 14 (2004) 1077.
- [1.35] G. Yu, J. Gao, J. Hummelen, F. Wudl, A. Heeger, *Science* 270 (1995) 1789.
- [1.36] C. J. Brabec, G. Zerza, G. Cerullo, S. De Silvestri, S. Luzzati, J. C. Hummelen, S. Sariciftci, *Chem. Phys. Lett.* 340 (2001) 232.

- [1.37] J.J.M. Halls, C.A. Walsh, N.C. Greenham, E.A. Marseglia, R.H. Friend, S.C. Moratti, A.B. Holmes, *Nature* 376 (1995) 498.
- [1.38] M. Gratzel, *Nature* 414 (2001) 338.
- [1.39] B. O'Regan, M. Gratzel, *Nature* 353 (1991) 737.
- [1.40] M. Granstrom, K. Petritsch, A. C. Arias, A. Lux, M. R. Andersson, R. H. Friend, *Nature* 395 (1998) 257.
- [1.41] R. Koeppel, N. S. Sariciftci, *Photochem. Photobiol. Sci.* 5 (2006) 1122.
- [1.42] *Photoinduced Electron Transfer* (Eds.: M. A. Fox, M. Chanon), Elsevier, Amsterdam, (1988).
- [1.43] F. C. Krebs, H. Spanggaard, *Chem. Mater.* 17 (2005) 5235.
- [1.44] F. C. Krebs, K. Norrman, *Prog. Photovolt. Res. Appl.* 15 (2007) 697.
- [1.45] E. A. Katz, S. Gevorgyan, M. S. Orynbayev, F. C. Krebs, *Eur. Phys. J. Appl. Phys.* 36 (2007) 307.
- [1.46] F. Padinger, T. Fromherz, P. Denk, C. J. Brabec, J. Zettner, T. Hierl, N. S. Sariciftci, *Synth. Met.* 121 (2001) 1605.
- [1.47] F. C. Krebs, *Sol. Energy Mater. Sol. Cells* 92 (2008) 715.
- [1.48] M. Jørgensen, K. Norrman, F. C. Krebs, *Sol. Energy Mater. Sol. Cells* 92 (2008) 686.
- [1.49] K. Kawano, R. Pacios, D. Poplavskyy, J. Nelson, D. D. C. Bradley, J. R. Durrant, *Sol. Energy Mater. Sol. Cells* 90 (2006) 3520.
- [1.50] J. A. Hauch, P. Schilinsky, S. A. Choulis, R. Childers, M. Biele, C. J. Brabec, *Sol. Energy Mater. Sol. Cells* 92 (2008) 727

CHAPTER TWO

COMPARATIVE STUDY: THE EFFECTS OF SOLVENT ON THE MORPHOLOGY, OPTICAL AND STRUCTURAL FEATURES OF REGIOREGULAR POLY(3-HEXYLTHIOPHENE): FULLERENE THIN FILMS

ABSTRACT

In this report the effect of solvent to control the degree of mixing of the polymer and fullerene components, as well as the domain size and charge transport properties of the blends were investigated in detail using P3HT:C₆₀ films. The polymer blend films spin coated from faster evaporating, non-aromatic solvents demonstrated an improved ordering and optical absorption in P3HT and blended films, indicating that the limited solubility of P3HT:C₆₀ in a marginal solvent can lead directly to optimal morphologies on the films. The PL quenched by a factor of 3 after blending the P3HT with C₆₀ in a 1:1 wt. ratio using CB, xylene, DCB, and toluene as solvents, indicating a partially charge transfer from P3HT to C₆₀. A complete reduction in the PL intensity was observed in the film spin-coated from chloroform.

The content of this chapter was published in: Synthetic Metals 160 (2010) 876–882

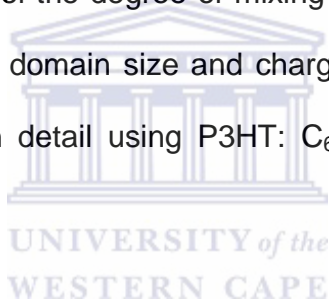
2.1. INTRODUCTION

In the last decade, solution processible organic conducting and semiconducting polymers have been extensively studied for use in organic solar cells due to their low-cost synthesis, low thermal budget and direct-writing printing techniques [2.1-2.4]. However, various properties of conducting polymers such as the charge mobility and electrical conductivity need to be improved in order to achieve the performance level of solar cells based on its inorganic crystalline and amorphous counterparts.

Poly(3-hexylthiophene) (P3HT) is a widely used organic semiconductor and therefore it is a good candidate for application in polymer solar cells [2.5]. P3HT shows good environmental stability [2.6], proper field-effect mobility of 0.01- 0.1 cm^2/Vs , reasonably high hole mobility in the range of $10^{-3} \text{ cm}^2 \text{ V}^{-1} \text{ s}^{-1}$ [2.7], has an absorption edge around 1.9 - 2.0 eV [2.8] and has a high solubility (solution processability). The excellent mobility of P3HT is thought to be due to the lamella-type stacking of the side chains and the stacking of thiophene rings, and thus the strong interchain interactions [2.9, 2.10]. In the past few years the technology of polymer photovoltaics has seen some drastic improvements in their power conversion efficiency [2.11]. Power conversion efficiencies in the 5% range have been achieved [2.12, 2.13] by optimizing the fabrication process, such as by annealing devices in a particular range of temperatures [2.13] or in a microwave oven [2.14] for an adequate period, or by carefully controlling the solvent evaporation rate [2.15]. This annealing process was carried out in order to induce the formation of a nanoscaled bi-continuous interpenetrating network

with a high interfacial area to increase exciton dissociation efficiency and the ordered stacking structure of the polymer chains and thereby enhance the charge mobility. For achieving such a high interfacial area, the electron acceptor material must have a high solubility in the organic solvent. Therefore, fullerene derivatives should be used as the electron acceptor for homogeneous, thin film formation from solutions with optical quality [2.16].

In spite of these recent works no unambiguous result as to the optimal processing for device performance has been established to date. In this work, the effect of solvent to control the degree of mixing of the polymer and fullerene components, as well as the domain size and charge transport properties of the blends were investigated in detail using P3HT: C₆₀ films with different weight ratios.



2.2. EXPERIMENT DETAILS

2.2.1. Sample preparation

Sample preparations were done according to the following procedure. All chemicals used in this experiment were purchased from Sigma Aldrich. Regioregular poly(3-hexylthiophene) (rr-P3HT) was used as a light absorption and electron donating material; while the C₆₀ fullerene was used as an electron acceptor material. The molecular weight (M_n) of P3HT reported by Sigma Aldrich was $\sim 64,000 \text{ g mol}^{-1}$; with regularity that is greater than 98.5 % for head-to-tail. Regioregularity denotes the percentage of stereo-regular head-to-tail (HT)

attachments of the hexyl side chains to the 3-position of the thiophene rings [2.17]. These materials were used as received, without any further purification. Indium tin oxide (ITO) coated on a 1 mm glass substrate with a resistance between 8 and 12 Ωsq^{-1} , and silicon (Si) (100) substrates were successfully cleaned by consecutive ultrasonication in acetone, isopropanol and de-ionized water for 10 min and dried in dry nitrogen. The active layer (i.e. the layer in which the majority of the incident light is absorbed and charges are generated) containing rr-P3HT and C₆₀ with different weight ratios (P3HT: C₆₀, e.g. 1:0, 1:1 wt. ratio) was dissolved in 1mL of non-aromatic solvents (Tetrahydrofuran (THF) and Chloroform) and aromatic solvents (Dichlorobenzene (DCB), Toluene, Xylene and Chlorobenzene (CB) solutions). The solutions were stirred overnight on a hot plate at a temperature of 50 °C to promote a complete dissolution. P3HT and its blends with a thickness of about 100 nm were spin coated onto the ITO and Si substrates. The spinning rate and time of spin-coating were 2500 rpm and 30 s. The samples were dried on a hot plate at a temperature of 50 °C for 15 min.

2.2.2. Characterization

The microstructure of the P3HT and its blends was studied with a Carl Zeiss Imager Z1M polarised optical microscope (POM). Spin-coated thin films were placed between two covering glasses and placed on a Linkam hot-stage (Linkam Scientific Instruments Ltd, UK), mounted on a POM instrument. Samples were heated from room temperature up to 250 °C at a heating rate of 10 °C.min⁻¹, held

at 250 °C for 1 min and then cooled down to room temperature at a precisely controlled cooling rate of 10 °C.min⁻¹. The films thickness was measured using a Veeco DEKTAK 6M Stylus profilometer.

The orientation and crystallinity of the P3HT and blends films spin-coated onto Si substrates, perhaps the most significant factors enhancing P3HT thin film properties, were characterized by Panalytical X'pert PRO PW 3040/60 x-ray diffractometer with a Cu K_α ($\lambda = 0.154$ nm) monochromated radiation source, operating at 45.0 kV and 40.0 mA. XRD data were collected in the 2 θ ranging from 3 to 25° with a step size of 0.02°. The absorption spectra of the active layer of P3HT and C₆₀ organic layers were measured by a PerkinElmer Ultra Violet-Visible (UV-vis) spectrometer from 900 to 300 nm. For Photoluminescence (PL), Raman and Fourier transform infrared spectroscopy (FTIR) measurements; samples were spin-coated on Si substrates. The photoluminescence (PL) spectra were taken from 300 to 900 nm by exciting the samples with a 350 nm line of deuterium lamp. The emission was detected with a Jobin-Yvon PMT detector. The structural properties of P3HT and its blend were investigated by PerkinElmer Fourier transform infrared spectroscopy spectrometer and Horiba Jobin Yvon HR800 micro-Raman spectrometer in backscattering geometry at room temperature. The Raman spectra were collected in the region 100–3000 cm⁻¹ with a spectral resolution of 0.4 cm⁻¹, using an excitation wavelength of 514.5 nm which was directed perpendicular to the Si substrate.

2.3. RESULTS AND DISCUSSION

2.3.1. Morphology

The microstructure of the blends spin-coated on Si substrates and prepared from different solvents was studied using the polarised optical microscopy (POM) technique. It is evident in Fig. 2.1a-c and f that the films investigated at room temperature shows small aggregates, which are related to C₆₀ fullerene clusters embedded in a polymer-rich skin layer, while the films prepared from CB and DCB (Fig. 2.1d and e) shows less or no aggregates associated with C₆₀. This is due to their high solubility in C₆₀ fullerene. The observed C₆₀ clusters, especially in the case of the THF and chloroform (Fig. 2.1b and f) solutions can be related to the lower solubility of C₆₀ (Table 2.1) and could act as better pathways for charge-carrier transport in the polymer phase [2.18].

To study the effect of temperature on the P3HT:C₆₀ (1:1 wt. ratio) films, the samples spin-cast from chloroform solvent were heated from room temperature to 250 °C at a heating rate of 10 °Cmin⁻¹, dwelled at 250 °C for 1 min and then cooled down to room temperature at a precisely controlled cooling rate of 10 °C min⁻¹. It can clearly be seen in Fig. 2.1g-i as well as on the inset (Fig. 2.1g) that, during heating treatment, the changes in colour visible of as-prepared film is observed. The changes in colour visible during this treatment may correspond to P3HT crystallization and a slight depletion of C₆₀ which would occur between around 72 to 170 °C, followed by melting from 200 to 250 °C.

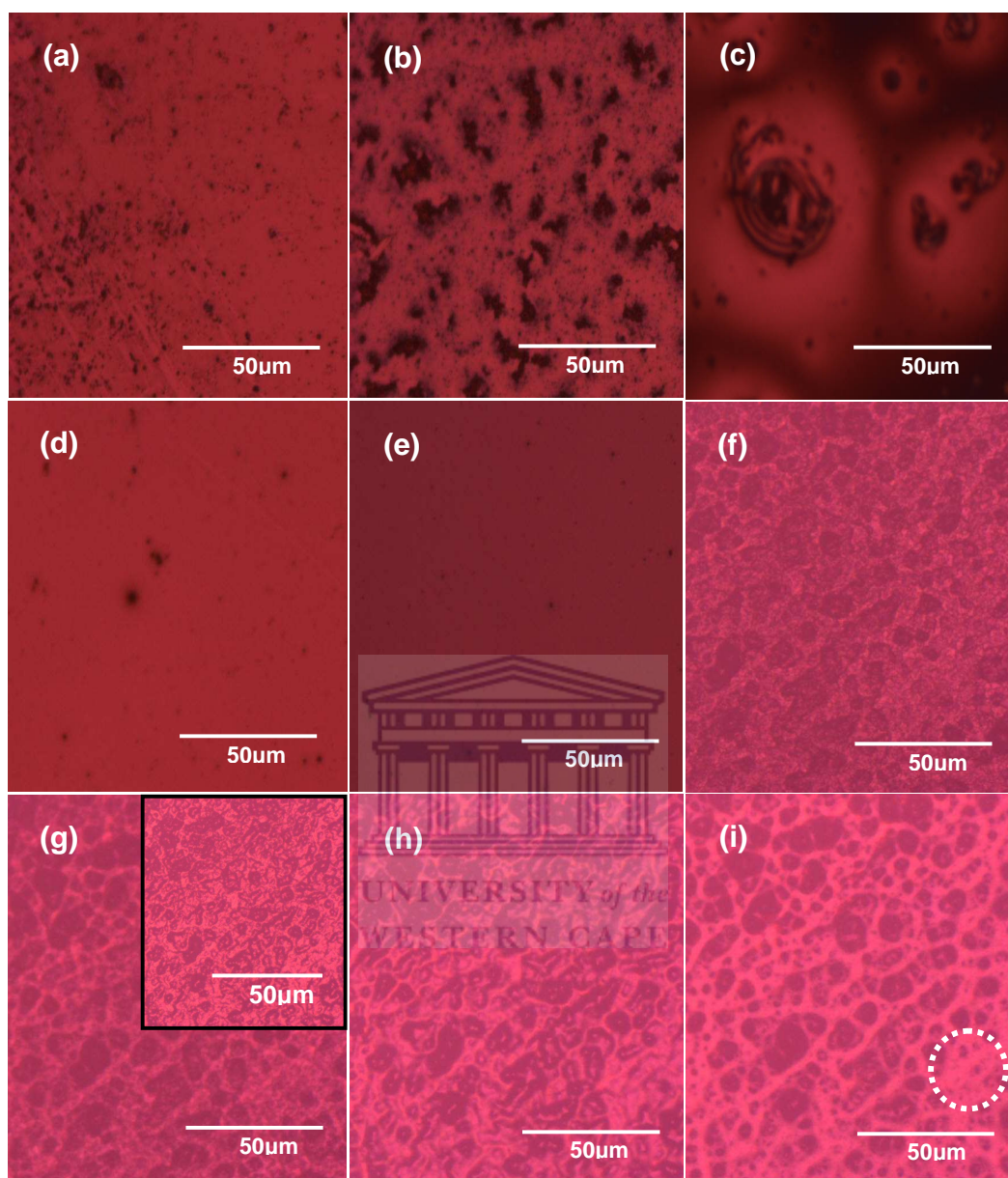


Figure 2. 1: Polarized optical microscopy micrographs of the surface of a P3HT:C₆₀ (1:1 wt. ratio) prepared from different solvents: (a) Toluene, (b) THF, (c) Xylene (d) CB, (e) DCB and (f-i) Chloroform. The images in g-i correspond to temperatures of 72, 170 (inset), 200 and 250 °C, respectively. Note: images in a-f were taken at room temperature.

TABLE 2. 1:Boiling points of different solvents and their solubility in C₆₀ fullerene [2.19, 2.20].

Solvents	Boiling points (°C)	C₆₀ Solubility (mg mL⁻¹)
Dichlorobenzene (DCB)	180.3	27.0
Chlorobenzene (CB)	111.0	7.0
Xylene	62.0	5.2
Toluene	66.0	2.8
Chloroform	132.0	0.16
THF	144.0	0.006

At a temperature of 250 °C (Fig. 2.1i), the surface of the film becomes smoother at certain areas. Hence some of the aggregate domains, probably related to C₆₀ diminish with an increase in temperature, while larger clusters remaining on the film surface.

A similar behavior in colour change and a depletion of a soluble fullerene derivative, phenyl-C₆₁-butyric acid methyl ester (PCBM) around 250 °C was also observed by Campoy-Quiles *et al.* [2.21]. Differential scanning calorimetry (DSC) measurements showed that, rr-P3HT exhibit an exothermic transition from a crystalline to a liquid crystalline state around 229 °C [2.22]. Chen *et al.* [2.23] also showed a melting temperature of 240–245 °C for head-to-tail rr-P3HT. Previous experimental POM results [2.24] showed that during annealing the P3HT films and its blend exhibit larger stains (aggregate domains). An increase

in aggregates related to C₆₀ clusters, diffused out of the polymer matrix during annealing.

2.3.2. Structural properties

To determine the structural information (chain orientation and crystallinity) of the P3HT film and its blend, the x-ray diffraction (XRD) measurements were carried out on the films spin-coated on Si (100) substrates. Fig. 2.2 depicts the XRD patterns of the P3HT film as well as the blend of P3HT:C₆₀ (1:1 wt. ratio) prepared from different solvents. The P3HT polymer prepared from non-aromatic solvents such as chloroform and THF shows well defined diffraction peaks around $2\theta = 5.5, 10.7$ and 15.9° (Fig. 2.2a) and (Table 2.2). These well defined diffraction patterns correspond to an ordered, self-organized lamellae structure with an interlayer spacing, which is formed by parallel stacks of polymer main chains that are separated by regions that are filled with the alkyl side-chains [2.23, 2.25-2.29]. The films spin-cast from DCB and CB solvents showed only the (100) diffraction patterns.

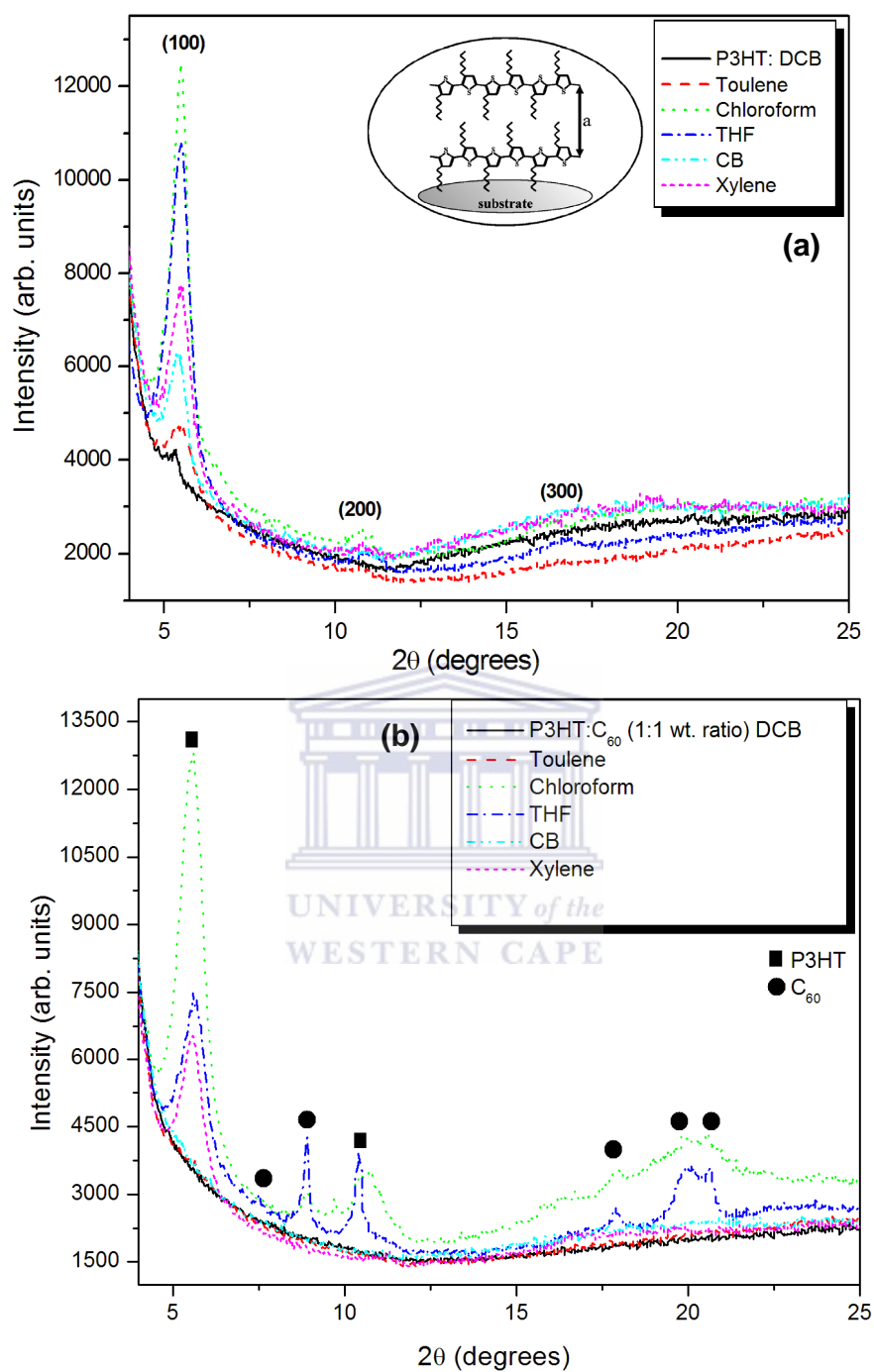


Figure 2. 2: Diffraction patterns of (a) rr-P3HT and (b) P3HT:C₆₀ (1:1 wt. ratio) blend prepared from different solvents. The inset depicts the orientation of the P3HT crystalline domains with respect to the substrate (Fig. 2.2a).

TABLE 2. 2: Summary of the peak positions and grain sizes of the as-prepared P3HT films prepared from different solvents.

Solvents	Peak height (cts)	d-spacing (nm)	FWHM (°)	Grain size (nm)
DCB	1380.6	1.65	0.82	9.7
Toluene	2109.2	1.59	0.77	10.3
Chloroform	8853.5	1.59	0.56	14.2
THF	8108.1	1.55	0.60	13.3
CB	3384.4	1.61	0.65	12.2
Xylene	4707.0	1.59	0.71	11.2

When P3HT polymer is blended with C₆₀ fullerene (Fig. 2.2b), the P3HT diffraction peaks for (100), (200) and (300), as well as the (220), (311), (222) and (331) diffraction peaks at 17.7, 20.9 and 21.7° associated with C₆₀ were only observed on the films spin cast from THF and chloroform, respectively [2.30]. The observed diffraction peaks for blend films spin-cast from chloroform and THF solutions illustrate that the P3HT material still maintains its structure and it is not hindered by the addition of C₆₀, due to their low boiling point (Table 2.1) which offers an advantage of fast solvent drying time to deposit highly crystalline P3HT film [2.31]. The low intensity (lower crystallinity) peaks observed for blends spin-coated from aromatic solvents, such as Toluene, DCB and CB, indicates that P3HT crystallization is hindered and disordered with an addition of C₆₀ fullerene.

However, Kline *et al.* [2.32] found that P3HT films cast in xylene have substantially higher crystallinity than their chloroform counterparts. Considering, the above results (Fig. 2.2), it can be suggested that, the faster evaporation time and limited solubility of rr-P3HT and C₆₀ in both solvents (chloroform and THF solution) for spin-casting offers rr-P3HT and its blend to form a more kinetically favourable crystal structure and crystallization [2.31], where hexyl side chains of rr-P3HT are oriented parallel to the substrate, i.e., vertically π - π stacking of inter-rr P3HTs on the substrate (inset in Fig. 2.2a). In addition, it can also be inferred that in the non-aromatic solvents the beam is more highly scattered due the substantial ordering of the polymer as well by C₆₀ clusters formation induced by lower solubility solvents in C₆₀. However, in the films spin-cast in aromatic solvents the scattered beam experiences a smooth interface between P3HT and C₆₀ induced by high solubility of C₆₀ in aromatic solvents (Table 2.1).

Using Bragg's equation [2.28, 2.29, 2.33, 2.34], the d-spacing for the primary (100) peak of P3HT and its blend was found to be between 1.55 and 1.65 \pm 0.03 nm as shown in Table 2.2. Thus, comparing these values with the data from the literature [2.25, 2.33-2.38], it can be concluded, that the detected peak originates from polymer crystallites with *a*-axis orientation (backbone parallel and side-chains perpendicular to the substrate, as depicted in the inset in Fig. 2.2a). The domain size along the *b* and *c* axes [2.28] could not be estimated from our measurements. Furthermore, using Scherrer's equation [2.33, 2.34] with the full width at half maximum (FWHM) of the (100) diffraction peak of the P3HT film revealed that the crystallite sizes of P3HT and blend films ranges

between 9.0 and 15.0 ± 0.03 nm as presented in Table 2.2. An increase in crystal size (reduction in FWHM) was observed for the P3HT prepared from non-aromatic solvents. This indicates an increase in the ordering of the alkyl chains within the main thiophene chains. It was previously observed, using high resolution transmission electron microscopy (HR-TEM) as well as XRD, that the structure of rr-P3HT films consists of crystallites embedded in an amorphous polymer matrix [2.22, 2.32, 2.39].

To complement XRD, Raman spectroscopy measurements were performed on spin-coated P3HT and P3HT: C₆₀ (1:1 wt. ratio) films. Fig. 2.3 present the Raman spectra of the P3HT and its blend (1:1 wt. ratio) film prepared from different solvents. In the spectrum of P3HT (Fig. 2.3) intensive Raman bands at about 715 , 1380 and 1440 cm⁻¹ are observed and are assigned to the C–S–C ring deformation, C–C skeletal stretching and C=C ring stretching, respectively [2.40-2.42]. However, no Raman features attributable to C₆₀, such as the A_{1g} 1469 cm⁻¹ mode of fullerenes, could be resolved.

To investigate the effect of solvents on the structural properties of P3HT, we compare the 1350-1500 cm⁻¹ region for non-aromatic and aromatic solvents. A Lorentzian function was carried out on the Raman spectra around 1445 cm⁻¹ and the data is summarized in Table 2.3. For rr-P3HT films prepared from non-aromatic solvents (Fig. 2.3a), an increase on the intensity of C=C ring stretching bands is observed, indicating an ordering in the polymer. However, when P3HT is blended with C₆₀ fullerene (Fig. 2.3b), significant changes on the C=C stretching deformation is observed.

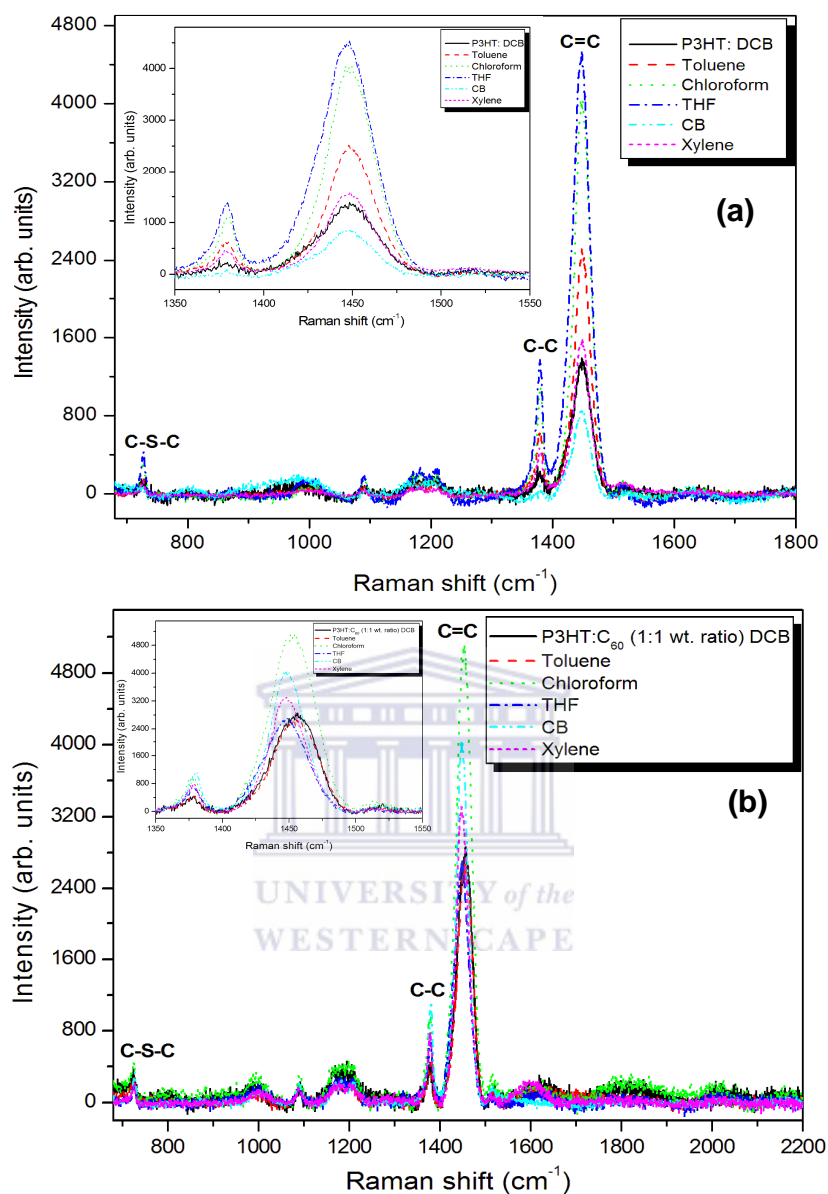


Figure 2. 3: Raman spectrum of (a) P3HT film, as well as its blend, (b) 1:1 wt. ratio, prepared from different solvents and spin-coated on Si substrate.

The peak position shifts to higher wavenumbers (cm⁻¹) and the FWHM also increased with the addition of C₆₀. A downward shift in the wavenumber generally indicates an increase in the crystallinity of P3HT polymer and the

extension of the effective conjugation length along the polymer backbone [2.43].

Similar results were also observed by Malgas *et al.* [2.44].

TABLE 2. 3: Raman measurements of the C=C stretching deformations for the P3HT film and its blend (1:1 wt. ratio) prepared from different solvents and spin-coated on Si substrates.

Solvents	<i>P3HT film</i>			<i>P3HT: C₆₀ (1:1 wt. ratio) film</i>		
	Peak position (cm ⁻¹)	FWHM (cm ⁻¹)	Intensity (a. u)	Peak position (cm ⁻¹)	FWHM (cm ⁻¹)	Intensity (a. u)
DCB	1447.7	31.0	1401.8	1454.2	46.3	3599.3
Toluene	1449.0	33.9	2878.0	1454.8	44.3	3313.0
Chloroform	1448.7	33.9	4682.2	1452.5	47.7	6579.9
THF	1447.5	38.8	5174.2	1449.4	44.3	3280.3
CB	1447.6	38.3	1005.6	1448.9	34.5	4634.2
Xylene	1448.2	32.5	1724.0	1448.8	36.2	3930.8

Fig. 2.4 presents Fourier transform infrared spectroscopy (FTIR) absorbance spectra of P3HT and blended films measured in the range of 4000–400 cm⁻¹. The absorption band at 3054 cm⁻¹ is assigned to aromatic CH stretching. This band is only observed for the P3HT films prepared from chloroform, indicating better ordering on the polymer structure. However, for the P3HT:C₆₀ (1:1 wt. ratio) film (Fig. 2.4b), this band disappears, which is probably

due to the addition of the C₆₀ fullerene. The bands around 2921, 2935 and 2854 cm⁻¹ are assigned to aliphatic CH stretching; while the bands at 1460 and 1510 cm⁻¹ are associated with symmetric and asymmetric ring stretching vibrations, respectively. The relative intensity ratio of the 1510 cm⁻¹ band to the 1460 cm⁻¹ band (I_{1508}/I_{1460}) provides information on the P3HT the conjugation length [2.45, 2.46]. In brief, conjugation length is the length of a completely undisturbed alternating single bond / double bond segment, being planar and allowing maximum overlap of π -electrons. In the present case for as-prepared P3HT prepared from different solvents, the I_{1508}/I_{1460} ratios ranges between 0.25 and 2.0.

The absorption bands at 1377, 819 and 725 cm⁻¹ corresponds to the methyl deformation, aromatic C-H out-of plane and to the methyl rocking. The band at 1045 cm⁻¹ are assigned to C=S⁺-O⁻ residues [2.47]. The films prepared from chloroform and THF as depicted in the inset (Fig. 2.4) shows enhanced intensity on the aromatic C-H out-of plane and this band can be used to study the charge-transfer effect in P3HT. However, no significant changes, such as shifting of the peaks were observed on the bands. A new band appears (inset Fig. 2.4a) at 798 cm⁻¹ and disappears for the blended films. Gustafsson *et al.* [2.48] observed two peaks (at 2480 and 774 cm⁻¹) for fully FeCl₃ doped P3HT and assigned them to the formation of bi-polarons. Therefore, we can conclude that an increase in the intensity of C=C ring stretching bands (Fig. 2.3) and the formation of absorption band at 3054 cm⁻¹ provide evidence of the better ordering of the polymer matrix

in the fast drying solvents, which is confirmed by the enhanced crystallinity observed in the corresponding XRD spectra (Fig. 2.2).

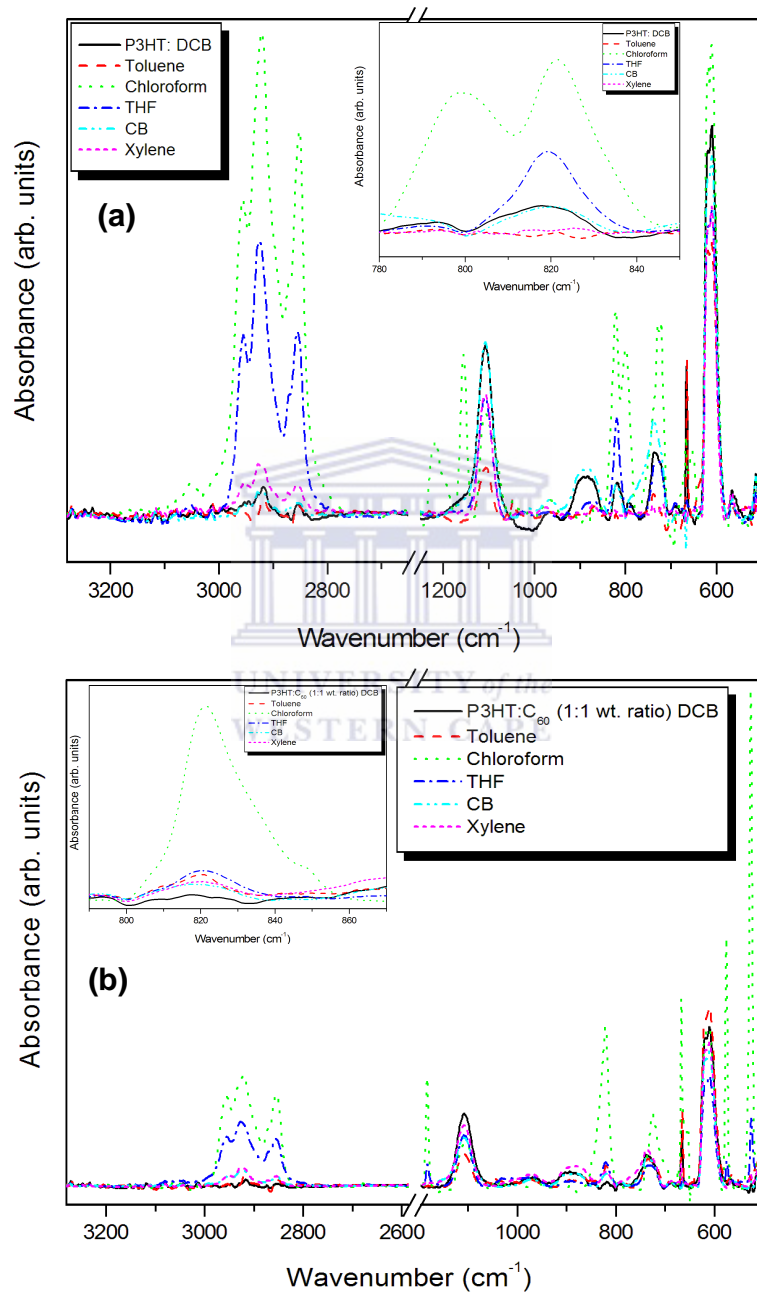


Figure 2. 4: FITR spectra of (a) P3HT film, as well as its blend, (b) 1:1 wt. ratio, prepared from different solvents and spin-coated on Si substrates.

2.3.3. Optical properties

Fig. 2.5 depicts the UV-vis absorption spectra of the rr-P3HT film and its blend of P3HT:C₆₀ (1:1 wt. ratio) prepared from different solvents. It is evident from Fig. 2.5a that the films spin-coated in non-aromatic solvents have higher absorption intensity than the aromatic solvents. This indicates that the degree of the P3HT chain ordering intra-chain interactions is higher in the case of using non-aromatic solvents [2.35, 2.49, 2.50] and is in agreement with observations made from the structural analysis. The absorption maxima are observed at the wavelengths of between 522 and 560 nm, for the film prepared from aromatic solvents. However, for non-aromatic solvents, the absorption maxima were observed around 518 and 556 nm, respectively. These bands can be ascribed to the π - π^* transition [2.23]. The development of vibronic structures (i.e. the strong shoulders peaks) is also observed around 604 nm.

When P3HT is blended with C₆₀ (1:1 wt. ratio) as shown in Fig. 2.5b, an interesting effect was observed. The reduction in maximum absorption intensity and shifting in the wavelength was observed. This reduction in intensities and the shift might originate from a tighter chain coil, produced by twisting of the polymer backbone or broken conjugation in the presence of C₆₀, resulting in segments with a shorter conjugation length and weaker interchain interaction. This result can also be explained by a change in the stacking conformation of the polymer structure from high crystallinity to lower crystallinity, and a reduction of intraplane and interplane stacking, which causes a poor π - π^* transition and lower

absorbance. This reduction in intensities was also observed in the literature [2.51, 2.52].

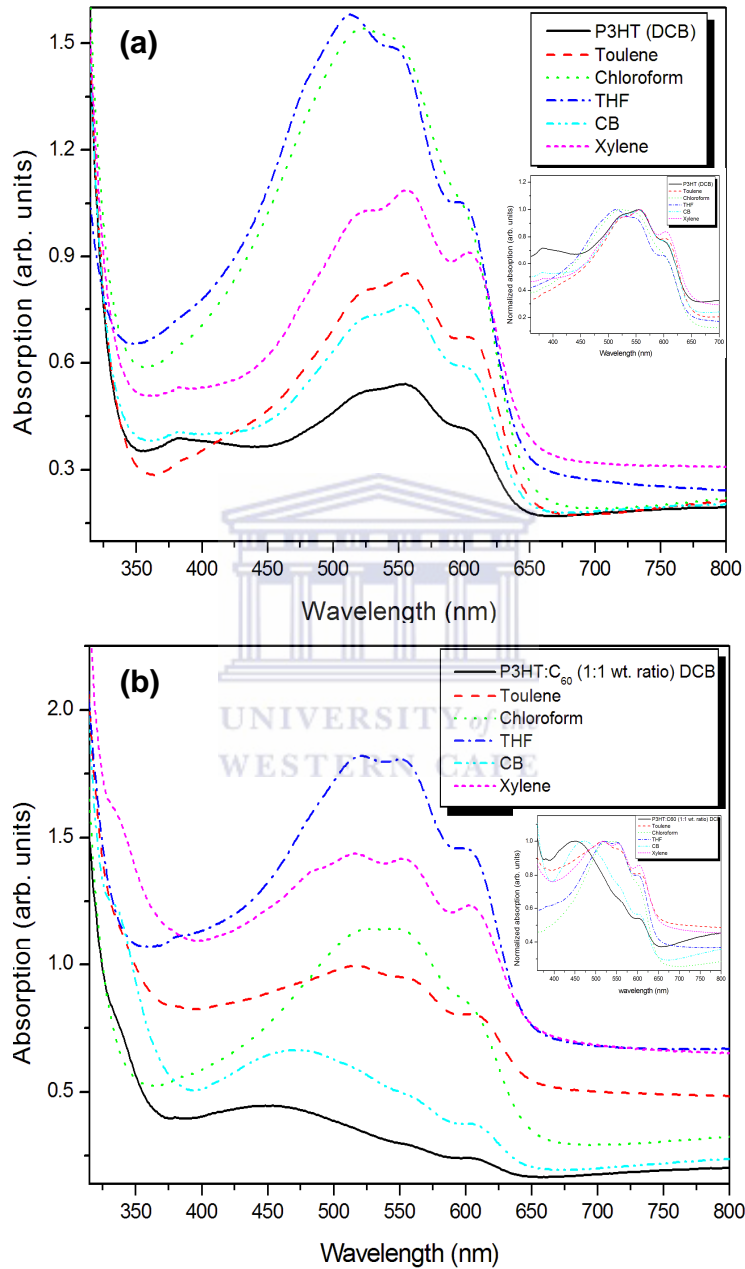


Figure 2. 5: UV-vis absorption spectra of (a) pure P3HT film, (b) P3HT:C₆₀ (1:1 wt. ratio) blend prepared from different solvents and spin-coated on ITO glass substrates.

Photoluminescence quenching in a bulk heterojunction (BHJ) is a useful indication of the degree of success of exciton dissociation. Fig. 2.6 shows the PL spectra of P3HT and P3HT:C₆₀ (1:1 wt. ratio) films spin-coated from different solvents. It is apparent in Fig. 6a that the films spin-coated from chloroform as well as in xylene solvent exhibit a reduced PL intensity. Upon introducing a C₆₀ fullerene as an acceptor material in the P3HT films (Fig. 2.6b) the PL is quenched by a factor of 3. It is also observed that the chloroform prepared film exhibits a red-shift, showing its maximum at 700 nm and a shoulder at 718 nm. The red-shift and the reduction in the PL intensity in the case of chloroform is probably due to less coarse phase separation, which promote the C₆₀ to be in close enough contact with the polymer to undergo a charge transfer.

Films spin-coated in other solvents, such as CB, xylene, DCB, and toluene solvents; reveal a higher PL intensity (incomplete quenching), showing that not all the excitons generated on one polymer within the film reached an interface with the other polymer. This is probably due to their higher solubility of the C₆₀ fullerene (Table 2.1) thereby inducing a finer phase separation and smaller grain size observed. Koeppe *et al.* [2.53] reported that, in a finer phase separation, the photogenerated charge carriers overcome much more interfaces during their travel in a fine mixture. Therefore, it can be concluded that, the formation of inter-chain exciton and its easy dissipation to a long distance overcomes over exciton dissociation [2.54], as chain planarity/crystallinity (Fig. 2.2) increases and causes a decrease in PL intensity. The PL quenching observed here is suggested to be a case of self-quenching, where plainer chains allow easy

going/dissipation for excitons to a long distance (10-20 nm). This will allow excitons to lose their energy and lessen the probability of radiative decay.

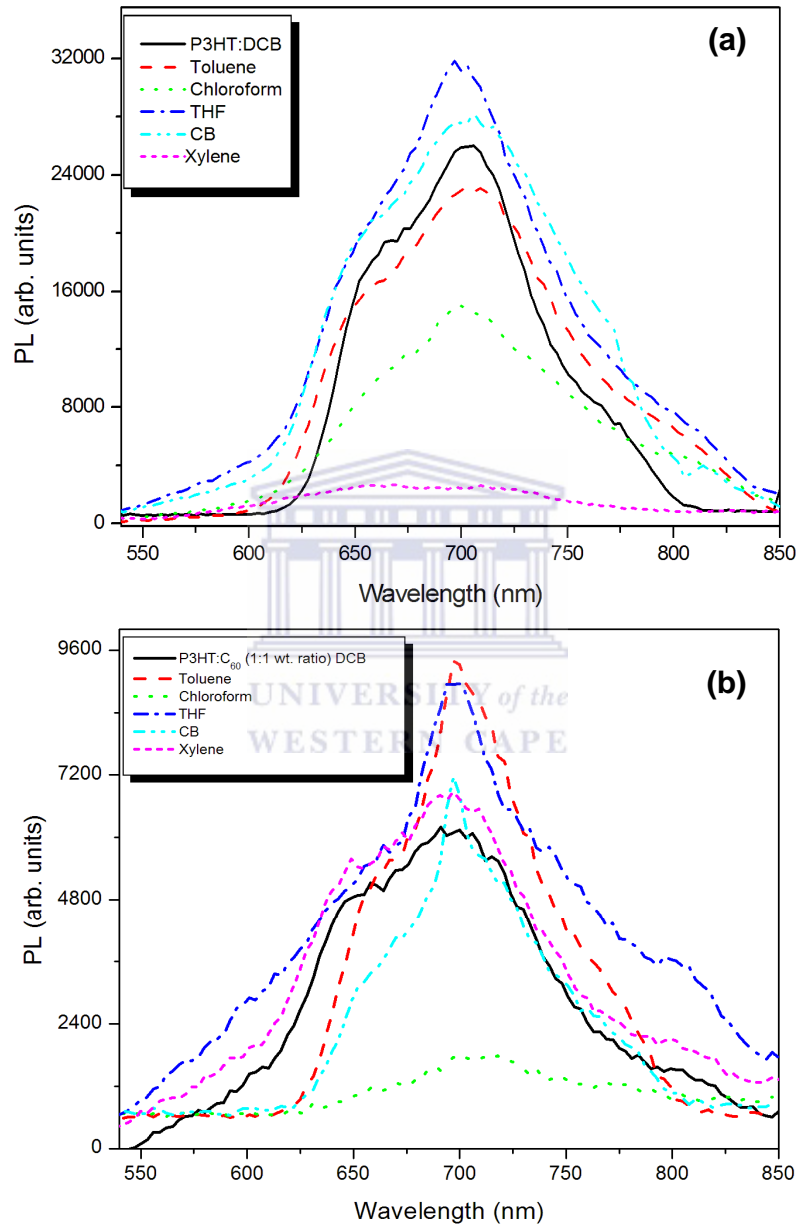


Figure 2. 6: Photoluminescence (PL) spectra of (a) P3HT film and (b) P3HT:C₆₀ blend film spin cast from different solvents on Si (100) substrates. Variation in intensity is observed for different solvents.

2.4. CONCLUSION

We have studied the effect of solvents on the crystallization and interchain interaction of P3HT and C₆₀ fullerene films using XRD, UV-vis, PL, Raman and FTIR spectroscopy. The polymer blends formed with non-aromatic solvents exhibited an improved crystallinity and polymer morphology than that formed with aromatic solvents. An improved ordering was demonstrated in the polymer films spin coated from non-aromatic solvents. This indicates that the limited solubility of rr P3HT in a marginal solvent such as non-aromatic solvents can offer a strategy to obtain highly ordered crystal structures. A red-shift and a complete quenching in the PL intensity were observed in the films spin-cast from chloroform. The PL quenched by a factor of 3 after blending the P3HT with C₆₀ in a 1:1 wt. ratio using CB, xylene, DCB, and toluene as solvents, indicating a partially charge transfer from P3HT to C₆₀.

2.5. REFERENCES

- [2.1] C. W, Tang, Appl. Phys. Lett. 48 (1986) 183.
- [2.2] S. E. Shaheen, R. Radspinner, N. Peyghambarian, G. E. Jabbour, Appl. Phys. Lett. 79 (2001) 2996.
- [2.3] F.C. Krebs, J. Alstrup, H. Spangaard, K. Larsen, E. Kold, Sol. Energ. Mater. Sol. Cells 83 (2004) 293.
- [2.4] T. Aernouts, in: 19th European Photovoltaics Conference, 7–11 June 2004, Paris, France.
- [2.5] J. Y. Seong, K. S. Chung, S. K. Kwak, Y. H. Kim, D. G. Moon, J. I. Han and W. K. Kim, J. Korean Phys. Soc. 45, (2004) 5914.
- [2.6] H. Sirringhaus, N. Tessler, R. H. Friend Science 280 (1998) 1741.
- [2.7] S. S. Pandey, W. Takashima, S. Nagamatsu, T. Endo, M. Rikukawa, K. Kaneto, Japan. J. Appl. Phys. 39 (2000) 94.
- [2.8] D. H. Kim, Y. D. Park, Y. S. Jang, H. C. Yang, Y. H. Kim, J. I. Han, D. G. Moon, S. J. Park, T. Y. Chang, C. W. Chang, M. K. Joo, C. Y. Ryu, K. W. Cho, Adv. Func. Mat. 15 (2005) 77.
- [2.9] H. Sirringhaus, P. J. Brown, R. H. Friend, M. M. Nielsen, K. Bechgaard, B. M. W. Langeveld-Voss, A. J. H. Spiering, R. A. J. Janssen, E. W. Meijer, P. Herwig and D. M. de Leeuw, Nature 401 (1999) 685.
- [2.10] X. Jiang, R. Osterbacka, O. Korovyanko, C. P. An, B. Horowitz, R. A. J. Janssen and Z. V. Vardeny, Adv. Funct. Mater. 12 (2002) 587.
- [2.11] Special Issue: Organic-Based Photovoltaics, MRS Bull. 30 (2005) issue 1.

- [2.12] G. Li, V. Shrotriya, J. Huang, Y. Yao, T. Moriarty, K. Emery, Y. Yang, Nature Mater. 4 (2005) 864.
- [2.13] W. Ma, C.Y. Yang, X. Gong, K. Lee, A.J. Heeger, Adv. Funct. Mater. 15 (2005) 1617.
- [2.14] C. J. Ko, Y. K. Lin, F. C. Chen, Adv. Mater. 19 (2007) 3520.
- [2.15] G. Li, V. Shrotriya, J. Huang, Y. Yao, T. Moriarty, K. Emery, Y. Yang, Nature Mater. 4 (2005) 864.
- [2.16] G. Yu, J. Gao, J. C. Hummelen, F. Wudl, A. J. Heeger, Science 270 (1995) 1789.
- [2.17] R. D. McCullough, Adv. Mater. 10 (1998) 93.
- [2.18] Mao-Yuan Chiu, U-Ser Jeng, Chiu-Hun Su, Keng S. Liang, and Kung Hwa Wei, Adv. Mater. 20 (2008) 2573.
- [2.19] R. S Ruoff, D. S Tse, R. Malhotra, D. C. Lorents, J. Phys. Chem. 97 (1993) 3379.
- [2.20] D. R. Lide, CRC Handbook of Chemistry and Physics, 82nd Ed., CRC Press, 06/2001.
- [2.21] M. Campoy-Quiles, T. Ferenczi, T. Agostinelli, P. G. Etchegoin, Y. Kim, T. D. Anthopoulos, P. N. Stavrinou, D. D. C. Bradley, J. Nelson, Nature Mater 7 (2008)158.
- [2.22] D. E. Motaung, G. F. Malgas, C. J. Arendse, S. E. Mavundla, C. J. Oliphant, D. Knoesen, Solar Energy Materials & Solar Cells 93 (2009) 1674.
- [2.23] T-A. Chen, X. Wu and D. Rieke J. Amer. Chem. Soc. 117 (1995) 233.

- [2.24] D. E. Motaung, G. F. Malgas, C. J. Arendse S. E. Mavundla, C. J. Oliphant, D. Knoesen, J. Mater. Sci. 44 (2009) 3192.
- [2.25] W. R. Salaneck, O. Inganas, B. Themans, J. O. Nilsson, B. Siogren, J-E. Osterholm, J-L. Bredas and S. Svensson, J. Chem. Phys. 89 (1988) 4613.
- [2.26] P. Vanlaeke, G. Vanhoyland, T. Aernouts, D. Cheyns, C. Deibel, J. Manca, P. Heremans, J. Poortmans, Thin Solid Films 511–512 (2006) 358.
- [2.27] P. Vanlaeke, A. Swinnen, I. Haeldermans, G. Vanhoyland, T. Aernouts, D. Cheyns, C. Deibel, J. D'Haen, P. Heremans, J. Poortmans, J.V. Manca, Sol. Energy Mater. Sol. Cells 90 (2006) 2150.
- [2.28] T. Erb, U. Zhokhavets, G. Gobsch, S. Raleva, B. Stühn, P. Schilinsky, C. Waldauf, C.J. Brabec, Adv. Funct. Mater. 15 (2005) 1193.
- [2.29] U. Zhokhavets, T. Erb, H. Hoppe, G. Gobsch, N.S. Sariciftci, Thin Solid Films. 496 (2006) 679.
- [2.30] International Centre for Diffraction Data (ICDD): P3HT (48-2040), C₆₀ fullerene (47-0787, 44-0558).
- [2.31] D. M. DeLongchamp, B. M. Vogel, Y. Jung, M. C. Gurau, C. A. Richter, O. A. Kirillov, J. Obrzut, D. A. Fischer, S. Sambasivan, L. J. Richter, and E. K. Lin, Chem. Mater. 17 (2005) 5610.
- [2.32] R. J. Kline, M.D. McGehee, E.N. Kadnikova, J.S. Liu, J.M.J. Fréchet, M.F. Toney, Macromolecules 38 (2005) 3312.
- [2.33] T. Erb, U. Zhokhavets, H. Hoppe, G. Gobsch, M. Al-Ibrahim, O. Ambacher, Thin Solid Films 511 (2006) 483.

- [2.34] B. E Warren, X-Ray Diffraction (New York: Dover) p. 251 (1990).
- [2.35] Y. Kim, S. Cook, S.M. Tuladhar, S.A. Choulis, J. Nelson, J.R. Durrant, D. D. C. Bradley, M. Giles, I. McCulloch, C.S. Ha, M. Ree, Nat. Mater. 5 (2006) 197.
- [2.36] T. J. Prosa, M.J. Winokur, Macromolecules 25 (1992) 4364.
- [2.37] K. E. Aasmundtveit, E.J. Samuelsen, M. Guldstein, C. Steinsland, O. Flornes, C. Fagermo, T.M. Seeberg, L.A.A. Pettersson, O. Ingana's, R. Feidenhans'l, S. Ferrer, Macromolecules 33 (2000) 3120.
- [2.38] T. Erb, S. Raleva, U. Zhokhavets, G. Gobsch, B. Stuhn, M. Spode, O. Ambacher, Thin Solid Films 450 (2004) 97.
- [2.39] A. Zen, J. Pflaum, S. Hirschmann, W. Zhuang, F. Jaiser, U. Asawapirom, J.P. Rabe, U. Scherf, D. Neher, Adv. Funct. Mater. 14 (2004) 757.
- [2.40] M Baibarac, M Lapkowski, A. Pron, S. Lefrant, I. Baltog, J. Raman Spectrosc. 29 (1998) 825.
- [2.41] P.J. Brown, D.S. Thomas, A. Köhler, J.S. Wilson, J.-S. Kim, C.M. Ramsdale, H. Sirringhaus, R.H. Friend, Phys. Rev., B 67 (2003) 064203.
- [2.42] G. Louarn, M. Trznadel, J.P. Buisson, J. Laska, A. Pron, M. Lapkowski, S.J. Lefrant, Phys. Chem. 100 (1996) 12532.
- [2.43] C. Heller, G. Leising, G. Godon, S. Lefrant, W. Fischer, F. Stelzer, Phys. Rev., B 51 (1995) 8107.
- [2.44] G. F. Malgas, C. J. Arendse, S. E. Mavundla, F. R. Cummings, J. Mater. Sci. 43 (2008) 5599.
- [2.45] Y. Furukawa, M. Akimoto, I. Harada, Synthetic Metals 18 (1987) 151.

- [2.46] S.S. Pandey, W. Takashima, S. Nagamatsu, K. Kaneto, *IEICE Trans. Electron.*, E83-C (2000) 1088.
- [2.47] M. S.A. Abdou, S. Holdcroft, *Can. J. Chem.* 73 (1995) 1893.
- [2.48] G. Gustafsson, O. Inganäs, J.O. Nilsson, B. Lieberg, *Synth. Met.* 26 (1988) 297.
- [2.49] X. Jiang, R. Osterbacka, O. Korovyanko, C. P. An, B. Horowitz, R. A. J. Janssen and Z. V. Vardeny, *Adv. Funct. Mater.* 12 (2002) 587.
- [2.50] P.J. Brown, D.S. Thomas, A. Köhler, J.S. Wilson, J.S. Kim, C.M. Ramsdale, H. Sirringhaus, R.H. Friend, *Phys. Rev. B* 67 (2003) 064203.
- [2.51] V. Shrotriya, J. Ouyang, R. J. Tseng, G. Li, Y. Yang, *Chemical Physics Letters* 411 (2005) 138.
- [2.52] D. Valentin, Mihailetchi, Hangxing Xie, Bert de Boer, L. Jan Anton Koster, and P. W. M. Blom, *Adv. Funct. Mater.* 16 (2006) 699.
- [2.53] R. Koeppe and N. S. Sariciftci, *Photochem. Photobiol. Sci.* 5 (2006) 1122.
- [2.54] M. P. Jeffrey, D. S. Richard, W. Donald. *J Am Chem Soc* 126(38) (2004) 11752.

CHAPTER THREE

STRUCTURAL AND PHOTO-PHYSICAL PROPERTIES OF SPIN-COATED POLY(3-HEXYLTHIOPHENE) THIN FILMS

ABSTRACT

Regioregular poly(3-hexylthiophenes) (P3HTs) and its blends were studied regarding their structural and photo-physical properties using fullerene as an electron acceptor material. Photo-physical and structural characteristics of the polymer blends were studied using UV-vis spectroscopy, photoluminescence (PL), Fourier transform infrared absorption (FTIR) spectroscopy and Raman spectroscopy analysis. Films based on the polymer blends with C₆₀ showed photo-induced absorption characteristic for charged excitations. The absorption spectra of the rr-P3HT exhibit a shift to higher energies (blue shift) of the π - π^* interband transition upon mixing with C₆₀. A distinctive photoluminescence quenching effect is observed indicating photo-induced electron transfer. The complete reduction of PL of P3HT after mixing with C₆₀ in a 1:1 weight ratio indicates an effective charge transfer from P3HT to C₆₀.

The content of this chapter was published in: Materials Chemistry and Physics 116 (2009)

279–283

3.1. INTRODUCTION

The use of polymeric materials in the fabrication of low cost photovoltaic devices or plastic electronics has been extensively studied due to its low-cost synthesis and easy manufacture of thin film devices by vacuum evaporation/sublimation or solution cast or printing technologies. Organic semiconductor thin films also show high absorption coefficients **[.31]** exceeding 10^5 cm^{-1} , which makes them good chromophores for optoelectronic applications. It has been shown by Roncali **[3.2]** that the electronic band gap of organic semiconductors can be engineered by chemical synthesis for simple colour changing of light emitting diodes (LEDs). Despite the good properties mentioned above great progress in both power conversion efficiency and stability is needed for practical device applications.

In order for a major breakthrough to take place, a significant improvement in the device efficiency-to-cost ratio is essential. There are several factors that influence the efficiency of OPVs, e.g. the structure of the polymer, the morphology of the film, the interfaces **[3.3]** between the layers (organic/metal, organic/organic) and the choice of electron acceptor and the ratio between this and the polymer **[3.4]**. Intensive research in organic photovoltaics has led to a wide variety of different structure designs and different types of hole and electron acceptor materials **[3.5 –3.7]**. With regard to improving the efficiency, low band gap polymers which harvest the red part of the solar spectrum are being examined **[3.8]**. Studies on the stability of organic photovoltaic cells have typically focussed on optimisation of the stability of encapsulated devices under

continuous light illumination [3.8-3.11]. Lifetimes of up to 2000 h continuous operation have been reported for devices protected from oxygen and water ingress [3.11]. In this work, we report on the structural and photophysical properties of P3HT thin films using spectroscopy investigations to study the photoinduced charge generation in photoexcited P3HT films and its blends with fullerene as an electron acceptor material.

3.2. EXPERIMENTAL DETAILS

The bilayer or blended structures were prepared according to the following procedure. Regioregular poly(3-Hexylthiophene) (P3HT), $M_n \sim 64000$ g/mol, and fullerene (C_{60}) were purchased from Sigma Aldrich and were used as received without further purification. The regioregularity of the regioregular material was specified as $> 98\%$. The ratio of the number-average molecular weight M_n of the polymer and the molecular weight of the monomer is known as the degree of polymerization (DP). Since the molecular weight of a hexylthiophene unit is 170 g/mol and the molecular weight of the rr-P3HT is about 64000 g/mol the degree of polymerization can be calculated as about 376.47. The chemical structures of rr-P3HT and C_{60} are shown in Fig. 3.1.

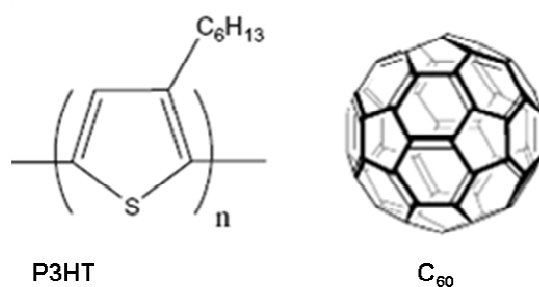


Figure 3. 1: Chemical structures of P3HT and C_{60} .

The ITO coated on 1 mm glass substrates, with a resistance $\leq 20 \Omega/\text{square}$, was first cleaned thoroughly with solvents and dried in dry nitrogen. A thin layer of poly(3,4-ethylenedioxythiophene):poly (styrenesulfonate) (PEDOT:PSS) solution was spin coated onto the ITO structure. The spinning rate and time of spin-coating were between 2000 and 3000 rpm and 30 s, respectively. The PEDOT layer was subsequently annealed in ambient at 100 °C for 15 min on a hotplate. The active layer containing regioregular poly(3-hexylthiophene) (rr-3HT) was dissolved in 1 ml of chloroform solution and spin coated on top of the PEDOT:PSS layer. For the blended samples; rrP3HT (~ 5 mg or a weight percentage of 50 %) and C₆₀ with different concentrations (~5 mg and 20 mg) was dissolved in 1 ml of chloroform solution to obtain ratios of 1:1 and 1:4. This corresponds to a C₆₀ weight percentage of 50 % and 80 %, respectively. The solution was stirred overnight on a hotplate at 50 °C. The precursor solution prepared for this study had a molar concentration of 0.15 M. The solution were spin coated on top of the PEDOT:PSS layer. The spinning rate and time of spin-coating were 2500 rpm and 30 s.

UV-vis spectra were recorded by a Perkin Elmer λ 20 spectrometer from 900 to 300 nm. The photoluminescence (PL) spectra were measured by exciting the samples with 350 nm line of deuterium lamp. It should be noted that for some photoluminescence measurements, the PEDOT:PSS layer was omitted in order to avoid masking of P3HT features which overlap with those of PEDOT. The emission was detected by a Jobin Yvon PMT detector. The structure of pure P3HT with different concentrations of C₆₀ was characterized by Fourier transform

infrared spectroscopy (FTIR) using a Perkin Elmer FT-IR spectrometer and Raman spectroscopy using a Horiba Jobin Yvon HR800 micro-Raman spectrometer. The Raman spectroscopy measurements were conducted at room temperature using a 514 nm excitation laser with a spectral resolution of 0.4 cm^{-1} . It should also be noted that for some FTIR and Raman spectroscopy measurements that the blends were spin-coated on a Si (100) substrate.

3.3. RESULTS AND DISCUSSION

The PL technique has been widely used to investigate the energy level of materials and to provide fundamental information on the properties of the energy levels lying within the band gap. The PL of P3HT and its blend with fullerene (C_{60}) was measured to check if there is interaction of the two components in the excited state. Saricifti *et al.* [3.12] reported that the PL quenching of an appropriate donor polymer by a suitable acceptor gives an indication of an effective donor–acceptor charge transfer for composites of p-conducting polymers and fullerene derivatives. Fig. 3.2 compares the PL spectra of P3HT film with that of blends of P3HT with different fullerene ratios. The PL spectra of P3HT and its blends were obtained by using an excitation wavelength of 350 nm in the range from 400 to 900 nm. An incomplete quenching is observed for the PL spectra of P3HT and the blend of P3HT: C_{60} with a weight ratio of 1:4. The PL spectra of the blend of P3HT: C_{60} with a 1:4 wt. ratio also shows a blue shift (shift to higher energies or lower wavelengths) compared to the spectra of a P3HT film, suggesting that the polymer chains are twisted and not π -stacked on each other.

At this point, it is unclear whether the incomplete quenching resulted from the reduced exciton mobility on the polymer chains or from the pore size (not measured) simply being too large given the small exciton diffusion length that has been observed in thiophene-based polymers [3.13]. The larger intensity of PL emission from the P3HT film can also be attributed to the surface oxidation defects of the exposed film. The degree of PL quenching is also related to oxygen adsorbed on surface-active sites or possible structural order of the polymer film on the silicon substrate [3.14]. Al-Ibrahim *et al.* [3.15] reported that materials with high absorption coefficient are necessary for application in polymer solar cells, because the film thickness of the photoactive layer should not be normally over some hundreds of nanometers (typical are 100–300 nm).

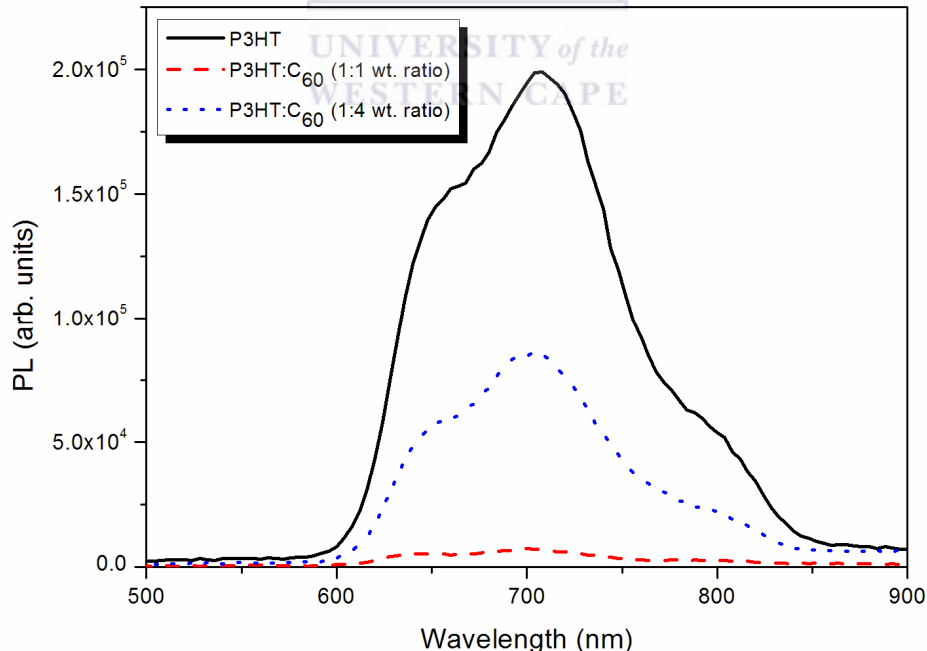


Figure 3. 2: Photoluminescence spectra of films of P3HT, P3HT:C₆₀ (1:1 wt. ratio) and P3HT:C₆₀ (1:4 wt. ratio) dissolved in chloroform

This limitation is predicted by the much lower charge mobility compared with inorganic semiconductors. The P3HT shows PL, which is completely quenched when it is mixed with a 1:1 wt. ratio of C₆₀. Therefore, the excitons created during the PL have a finite lifetime and during the diffusion process (charge transfer process) they decay or dissociate through several mechanism. In order to achieve efficient photovoltaic conversion, the excitons have to dissociate into free electrons and holes, before they decay radiatively, thermally or vibronically. The most common way to achieve exciton dissociation into free electrons and holes is through a photo-induced charge transfer process.

We conclude that the change of the photoluminescence intensity originates from a phase separation and thus changes in the morphology of the active layer. The fullerene surplus at higher concentrations (P3HT:C₆₀ film with a 1:4 wt. ratio) is not homogeneously dispersed within the polymer matrix, but diffuses away and creates phase separated clusters, agglomerates or C₆₀ islands. The complete quenching of the P3HT:C₆₀ film with a 1:1 wt. ratio indicates that due to the finer phase separation in the chloroform blend, all of the C₆₀ is in close enough contact with the polymer to undergo a charge transfer. In solar cells a significant amount of light absorption is in the C₆₀ phase, the amount of generated charge carriers and therefore the photocurrent is reduced in the coarsely phase separated blend (1:4 wt. ratio). Charges become trapped on C₆₀ islands and act as recombination sites for any opposite charge that then approaches. However, a finer phase separation and smaller grain size does not warrant increased photocurrent either,

since the photo-generated charge carriers will have to overcome much more interfaces during their travel in a fine mixture. Chrivase *et al.* [3.16] reported that atomic force microscopy measurements on a P3HT:PCBM composite disclose some variation in morphology due to the crystallization of PCBM. The concentration of the PCBM clusters and their size (up to 500 nm) were found to be correlated with the amount of PCBM in the blend. They also showed that PCBM concentrations above 50 %, leads to a partial damage of the absorber-metal interface due to the formation of voluminous PCBM clusters.

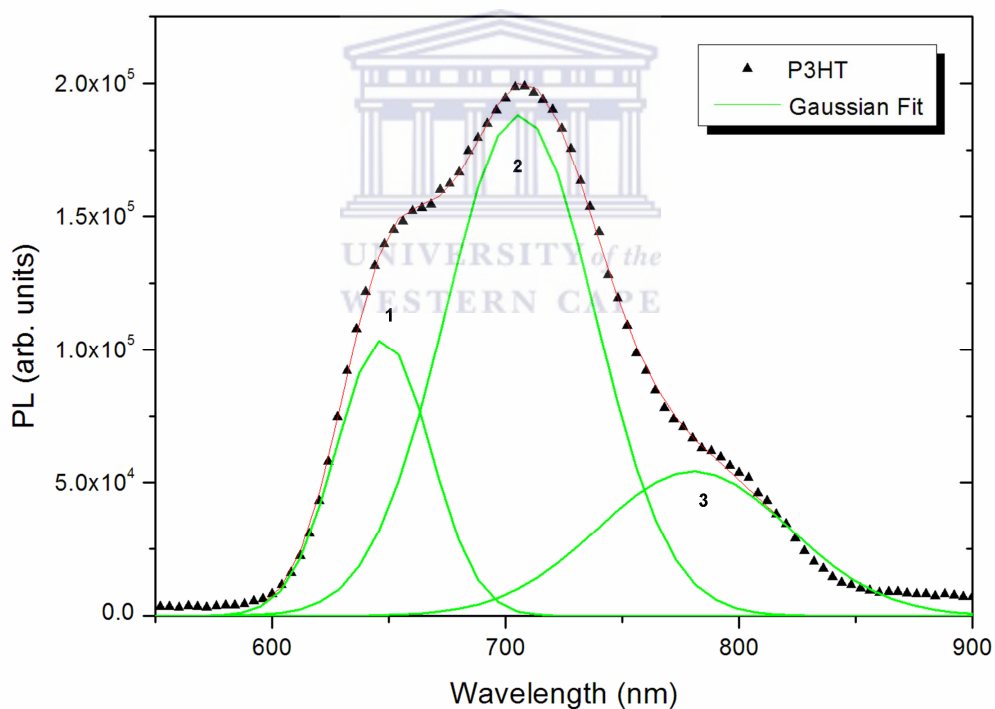


Figure 3. 3: PL spectra of a film of P3HT deposited on a Si substrate and their Gaussian band fits.

To obtain the electronic states in photo-excited P3HT, the PL curve of P3HT and the three PL emission peaks by Gaussian fitting are illustrated in Fig.3.3.

The PL spectra of P3HT (Fig. 3.2 and 3.3) show resolved vibronic structures at 645 nm, 700 nm, and 780 nm. It can be found that the Gaussian curves: 1, 2 and 3 fitted the PL curve perfectly. The data of the Gaussian fitting multi-peaks are shown in Table 3.1, in which calculated energies are indicated as well. The PL emission peaks located at around 645 nm (1.92 eV) was assigned to the pure electronic transition and the peak at around 700 nm (1.76) to the first vibronic band [3.17]. The PL emission in the higher wavelength region indicates ordering in the P3HT lamella structure within the spherulites [3.18, 3.19]. However, more precise work is necessary to confirm this.

TABLE 3. 1: PL bands, wavelength and calculated energies (eV) for P3HT

<i>Peak</i>	<i>Wavelength (nm)</i>	<i>Experimental (eV)</i>	<i>Width (nm)</i>	<i>Area (a.u)</i>
1	647.50	1.92	40.223	5.2239E6
2	706.05	1.76	63.927	1.5086E7
3	780.44	1.59	82.021	5.5765E6

The UV-Vis absorption spectra of fullerene, the P3HT film as well as different blends of P3HT:C₆₀ spin coated on an ITO coated glass substrate are presented in Fig. 3.4. In the spectra, absorption caused by P3HT is visible between 450 and 700 nm. For the P3HT film the solid-state absorption spectra showed two peaks at 507 nm and 538 nm and one shoulder at 586 nm. These first two bands can be attributed to the $\pi-\pi^*$ transition, whereas the shoulder

around 586 nm is due to the inter-chain interactions. Similar results and absorption values were obtained by Chen *et al.* [3.20] for regioregular P3HT.

The maximum absorption wavelength for the film with P3HT:C₆₀ (1:1 wt. ratio) was detected at ~ 501 nm showing a blue-shift. The peak absorption wavelength changed significantly for film with P3HT:C₆₀ using a 1:4 wt. ratio. The characteristic peak absorption wavelength (λ_{max}) for film with P3HT:C₆₀ (1:4 wt. %) are broad at a wavelength of ~ 501 nm. Since the concentration of P3HT was always kept the same in the solutions used for spin-coating, that is, the total amount of P3HT may be the same for all films, the quenching of the absorption for the film with the presence of C₆₀ can be attributed to the interaction between the polymer and C₆₀. One possible effect of the presence of C₆₀ molecules is the lowering of the interaction among the P3HT chains. However, the longer-wave absorption bands of P3HT and its blends at ~ 538 and ~586 nm remain nearly uninfluenced. This is an indication that these changes are not generated by ground state doping of the polythiophenes by C₆₀.

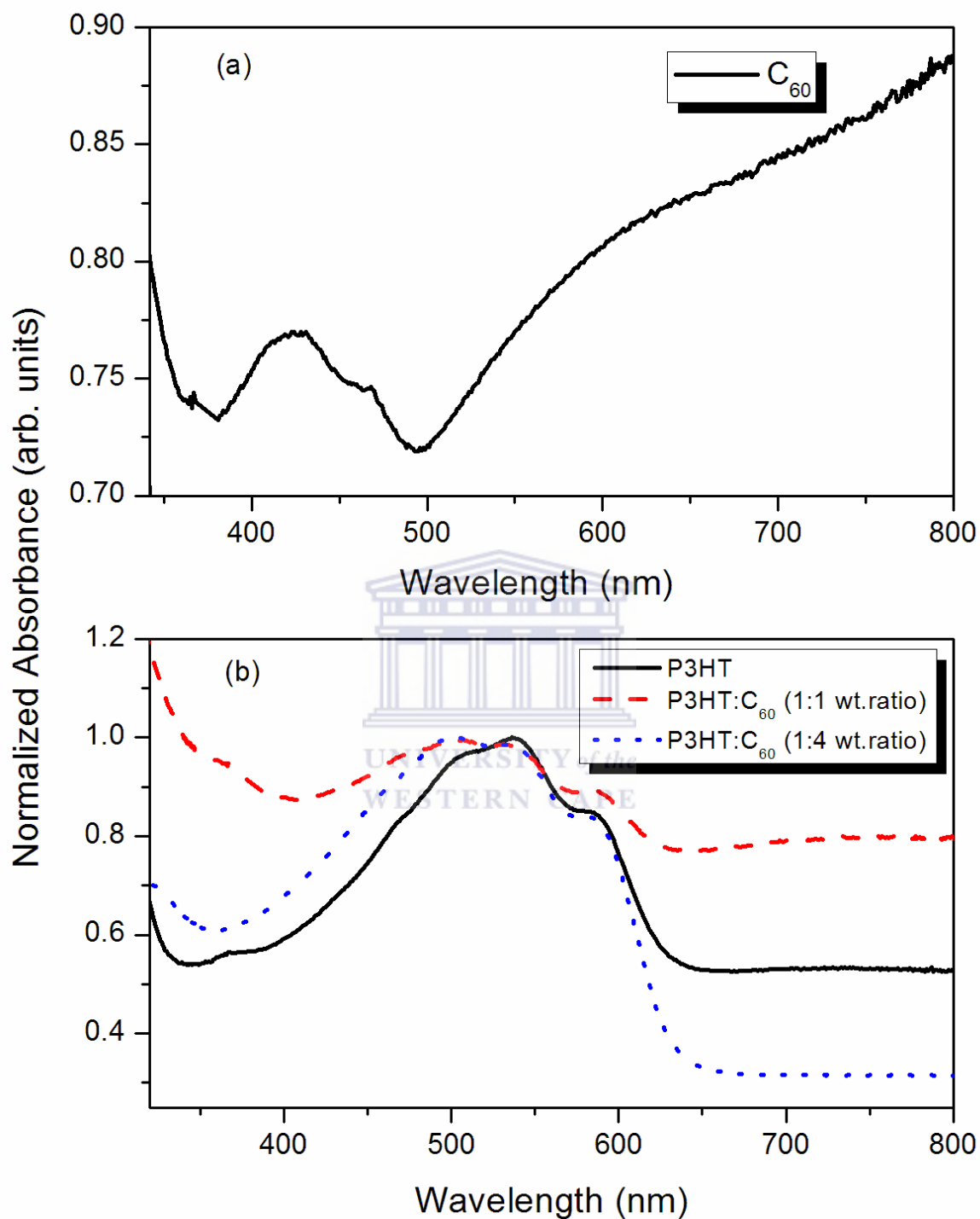


Figure 3. 4: UV-Vis absorption spectra for (a) fullerene (C_{60}) and (b) P3HT films compared with different blends of C_{60} .

The structure and charge transfer between P3HT and C₆₀ was further studied by FTIR spectroscopy as shown in Fig. 3.5. The FTIR absorption bands for rr-P3HT are given in Table 3.2. The peaks at 2852, 2923 and 2950 cm⁻¹ were assigned to CH₂ out of phase mode, CH₂ in phase mode and CH₃ asymmetry stretching mode, respectively. The peak at 1457 cm⁻¹ represents the symmetric ring stretching mode. The ratio between the intensity of the antisymmetric C=C stretching peak (mode at 1509 cm⁻¹) and the intensity of the symmetric stretching peak (mode at 1456 cm⁻¹) can be used to probe the average conjugation length (i.e., the length over which backbone planarity is maintained without interruption and which defines the chromophore) of P3HT [3.21, 3.22].

Therefore using this relation (I_{1510}/I_{1456}) we observed that the conjugation length of P3HT chains actually shows a decrease from 0.50 for P3HT to 0.45 over the range of the different blends studied, showing a decrease in the ordering of the films. Furukawa *et al.* [3.21] reported that the average conjugation length will increase if the relative intensity of the FTIR peak at 1510 cm⁻¹ (asymmetric C=C stretching) increases. The vibrations of some compounds are sensitive to the charge on the compounds. It has been shown by Ouyang *et al.* [3.23, 3.24] that both the C=C and C-S stretching vibrations may shift when the amount of charge present on the compound changes. The C=C stretching vibrations are really complicated since both P3HT and C₆₀ have C=C stretching vibrations, and therefore, it is difficult to explain the charge-transfer effect by analyzing the C=C vibrations. Also it is not easy to find C-S peak in the IR spectra of P3HT [3.23].

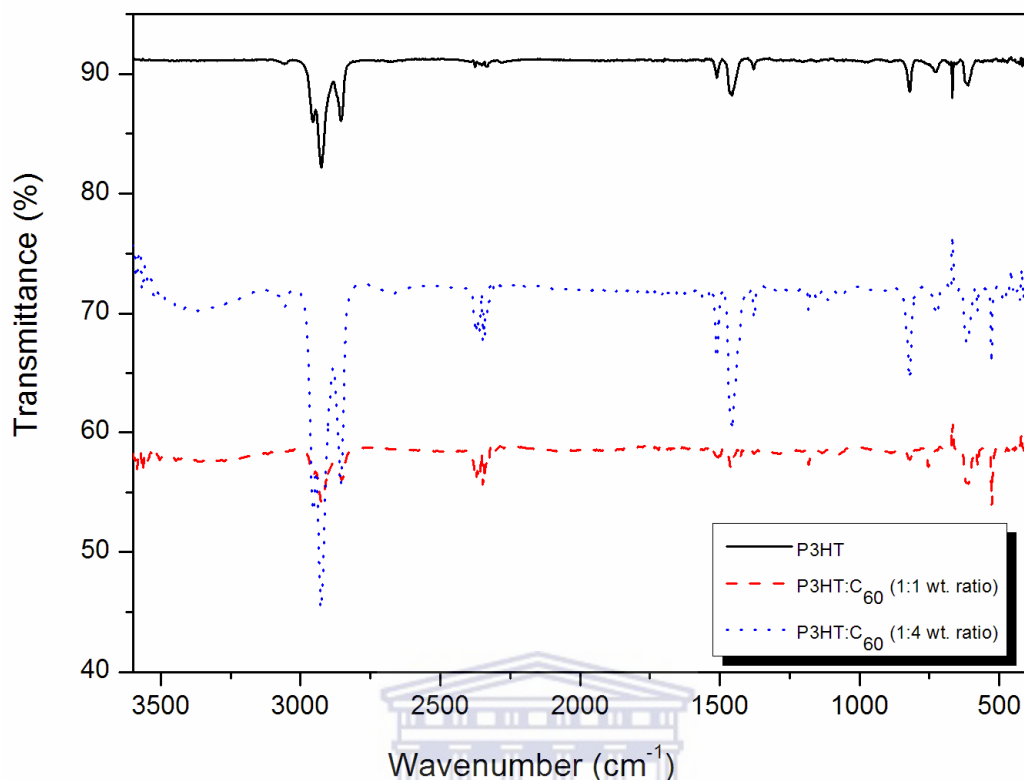


Figure 3. 5: FTIR spectra for thin films of P3HT and P3HT: C₆₀ in 1:1 and 1:4 wt. ratios.

However, the thiophene ring associated with P3HT shows an out of plane deformation of C-H, and the band at 819 cm⁻¹ is assigned to this C-H deformation vibration of P3HT. This change in the vibration energy can be used to study the charge-transfer effect in P3HT [3.25]. However, no changes are observed for the C-H band at 819 cm⁻¹ for the different P3HT:C₆₀ ratios. A new band appears at around 1182 cm⁻¹ and 2360 cm⁻¹ as for the 1:1 P3HT: C₆₀ film. These bands become intense with the increase of the amount of C₆₀. These bands at 1182 cm⁻¹ and 2360 cm⁻¹ are not from C₆₀. Hence, this change in vibration energy might be due to the charge transfer that occurs between sulphur atom in P3HT

molecule and C₆₀. Some charge is transferred from the sulphur atoms, to the conjugated chains of the C₆₀ molecules, and this result in a slight positive charge being present on the sulphur atoms.

TABLE 3. 2: FTIR band positions (cm⁻¹) and their assignments of P3HT films

<i>rr-P3HT</i> wavenumber (cm ⁻¹)	<i>Assignments</i>
721	Methyl rock
819	C-H out of plane mode
1182	-
1377	Methyl deformation
1507	Anti symmetric C=C stretching mode
1457	Symmetric C-C stretching mode
2360	-
2856, 2925, 2955	Aliphatic C-H stretching mode

Fig. 3.6 shows the Raman spectroscopy of the P3HT films as well as different blends of P3HT:C₆₀ films deposited on a Si substrate. The spectrum of the poly(3-hexylthiophene) film deposited on Si features all the vibrational frequencies expected for the conjugated polymer [3.26]. The data were stacked to avoid overlaying of the different peaks. The Raman peaks at 715 cm⁻¹, 1380

cm^{-1} and 1450 cm^{-1} are assigned to the P3HT C-S-C ring deformation, C-C skeletal stretching deformation and C=C ring stretching deformation, respectively [3.27–3.29]. It is observed that the peak position corresponding to the symmetric C=C stretching deformation, is shift to a higher wavenumber (cm^{-1}), if the polymer is blended with C_{60} . A downward shift in the wavenumber generally indicates an increase in the crystallinity of P3HT polymer and the extension of the effective conjugation length along the polymer backbone [3.30]. The intensity and the full-width at half maximum (FWHM) of P3HT and its blends of the C=C stretching deformation are often used as an indication of the ordering in the material. The high intensity in the pure P3HT/Si film indicates a highly order/crystalline material. When the P3HT is blended with C_{60} , a decrease in the intensity of the C=C stretching deformation are observed.

This might be due to a strong disordering of P3HT chains caused by an addition of C_{60} fullerene. This causes the C_{60} molecules to diffuse or migrate forming larger clusters which lead to a phase separation of P3HT and C_{60} . As a result, the polymer film prepared with a C_{60} -fullerene has the favourable molecular morphologies for the transport of charge carriers and is also responsible in the improvement of cell efficiencies. No Raman features attributable to C_{60} , such as the A_{1g} 1469 cm^{-1} mode of fullerenes could be resolved. Klimov *et al.* [3.31] showed that the Raman modes of P3HT in the blends are not influenced by the contributions of the C_{60} fluorescence.

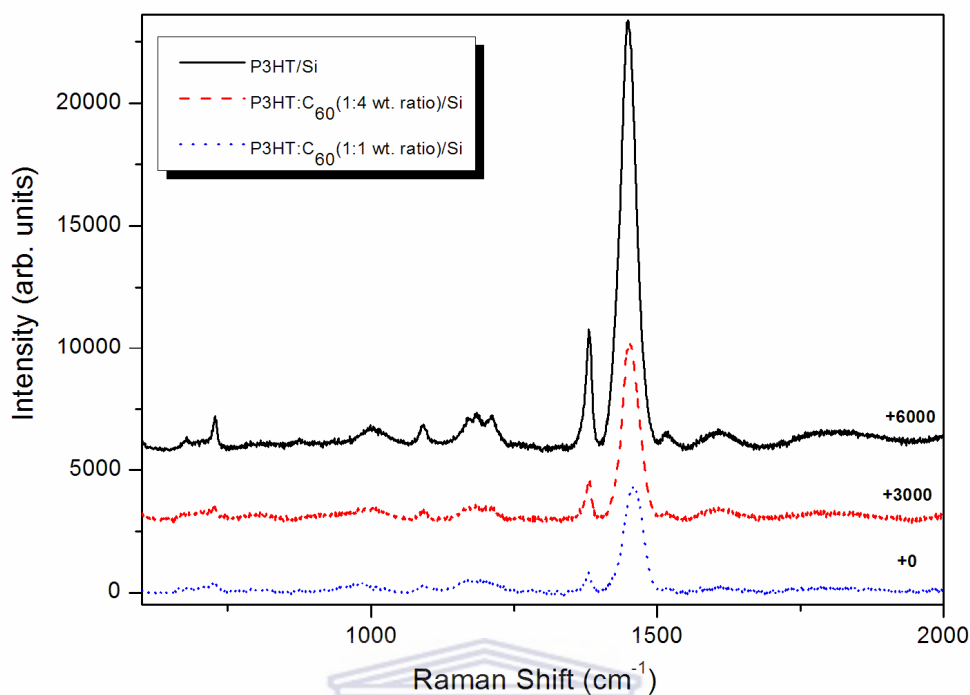


Figure 3. 6: Raman spectra of (a) P3HT, (b) P3HT:C₆₀ (1:1 wt. ratio) and (c) P3HT: C₆₀ (1:4 wt. ratio) films spun on a Si substrate.

UNIVERSITY of the
WESTERN CAPE

3.4. CONCLUSION

The interaction between P3HT and C₆₀ in solid-state thin films was studied by UV–Vis absorption, photoluminescence, FTIR and Raman spectroscopy analysis. In this study the spectroscopic investigations show that the films of P3HT and blends with different ratios of P3HT:C₆₀ exhibit an efficient photo-induced charge transfer. The blended P3HT:C₆₀ film with a 1:4 wt. ratio was found to be incompletely quenched whereas the blended P3HT:C₆₀ film with a 1:1 wt. ratio was completely quenched. The complete reduction of PL of P3HT after mixing with C₆₀ in a 1:1 wt. ratio indicates an effective charge transfer from

P3HT to C₆₀. The absorption spectra of regioregular P3HT show distinctive changes upon blending the polymers with C₆₀. The peak wave length of the $\pi-\pi^*$ inter-band transition of the P3HT blended with different fullerene ratios is shifted towards shorter wavelength. The detected shift to lower wavelength for blends may be due to differences in the molecular weights of the three polythiophenes or is a special feature of the applied solvent inducing unfavourable chain conformations and/or a disadvantageous interchain packaging. The FTIR spectroscopy showed no changes in peak assigned to C-H deformation vibration associated with the thiophene ring. The peaks at around 1180 cm⁻¹ and 2360 cm⁻¹ proved the occurrence of a charge-transfer process.

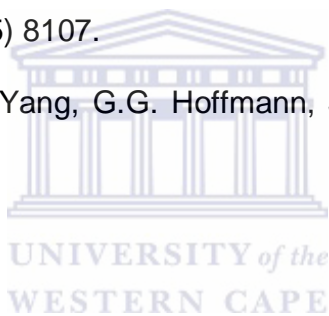


3.5. REFERENCES

- [3.1] H. Hoppe, N.S. Sariciftci, D. Meissner, *Mol. Cryst. Liq. Cryst.* 385 (2002) 113.
- [3.2] J. Roncali, *Chem. ReV.* 97 (1997) 173.
- [3.3] H. Ishii, K. Sugiyama, E. Ito, K. Seki, *Adv. Mat.* 11 (1999) 605.
- [3.4] H. Hoppe, N.S. Sariciftci, *J. Mater. Chem.* 16 (2006) 45.
- [3.5] C. W. Tang, *Appl. Phys. Lett.* 48 (1986) 183.
- [3.6] G. Yu, J. Gao, J. Hummelen, F. Wudl, A. J. Heeger, *Science* 270 (1995) 1789.
- [3.7] S. E. Shaheen, C. J. Brabec, F. Padinger, T. Fromherz, J. C. Hummelen, N. S. Sariciftci, *Appl. Phys. Lett.* 78 (2001) 841.
- [3.8] C. J. Brabec, C. Winder, N. S. Sariciftci, J. C. Hummelen, A. Dhanabalan, P. A. van Hal, R. A. J. Janssen, *Adv.Funct. Mater.* 12 (2002) 709.
- [3.9] H. Neugebauer, C. J. Brabec, J. C. Hummelen, N. S. Sariciftci, *Sol. Energy Mater. Sol. Cells* 61 (2000) 35.
- [3.10] F. Padinger, T. Fromherz, P. Denk, C. J. Brabec, J. Zettner, T. Hierl, N. S. Sariciftci, *Synth. Met.* 121 (2001) 1605.
- [3.11] C. J. Brabec, J.A. Hauch, P. Schilinsky, C. Waldauf, *MRS Bull.* 30 (2005) 50.
- [3.12] N. S. Sariciftci, L. Smilowitz, A.J. Heeger, F. Wudl, *Science* 258 (1992) 1474.
- [3.13] M. Theander, A. Yartsev, D. Zigmantas, V. Sundstrom, W. Mammo, M. R. Anderson, O. Inganasm, *Phys Rev B* 61 (2000) 12957.

- [3.14] K. Y. Jung, S. B. Park, M. Anpo, J. Photochem. Photobiol. A Chem. 170 (2005) 247.
- [3.15] M. Al-Ibrahim, H. Roth, U. Zhokhavets, G. Gobsch, S. Sensfuss, Solar Energy Mater. Solar Cell 85 (2005) 13.
- [3.16] D. Chirvase, J. Parisi, J. C. Hummelen and V. Dyakonov, Nanotechnology 15 (2004) 1317.
- [3.17] M. Sharma, D. Kaushik, R. R. Singh, and R. K. Pandey, J. Mater. Sci.: Mater. Electron. 17, (2006) 537.
- [3.18] L. Li, C.-M. Chan, K. L. Yeung, J.-X. Li, K.-M. Ng, and Y. Lei, Macromolecules 34, (2001) 316.
- [3.19] H. Yang T. Shin, J. L. Yang, K. Cho, C. Y. Ryu, and Z. Bao, Adv. Funct. Mater. 15, (2005) 671.
- [3.20] T.-A. Chen, X. Wu, R.B. Rieke, J. Am. Chem. Soc. 117 (1995) 233.
- [3.21] Y. Furukawa, M. Akimoto, I. Harada, Synthetic Metals 18 (1987) 151.
- [3.22] M. Trznadel, A. Pron, M. Zagorska, R. Chrzaszcz, J. Pielichowski, Macromolecules 31 (1998) 5051.
- [3.23] J. Ouyang, K. Yakushi, T. Kinoshita, N. Nanbu, M. Aoyagi, Y. Misaki, K. Tanaka, Spectrochim. Acta, Part A 58 (2002) 1643.
- [3.24] J. Ouyang, K. Yakushi, Y. Misaki, K. Tanaka, Phys. Rev. B 63 (2001) 054301.
- [3.25] V. Shrotriya, J. Ouyang, R. J. Tseng, G. Li, Y. Yang, Chemical Physics Letters, 411 (2005) 138.

- [3.26] R. Osterbacka, C.P. An, X.M. Jiang, Z.V. Vardeny, *Synthetic Metals* 116 (2001) 317.
- [3.27] M. Baibirac, M. Lapkowski, A. Pron, S. Lefrant, I. Baltog, *J. Raman Spectrosc.* 29 (1998) 825.
- [3.28] P. J. Brown, D. S. Thomas, A. Köhler, J. S. Wilson, J. S. Kim, C.M. Ramsdale, H. Sirringhaus, R. H. Friend *Phys. Rev. B* 67 (2003) 064203.
- [3.29] G. Louarn, M. Trznadel, J.P. Buisson, J. Laska, A. Pron, M. Lapkowski, S.J. Lefrant, *Phys. Chem.* 100 (1996) 12532.
- [3.30] C. Heller, G. Leising, G. Godon, S. Lefrant, W. Fischer, F. Stelzer, *Phys.Rev. B* 51 (1995) 8107.
- [3.31] E. Klimov, W. Li, X. Yang, G.G. Hoffmann, J. Loos, *Macromolecules* 39 (2006) 4493.



CHAPTER FOUR

CORRELATION BETWEEN THE MORPHOLOGY AND PHOTO-PHYSICAL PROPERTIES OF P3HT: FULLERENE BLENDS

ABSTRACT

The photo induced charge transfer and optoelectronic efficiency of the solar cells correlated to the morphology and the structure of P3HT:C₆₀ blend was studied by means of photoluminescence and electron spin resonance (ESR). The occurrence of photoinduced charge transfer, well-known for blends of P3HT with fullerenes, was evidenced in blends of P3HT:C₆₀ (1:1 wt. ratio) by the strong partially quenching of the P3HT luminescence. The ESR measurements allowed one to quantify the charge transfer between P3HT and C₆₀, which resulted in positive P3HT polarons. Wide angle x-ray scattering (WAXS) and UV-vis spectroscopy showed that an inclusion of a C₆₀ fullerene in the P3HT matrix lead to lower peak intensities and dark Debye rings and a blue shift on the $\pi-\pi^*$ interband transition of the P3HT as well as a reduction in the absorption coefficients. The SAED patterns of a well-ordered sample of P3HT exhibit distinct diffraction rings indicating that the P3HT forms polycrystalline film. The large-scale phase separation of P3HT and C₆₀ resulted from large C₆₀

agglomerations distributed uniformly across the film during spin coating was observed. A low power conversion efficiency of about $0.2 \times 10^{-4} \%$ was achieved.



The content of this chapter was published in: Journal of Material Science 45 (2010) 3276–

3283

4.1. INTRODUCTION

Since the discovery of charge separation in polymer/fullerene systems by Sariciftci *et al.* [4.1], organic photovoltaics (OPVs) became one of the most promising alternative concepts to the solar cells-based crystalline silicon technology. This is due to their low cost, low temperature processing, flexibility and a very high speed of processing [4.2]. The technology of polymer photovoltaics has seen some drastic improvements in their power conversion efficiency with the introduction of the bulk heterojunction consisting of an interpenetrating network of electron donor (D) and acceptor (A) materials [4.3, 4.4]. Power conversion efficiencies in the range of 6.5 % have been achieved [4.5] successfully through selection of materials with suitable energy levels, control of nano-morphology [4.6] either during film deposition [4.7] or using post-fabrication procedures such as thermal annealing [4.8, 4.9-4.14] and by optimisation of electrode materials [4.15].

Such progress makes polymer solar cells more competitive with amorphous silicon based solar cells. The main factors that limit the performance of polymer solar cells are charge carrier transport [4.16], narrow absorption in the visible range of the solar spectrum of the active layer and low open circuit voltage [4.17, 4.18]. In general, bicontinuous nanoscale morphology is pleasing for the D/A acceptor junctions, and high crystallinity in the D/A phases is also essential for better transportation ability of the charge carrier. Though, the ideal bicontinuous two-phase nanoscale morphology is difficult to obtain due to reduced solubility of the fullerene and inappropriate phase separation during the film cast process.

Currently, several works have been reported on making nanorods or nanowires structures of P3HT or C₆₀ to form a three-dimensional (3D) interpenetrating network such as the formation of fullerene nanorods structure with different sizes by solvent-vapour treatments at different vapour pressures [4.19].

These approaches provide promising protocols for morphology manoeuvring of conjugated polymer/C₆₀ for solar cells to obtain better charge carrier mobility and increase the absorption of solar energy. The C₆₀ derivative; PCBM was mainly used in published works, due to its higher solubility. However, C₆₀ may be a good candidate for an efficient acceptor material due to its higher electron mobility and crystalline structure compared to PCBM. The morphology fabrication of P3HT/C₆₀ blends remains a fundamental challenge in the field of conjugated polymer/C₆₀ solar cells [4.19, 4.20]. In this work, photo induced charge transfer and optoelectronic properties of photovoltaic cells correlated to the morphology and the structure of P3HT:C₆₀ blend was studied in detail.

4.2. EXPERIMENT DETAILS

4.2.1. Materials and solutions

A regioregular poly(3-hexylthiophene) (rr-P3HT) polymer with a molecular weight (M_n) of $\sim 64,000 \text{ g mol}^{-1}$; with regularity that is greater than 98.5 % for head-to-tail, buckminsterfullerene-C₆₀ with a purity of 99.5%, Indium tin oxide (ITO) coated on a 1 mm glass substrate with a sheet resistance of $8\text{-}12 \text{ } \Omega/\text{sq}^{-1}$,

poly(3,4-ethylenedioxythiophene):poly (styrenesulfonate) (PEDOT:PSS), as well as chloroform (CHCl_3) solution were purchased from Sigma-Aldrich.

4.2.2. Sample preparation

All materials used in this study were used as received, without any further purification. Regioregular P3HT was used as an electron donor material; while a fullerene- C_{60} was used as an electron acceptor material. A mixture of rr-P3HT (5 mg) and C_{60} (5 mg) dissolved in 1mL of CHCl_3 solution was stirred over night at a temperature of 50 °C in order to promote a complete dissolution. It should be noted that the solubility of C_{60} fullerene on chloroform is about 0.16 mg/mL [4.21].

For solar cells fabrication, a thin layer of PEDOT:PSS solution was spin coated onto the ultrasonically cleaned ITO glass substrates and silicon (Si) substrates with the spin rate of 2500 rpm for 30 s. This was followed by thermal treatment of the substrates at 100 °C for 30 min. The P3HT and blend films with a thickness of about 100 nm was spin coated onto the PEDOT:PSS layer. The spinning rate and time of spin-coating were 2500 rpm and 30 sec, respectively. The samples were dried on a hot plate at a temperature of 50 °C for 15 min to dry (or evaporate) the excess solvent. Solar cells were completed by evaporating about 100 nm of aluminium (Al) on top of the active layer (ITO/P3HT: C_{60} (1:1 wt. ratio)/Al) through a shadow mask by means of thermal evaporation in vacuum at a pressure of about 5×10^{-4} Pa resulting in an active device area of 0.14 cm².

4.2.3. Characterization

Surface morphological studies of P3HT and P3HT:C₆₀ (1:1 wt ratio) were carried out using an atomic force microscope (AFM) and a LEO 1525 SEM, operated at an accelerating voltage of 5 kV. The AFM images of the polymer films were acquired using a Veeco NanoScope IV Multi-Mode AFM with the tapping mode. A JEM-2100 JEOL high resolution transmission electron microscope (HR-TEM), operated at 100 kV was employed to examine the internal structure of the P3HT and the blends. Specimens for HR-TEM analysis were prepared by a placing a drop of P3HT dispersed in CHCl₃, onto a holey-carbon copper (Cu) grid and dried at ambient conditions. In order to determine the structural modification during heating; wide angle x-ray scattering (WAXS) measurements were performed using an Anton Paar SAXSess instrument, operating at an accelerating voltage of 40 kV and current of 50 mA. A Nickel (Ni) filtered CuK_α radiation source (0.154nm) (PW3830 x-ray generator PANanalytical) radiation was used. Intensity profiles were obtained with a slit collimated compact Krathy Camera and recorded with a two-dimensional (2-D) imaging plate. Sample to detector distance was 264.5 mm and covers the length of the scattering angle (2θ) from 0.1 to 30 °. The samples were heated in a paste cell at room temperature and 110 °C by a TCU50 (Anton-Paar) temperature control unit, which is attached to the SAXSess instrument.

The optical absorption study of spin-coated films was investigated by means of PekinElmer Lamda 750S Ultraviolet-visible (UV-vis) spectrophotometer. The photoluminescence measurements were carried out at room temperature by

exciting the samples with the 350 nm deuterium lamp. The emission was detected with Jobin-Yvon PMT detector. It should be noted that for some PL measurements, the PEDOT:PSS layer was omitted in order to avoid masking of P3HT features which overlap with those of PEDOT. The film thickness was determined by α -stepper DEKTAK 6M Stylus profilometer (Veeco instruments). Electron spins resonance (ESR) measurements were performed with a JEOL, X-band spectrometer JES FA 200 equipped with an Oxford ESR900 gas-flow cryostat and a temperature control (Scientific instruments 9700). Measurements were done at room temperature (23 °C). The power of 6.0 mW and frequency of 9.46 GHz were used.

The current density–voltage (J – V) characteristics of the polymer based organic solar cells were measured both in the dark and under illumination using a Keithley 2420. The devices were irradiated at 100 mW cm^{-2} using a xenon lamp-based Sciencetech SF150 150W solar simulator equipped with an AM1.5 filter as the white light source; the optical power at the sample was 100 mW cm^{-2} , detected using a daystar meter. All the photovoltaic properties were evaluated in air ambient at room temperature. The solar cells were illuminated through the side of the ITO-coated glass plate.

4.3. RESULTS AND DISCUSSION

The morphology of polymer/fullerene photo-active layers that plays a key role in the final solar cell performance was investigated using scanning electron microscopy (SEM) analysis. Fig. 4.1 shows the SEM micrographs of the surface

of P3HT and blended films spin-coated from a CHCl_3 solvent onto a silicon substrate. It is evident in Fig. 4.1a that the P3HT film shows a less ordered morphology with pores uniformly across the film surface. Smooth surface for the P3HT film prepared from pyridine-chloroform solution was observed by Verma *et al.* [4.22]. The micrograph in Fig. 4.1b shows that the surface has clusters/agglomerates of C_{60} fullerene in the polymer matrix which is uniformly distributed across the surface.

It is suggested that these clusters are nucleation sites for charge carrier transport and reduces the distance travelled by excitons to the respective polymer/ C_{60} interface which greatly enhancing the effectiveness of photo-induced charge transfer from the polymer to C_{60} . Large agglomerated nanotubes in a P3HT film blended with a non functionalized single walled carbon nanotubes (non-FSWCNTs–P3HT) were observed by Kumar *et al.* [4.23].

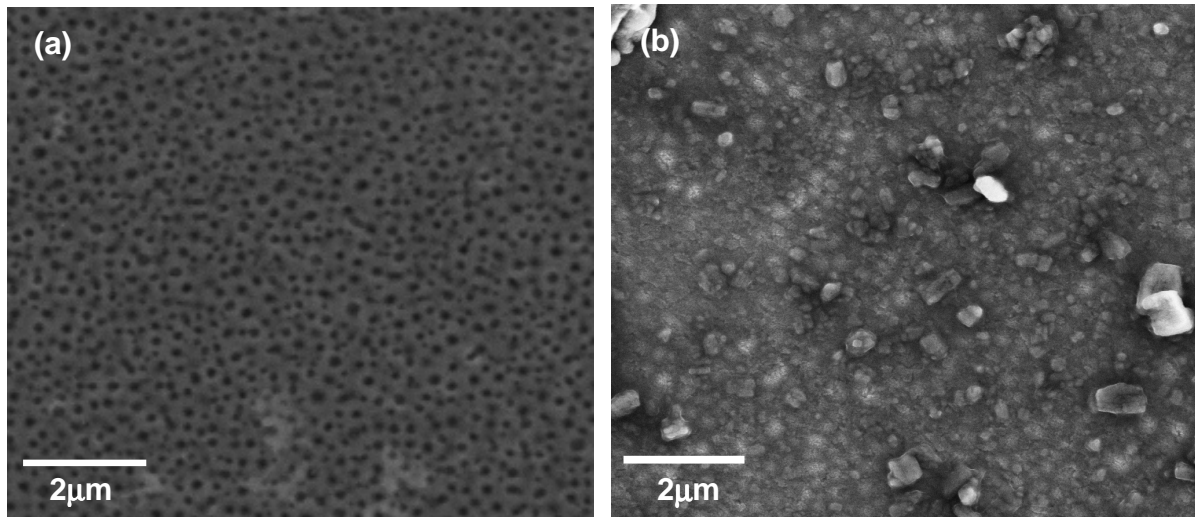


Figure 4.1: SEM micrographs of the surface morphology of (a) P3HT and (b) blended film showing a dispersed C_{60} fullerene on the P3HT matrix

To complement the HR-SEM analysis, AFM measurements were performed on the samples. Fig. 4.2 presents AFM height images of P3HT and blended film of P3HT:C₆₀ in a 1:1 wt. ratio. It is clear in Fig. 4.2a that the sample show pores with diameters ranging from 70-100 nm and lengths/depth that ranges between 3.5 and 9.0 nm. A series of small clusters is observed in the P3HT:C₆₀ blended film (Fig. 2b), which may be attributed to the C₆₀ aggregates. The surface of P3HT and P3HT:C₆₀ (1:1 wt. ratio) films shows a root mean square (rms) roughness of 2.19 and 4.20 nm, respectively. It has been reported that the D/A blend morphology can be controlled by spin-casting the blend from a specific solvent preventing large-size phase separation or enhancing the polymer chain packing [4.6, 4.24].

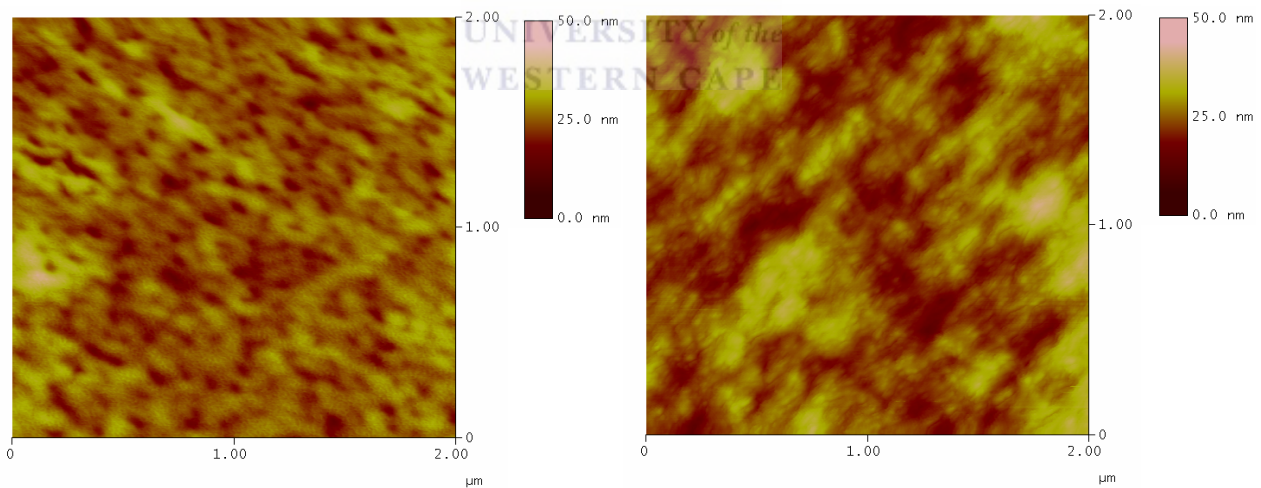


Figure 4.2: AFM height images of P3HT and blended (1:1 wt. ratio) films spin coated onto Si substrates.

High resolution TEM was used to further study the details of ordering of the P3HT active layer as shown in Fig. 4.3. The inset in Fig. 4.3a corresponds to the (200) plane, with a d-spacing of 0.86 nm. The selected area electron diffraction (SAED) pattern (Fig. 4.3b) of a well-aligned sample of P3HT exhibits distinct diffraction rings (spots) indicating that the P3HT forms a polycrystalline film. The P3HT structure shows the (100), (300) as well as the (010) reflections, with a d-spacing of 1.73, 0.52 and 0.37 nm, plane respectively, which are consistent with the WAXS results.

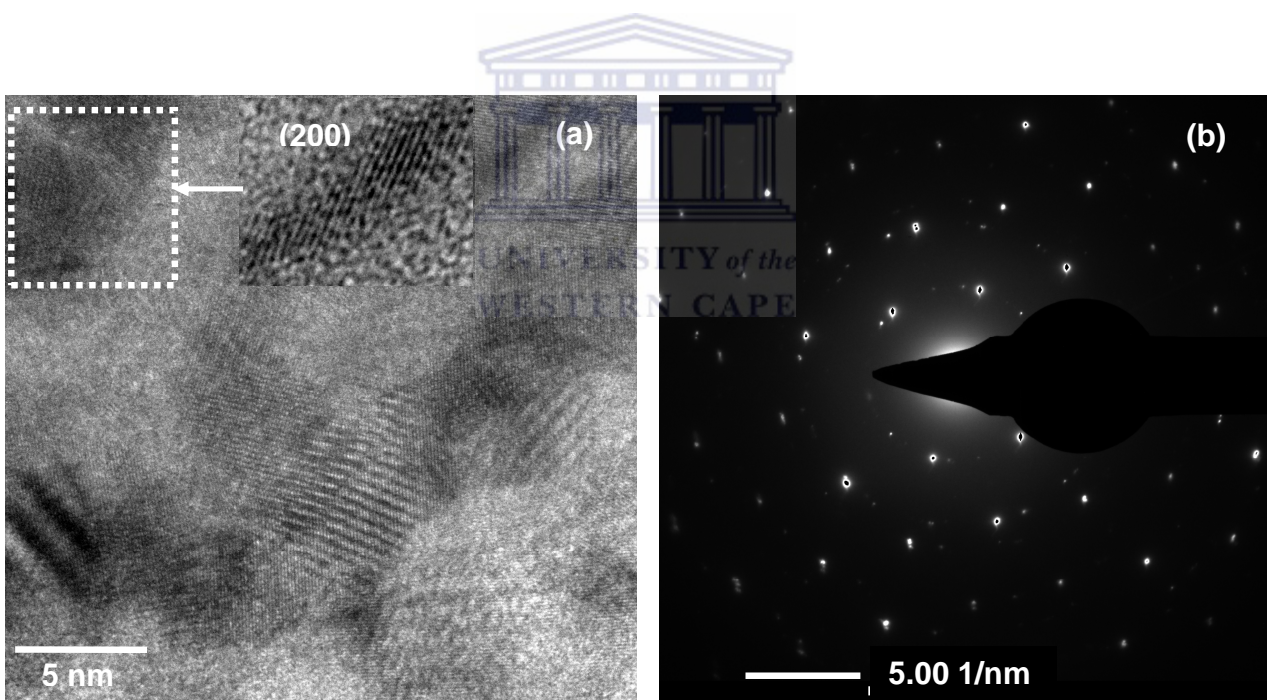


Figure 4.3: HR-TEM images of (a) P3HT dissolved in CHCl_3 solution and (b) SAED pattern of the P3HT. The inset corresponds to (200) plane.

The microstructure and domain spacing for P3HT and blend were examined using wide-angle x-ray scattering technique (WAXS). Representative WAXS patterns for the as prepared P3HT and its blended samples measured at room temperature (RT) and heated at 110 °C are presented in Figs. 4.4 and 4.5. It is noticeable in Figs. 4.4 and 4.5 that P3HT depicts its characteristic peaks at $2\theta \approx 5.2, 10.7, 16.3$ and 23.4° at RT, with broadly bright Debye rings of (*h*00) assigned to (100), (200) (300) and (010) reflections [4.25].

The P3HT:C₆₀ (1:1 wt. ratio) blend in Figs. 4.4 and 4.5c and d shows low peak intensities and diffused Debye rings of (100) and (010) crystalline reflections assigned to P3HT and (111), (220), (311) assigned to C₆₀ fullerene. This indicates that the blended sample has low crystallinity and less ordered structure crystal orientation than a pure P3HT sample. The intensity of the (100) reflection due to lamella layer structure (1.64 nm) is strong, while the intensity of the (010) reflection due to π - π interchain stacking (0.38 nm) is very weak [4.26]. The C₆₀ diffraction patterns (Fig. 4.5e and f) are also consistent with the previously observed results for buckminsterfullerene, which is known to have a face-centred-cubic (fcc) crystal structure at room temperature, and shows reflections for the (111), (220), (311), (222) and (331) diffraction peaks at 10.6, 17.7, 20.9, 21.7 and 27.4° [4.25, 4.27-4.29]. From the WAXS patterns of P3HT and the blended sample, the d-spacing ranges between 0.37 and 1.96 nm, and were estimated using Bragg's law [4.30], while the crystal sizes were estimated using Scherrer's relation [4.31] as shown in Table 4.1.

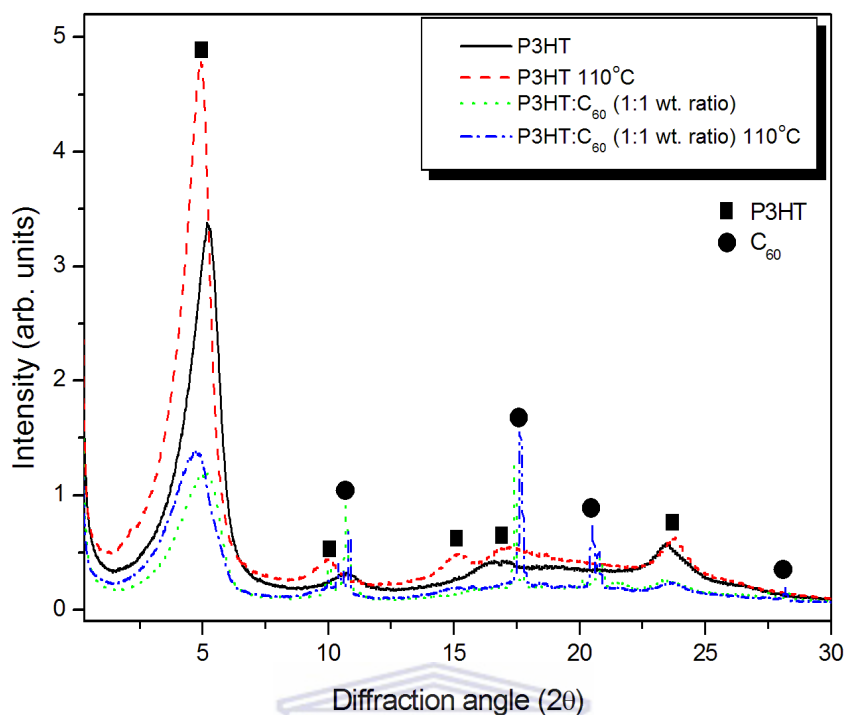


Figure 4.4: Wide-angle X-ray scattering patterns measured at RT and 110 °C of P3HT and its blend.

However, when the P3HT sample is heated at a temperature of 110 °C, diffraction peaks shift to lower angles ($2\theta \approx 4.7, 9.8$ and 16.0°), giving a significant increase in d -spacing and grain sizes of the (100) plane, as depicted in Table 4.1. Similar behaviour was also observed for the blended samples with C_{60} . This indicates an increase in the ordering of the alkyl chains within the main thiophene chains. It is interesting to note that at 110 °C a broad peak formed around 17.1° with a d -spacing and crystal size of 0.51 nm and 1.99 nm, respectively (Fig. 4.4). The formation of this peak is clear in Fig. 4.5b as indicated by an arrow.

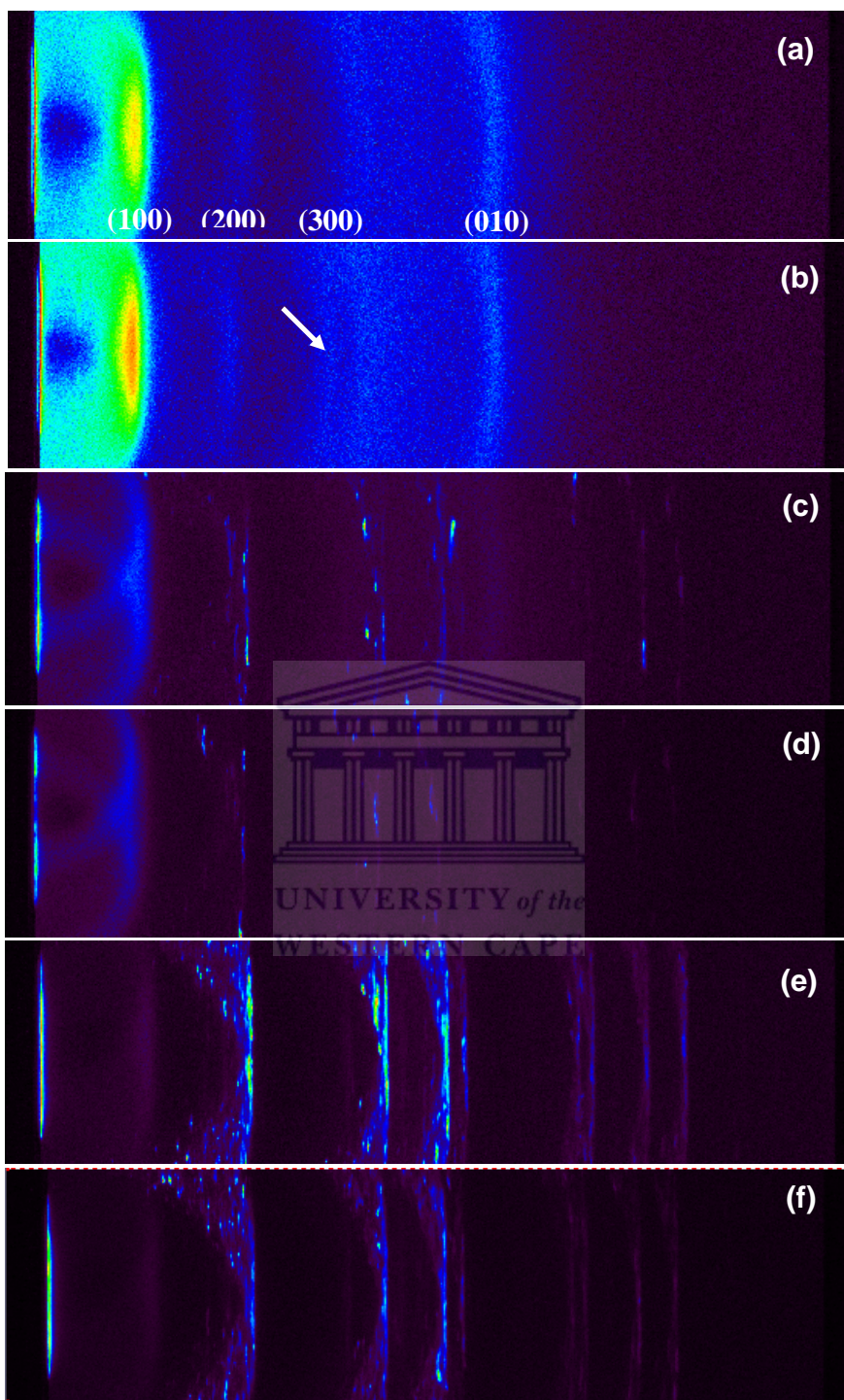


Figure 4.5: 2-D Wide-angle X-ray scattering patterns of: (a) P3HT at RT, (b) P3HT at 110 °C, (c) P3HT:C₆₀ (1:1 wt. ratio) at RT, (d) 1:1 wt. ratio at 110 °C, (e) fullerene C₆₀ at RT and (f) C₆₀ at 110 °C.

Table 4.1: Summary of the full width at half maximum, d-spacing and grain sizes of the as-prepared rr-P3HT and samples heated at 110 °C.

Orientations	<i>As-prepared P3HT</i>			<i>P3HT (110 °C)</i>		
	d-spacing (nm)	FWHM (nm)	Grain sizes (nm)	d-spacing (nm)	FWHM (nm)	Grain sizes (nm)
(100)	1.70	1.38	5.80	1.87	1.26	6.32
(200)	0.83	1.41	5.73	0.90	1.01	7.99
(300)	0.54	3.60	2.29	0.55	2.49	3.32
(010)	0.38	1.53	5.66	0.37	1.25	6.94

Fig. 4.6 compares the optical absorption coefficients spectra of rr-P3HT films with C₆₀ fullerene and a blend of P3HT:C₆₀ in a (1:1 wt. ratio) spin coated on an ITO glass substrate. Both polymers showed the band gap edge at 1.9 eV which is in agreement to the literature [4.32-4.35] and an absorption maximum at around 2.4 eV, which is characteristic of the π - π^* transition between the highest occupied π electron band and the lowest unoccupied one of the polymer [4.36].

The development of a vibronic structure is also observed (refer to the shoulders peak around 2.25 eV and 2.06 eV), which is generally explained by a higher crystallization or ordering of intra-chain interactions in semiconducting polymers [4.37, 4.38]. The C₆₀ fullerene shows a small absorption peak at around 3.31 eV. Upon blending the polymer with a C₆₀ fullerene, a distinctive change in the peak wavelength is observed.

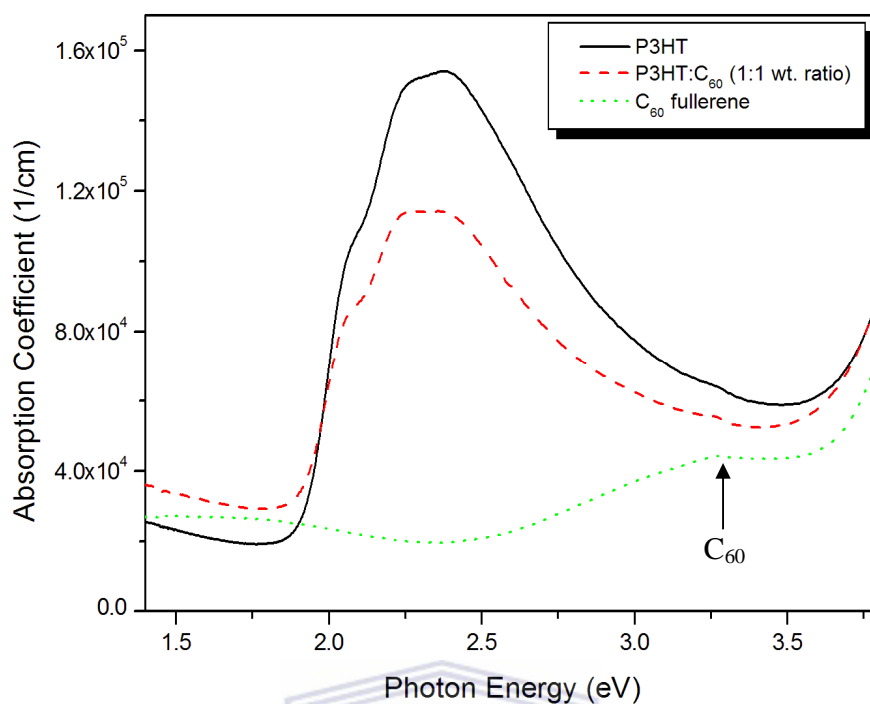


Figure 4.6: UV-vis spectra of films of P3HT, P3HT:C₆₀ (1:1 wt. ratio) blend and C₆₀ fullerene dissolved in CHCl₃ and spin coated on ITO substrates.

UNIVERSITY of the
WESTERN CAPE

A blue shift on the π - π^* interband transition of the P3HT blend as well as a reduction in the absorption coefficients is observed [4.35]. This is probably due to an altering in the stacking conformation of the polymer structure and a reduction of intraplane and interplane stacking, which causes a reduced π - π^* transition and a lower absorbance (Fig. 4.6). Chirvase *et al.* [4.39] reported that the modification in the absorption spectra of P3HT:PCBM composite films is due to the presence of PCBM which destructs the ordering in the P3HT chains.

Photoluminescence (PL) measurements were carried out extensively to evaluate the effectiveness of the photo-induced charge transfer in an electron

donor-acceptor pair. The PL spectra of P3HT and its blend with C₆₀ fullerene measured at room temperature (RT) are shown in Fig. 4.7. The P3HT film shows a strong PL signal around 1.75 eV and a shoulder around 1.92 eV which are assigned to the first vibronic band and the pure electronic transition respectively [4.40-4.43]. The PL emission peak in the shorter energy region (~1.55 eV) indicates an ordering in the P3HT lamella structure within the spherulites [4.40-4.43]. It is evident in Fig. 4.7 that, when fullerene is added in the P3HT matrix, the intense photoluminescence of the P3HT is almost completely quenched. The luminescence studies indicate a profound photoinduced charge transfer in the bulk of P3HT:C₆₀ (1:1 wt. ratio) blended film.

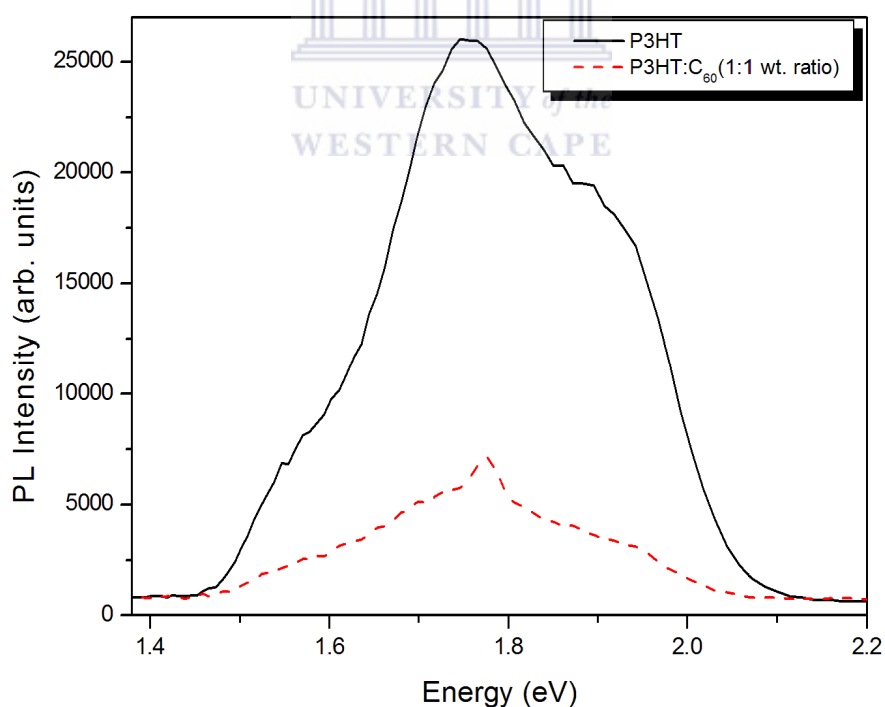


Figure 4.7: Photoluminescence spectra of films of P3HT and P3HT:C₆₀ (1:1 wt. ratio) dissolved in CHCl₃ and measured at room temperature.

The effective charge separation in the P3HT:C₆₀ (1:1 wt. ratio) system has been studied by ESR (electron spin resonance) signals. The spectrum of the blended film shown in Fig. 4.8 was extracted at a microwave power of 6.0 mW in the dark at room temperature. Large ESR signal caused by a partial charge transfer is observed between rr-P3HT and C₆₀ in the dark state. Similar results were observed in the literature [4.44, 4.45].

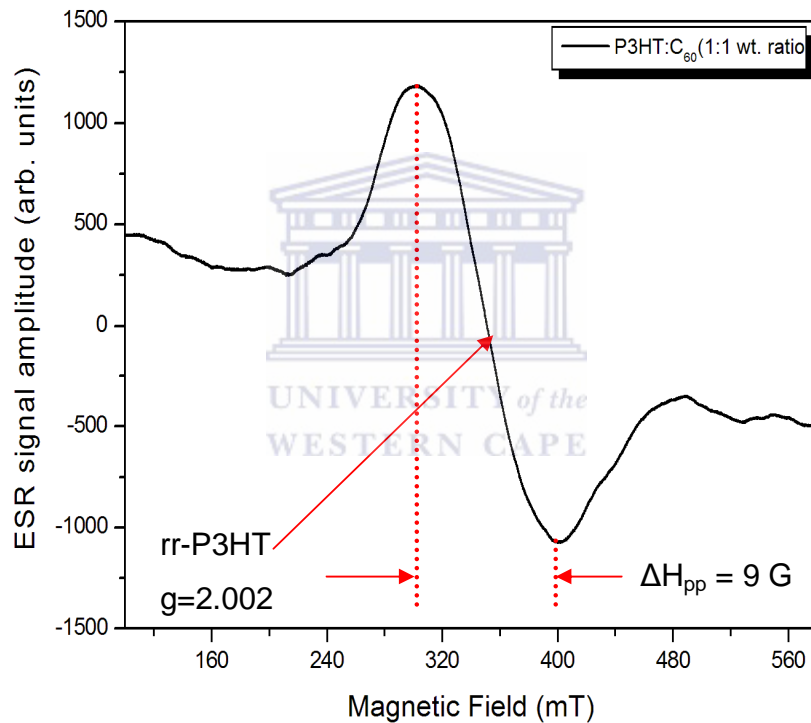


Figure 4.8: ESR spectra of the P3HT and blend films extracted at the power of 6.0 mW in the dark.

Only rr-P3HT signals can be observed at room temperature, due to the spin-relaxation time for the C₆₀ anions is short. The g-factor of the P3HT sample is about 2.0020, which can be attributed to the positive polarons in P3HT (P⁺).

These values as well as the observed peak to peak line width (ΔH_{pp}) of 9 G for rr-P3HT are in good agreement with the literature [4.46, 4.47]. However, the larger observed peak to- peak line width ($\Delta H_{pp}= 9$ G) of composites indicates that rr-P3HT orientation is disturbed [4.48], presumably caused by incomplete mixing of C_{60} . More detailed discussion, however, is beyond the scope of this work.

Fig. 4.9 presents the current density-voltage (J-V) characteristics of a P3HT: C_{60} (1:1 wt ratio) device measured in the dark and under AM1.5 conditions with a white light illumination. The device achieved a short-circuit current density (J_{sc}) of $2.55 \mu A cm^{-2}$, an open circuit voltage (V_{oc}) of 0.092 V, the fill factor of 0.20 and a final power conversion efficiency of about 0.2×10^{-4} %. The low V_{oc} , J_{sc} and efficiency may be attributed to the formation of large-size C_{60} crystals (Fig. 4.1), which causes not only a large-scale phase separation between P3HT and C_{60} , but also a rough P3HT: C_{60} (1:1 wt ratio) blend film as depicted in Fig 4.2. The rough P3HT: C_{60} layer may form some shunt paths after the top electrode deposition resulting in a low open circuit voltage.

Moulé *et al.* [4.49] reported that the morphology of the active layer strongly influences the performance of bulk heterojunction (BHJ) polymer solar cells. Previous studies of polycrystalline perylene diimide films have demonstrated exciton diffusion lengths of up to $2.5 \mu m$ [4.50]. However, the exciton diffusion length in conjugated polymers is merely about 10 nm, which are several orders of magnitude smaller than that in perylene diimide polycrystals. Therefore, the

large phase separation of P3HT:C₆₀ blend device might causes inefficient charge separation of excitons created in P3HT due to its short diffusion lengths.

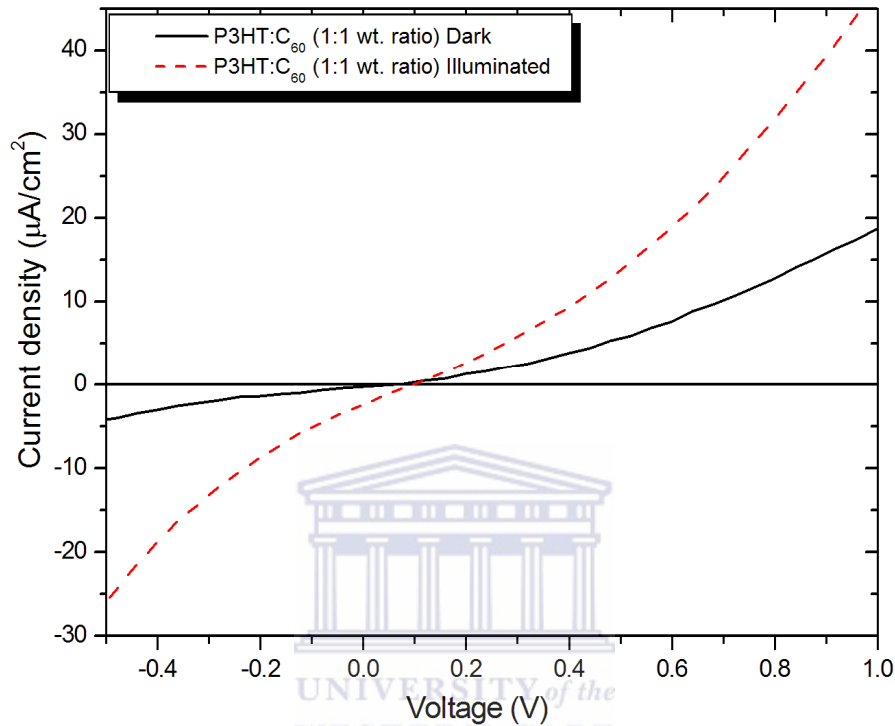


Figure 4.9: Current density–voltage (J – V) characteristics of P3HT:C₆₀ (1:1 wt. ratio) measured in the dark and under white light illumination.

4.4. CONCLUSION

In conclusion, we investigated the photo induced charge transfer correlated to the morphology and the structure of P3HT:C₆₀ blended organic solar cells. The occurrence of photo-induced charge transfer was evidenced in blends of P3HT:C₆₀ (1:1 wt. ratio) by a strong partially quenching of the P3HT luminescence. The ESR measurements allowed one to quantify the charge

transfer between P3HT and C₆₀, which resulted in positive polarons. WAXS data and UV-vis spectroscopy showed that an incorporation of C₆₀ in P3HT matrix lead to lower peak intensities, dark Debye rings and a blue shift on the $\pi-\pi^*$ interband transition of the P3HT as well as a reduction in absorption coefficients. The shift in diffraction peaks to lower angles, giving a significant increase in d -spacing and grain sizes of the (100) plane for films evaluated at 110 ° C was observed. The large-scale phase separation of P3HT and C₆₀ resulted from large C₆₀ agglomerations during spin coating, as observed by AFM and SEM, lead to a low power conversion efficiency of 0.2×10^{-4} %.



4.5. REFERENCES

- [4.1] N. S. Sariciftci, L. Smilowitz, A. J. Heeger, F. Wudl, *Science* 258 (1992) 1474.
- [4.2] E. Bundgaard, F. C. Krebs, *Sol. Energy Mater. Sol. Cells* 91 (2007) 954.
- [4.3] G. Yu, J. Gao, J. C. Hummelen, F. Wudl, A. J. Heeger, *Science* 270 (1995) 1789.
- [4.4] Special Issue: Organic-Based Photovoltaics, *MRS Bull.* 30 (2005) issue 1,
- [4.5] J. Y. Kim, K. Lee, N. E. Coates, D. Moses, Thuc-Quyen Nguyen, M. Dante, A. J. Heeger *Science* 317 (2007) 222.
- [4.6] S. E. Shaheen, C. J. Brabec, N.S. Sariciftci, F. Padinger, T. Fromherz, J. C. Hummelen, *Appl. Phys. Lett.* 78 (2001) 841.
- [4.7] G. Li, V. Shorriya, J. Huang, Y. Yao, T. Moriarty, K. Emery, Y. Yang, *Nat. Mater.* 4 (2005) 864.
- [4.8] W. L. Ma, C. Y. Yang, X. Gong, K. H. Lee, A. J. Heeger, *Adv. Funct. Mater.* 15 (2005) 1617
- [4.9] F. Padinger, R. S. Ritterberger, N. S. Sariciftci, *Adv. Funct. Mater.* 13 (2003) 85.
- [4.10] Y. Kim, S. A. Choulis, J. Nelson, D. D. C. Bradley, S. Cook, J.R. Durrant, *Appl. Phys. Lett.* 86 (2005) 063502.
- [4.11] Y. Kim, S. Cook, S. M. Tuladhar, J. Nelson, J.R. Durrant, D. D. C. Bradley, M. Giles, I. McCulloch, M. Ree, C. S. Ha, *Nat. Mater.* 5 (2006) 197.
- [4.12] C. J. Ko, Y. K. Lin, F. C. Chen, *Adv. Mater.* 19 (2007) 3520

- [4.13] M. Reyes-Reyes, K. Kim, J. Dewald, R. López-Sandoval, A. Avadhanula, S. Curran, D.L. Carroll, *Org. Lett.* 7 (2005) 5749.
- [4.14] P. Peumans, S. Uchida, S. R. Forrest, *Nature* 425 (2003) 158.
- [4.15] M. D. Irwin, D. B. Buchholz, A. W. Hains, R. P. H. Chang, T. J. Marks, *Proc. Nat. Acad. Sci.* 105 (2008) 2783.
- [4.16] W. L. Wang, H. B. Wu, C. Y. Yang, C. Luo, Y. Zhang, J. W. Chen, Y. Cao, *Appl. Phys. Lett.* 90 (2007) 183512.
- [4.17] M. A. Loi, S. Toffanin, M. Muccini, M. Forster, U. Scherf, M. Scharber, *Adv. Funct. Mater.* 17 (2007) 2111.
- [4.18] C. P. Chen, S. H. Chan, T. C. Chao, C. Ting, B. T. Ko, *J. Am. Chem. Soc.* 130 (2008) 12828.
- [4.19] G. Lu, L. Li, X. Yang, *Small* 4 (2008) 601.
- [4.20] X. N. Yang, G. H. Lu, L. G. Li, E. L. Zhou, *Small* 3 (2007) 611.
- [4.21] R. S. Ruoff, D. S. Tse, R. Malhotra, D. C. Lorents, *J Phys Chem.* 97 (1993) 3379.
- [4.22] D. Verma, V. Dutta, *J. Renewable Sustainable Energy* 1 (2009) 023107.
- [4.23] J. Kumar, R. K. Singh, V. Kumar, R.C. Rastogi, R. Singh, *Diamond & Related Materials* 16 (2007) 446.
- [4.24] J. K. J. van Duren, X. Yang, J. Loos, C. W. T. Bulle-Lieuwma, A.B. Sieval, J. C. Hummelen, R. A. J. Janssen, *Adv. Funct. Mater.* 14 (2004) 425.
- [4.25] International Centre for Diffraction Data (ICDD): P3HT (48-2040), C₆₀ fullerene (47-0787, 44-0558).

- [4.26] T. J. Prosa, M. J. Winokur, J. Moulton, P. Smith, A. J. Heeger, *Macromolecules* 25 (1992) 4364.
- [4.27] P. A. Heiny, J. E. Fischer, A. R. McGhie, W. J. Romanow, A. M. Denenstein, J. P. Jr. McCauley, A. B. III. Smith, D. E. Cox, *Phys. Rev. Lett.* 66 (1991) 2911.
- [4.28] M. E. Cagiao, A. O. Pozdnyakov, M. Krumova, V. V. Kudryavtsev, F. Balta Callej, *J. Compos. Sci. Technol.* 67 (2007) 2175.
- [4.29] J. Q. Li, Z. X. Zhao, Y. L. Li, D. B. Zhu, Z. Z. Gan, D. L. Yin, *Physica C*, 196 (1992) 135.
- [4.30] B. E Warren, *X-Ray Diffraction* (New York: Dover) (1990) 251.
- [4.31] B. D. Cullity, *Elements of X-Ray Diffraction*, 2nd ed.; Addison-Wesley Publishing Co.: Reading, MA, (1978).
- [4.32] T. Ahn, B. Choi, S. H. Ahn, S. H. Han, H. Lee, *Synth. Met.* 117 (2001) 219.
- [4.33] G. Dicker, T. J. Savenije, B.-H. Huisman, D. M. de Leeuw, M. P. de Haas, J. M. Warman, *Synth. Met.* 137 (2003) 863.
- [4.34] J. J. Apperloo, R. A. J. Janssen, M. M. Nielsen, K. Bechgaard, *Adv. Mater.* 12 (2000) 1594.
- [4.35] W. R. Salaneck, I. Lundstrom, B. Ranby (Eds.), *Conjugated Polymers and Related Materials Proceedings of the Eighty-first Nobel Symposium*, Oxford University Press, (1993), p. 290.
- [4.36] X. Jiang, R. Osterbacka, O. Korovyanko, C. P. An, B. Horowitz, R. A. J. Janssen, Z. V. Vardeny, *Adv. Funct. Mater.* 12 (2002) 587.

- [4.37] P. J. Brown, D. S. Thomas, A. Kohler, J. S. Wilson, J. S. Kim, C. M. Ramsdale, H. Sirringhaus, R. H. Friend, *Phys. Rev. B* 67, (2003) 064203.
- [4.38] T. C. Chung, J. H. Kaufman, A. J. Heeger, F. Wudl, *Phys. Rev. B* 30 (1984) 702.
- [4.39] D. Chirvase, J. Parisi, J. C. Hummelen, *Nanotechnology* 15 (2004) 1317.
- [4.40] M. Sharma, D. Kaushik, R.R. Singh, R.K. Pandey, *J. Mater. Sci.: Mater. Electron.* 17 (2006) 537.
- [4.41] D. E. Motaung, G. F. Malgas, C. J. Arendse, S. E. Mavundla, D. Knoesen, *Materials Chemistry and Physics* 116 (2009) 279.
- [4.42] L. Li, C.-M. Chan, K. L. Yeung, J.-X. Li, K.-M. Ng, Y. Lei, *Macromolecules* 34 (2001) 316.
- [4.43] H. Yang, T. Shin, J.L. Yang, K. Cho, C.Y. Ryu, Z. Bao, *Adv. Funct. Mater.* 15 (2005) 671.
- [4.44] K. Marumoto, N. Takeuchi, S. Kuroda, *Chem. Phys. Lett.* 382 (2003) 541.
- [4.45] K. Marumoto, N. Takeuchi, T. Ozaki, S. Kuroda, *Synth. Met.* 129 (2002) 239.
- [4.46] R. Dietmueller, A. R. Stegner, R. Lechner, S. Niesar, R. N. Pereira, M. S. Brandt, A. Ebbers, M. Trocha, H. Wiggers, M. Stutzmann, *App. Phys. Lett.* 94 (2009) 113301.
- [4.47] K. Marumoto, Y. Muramatsu, Y. Nagano, T. Iwata, S. Ukai, H. Ito, S. Kuroda, Y. Shimoj, S. Abe, *J. Phys. Soc. Jpn.* 74 (2005) 3066.
- [4.48] S. Watanabea, H. Tanaka, H. Ito, K. Marumoto, S. Kuroda, *Synth. Met.* 159 (2009) 893.

[4.49] A. J. Moulé, K. Meerholz, *Adv. Mater.* 20 (2008) 240.

[4.50] J. J. Dittmer, E. A. Marseglia, R. H. Friend, *Adv. Mater.* 12 (2000) 1270.



CHAPTER FIVE

INVESTIGATION OF THE EFFECTS OF SUBSTRATE ANNEALING ON THE PROPERTIES OF POLYMER BLENDS

ABSTRACT

In this manuscript, we investigated the effect of substrate annealing prior to the deposition of the active layer on the morphological, structural and opto-electrical properties of two variations of organic polymer blends of poly(3-hexylthiophene):C₆₀ fullerene and poly(3-hexylthiophene):[6,6]-phenyl C₆₁ butyric acid methyl ester films using atomic force microscopy, field emission scanning microscopy, x-ray diffraction and Hall effect measurements. P3HT films deposited on pre-annealed substrates exhibit an enhancement in the crystallization, and an increase in the electrical conductivity and Hall mobility of p-type P3HT. The microscopic morphology reveals self-assembled fibrillar structures due to the suppressed growth of fullerenes clusters induced by the controlled evaporation rate of the solvent. It is proposed that pre-substrate annealing controls the crystallization of P3HT, the phase separation and diffusion of the acceptor material (C₆₀ or PCBM).

The content of this chapter was published in: Materials Chemistry and Physics 124 (2010)

208–216

5.1. INTRODUCTION

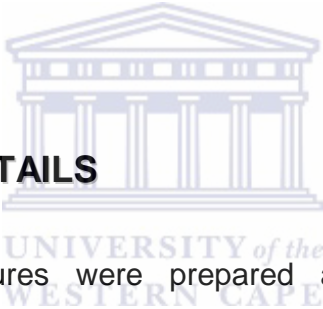
Organic photovoltaic cells (OPVs) have attracted great research interests as a potentially low-cost and lightweight source of renewable energy since the first thin film organic PV cell based on a donor/acceptor (D/A) heterojunction was reported by Tang in 1986 [5.1–5.3]. Among the various types of polymeric semiconductors, regioregular poly(3-hexylthiophene) (rr-P3HT) is considered as one of the most promising material, due to its good solubility in organic solvents, high hole mobility [5.4–5.8] and ease of synthesis [5.9–5.11]. Self-organized rr-P3HT exhibits semicrystalline microstructure, consisting of ordered crystallites separated by disordered grain boundary regions, where the crystal domain consists of lamellae of 2D plane with π - π stacked main chains.

Efficiencies over 5%, through optimization of processing parameters such as thermal annealing conditions and solvent evaporation time [5.12–5.24], have been reported. These parameters determine the degree of organization of polymers, nanoscale morphology and have a critical influence on the performance of electronic and optoelectronic devices. It has been reported that thermal annealing at temperatures up to 180 °C does not only improve the crystallisation of the rr-P3HT, but also improves the hole mobility of blended films [5.22–5.23].

Besides the introduction of low-band gap polymers into the photoactive layer, increasing the effective conjugation length and crystallinity of the materials involved in the bulk-heterojunction solar cells is also an efficient way to improve both the match of the optical absorption with the solar spectrum and charge

carrier mobility, and eventually the device performance [5.14, 5.17-5.19]. However, no conclusive work has been done using P3HT, C₆₀ and [6,6]-phenyl-C₆₁-butyric acid methyl ester (PCBM) to control and improve the evaporation rate such as by spin-coating an active layer onto an annealed substrate prior to active layer deposition. In this contribution, we therefore report on the effect of substrate annealing, prior to active layer deposition, on the morphology, structural properties and the mobility of two variations of organic polymer blends of poly(3-hexylthiophene):C₆₀ fullerene and poly(3-hexylthiophene):[6,6]-phenyl C₆₁ butyric acid methyl ester thin films.

5.2. EXPERIMENT DETAILS



The blended structures were prepared according to the following procedure. Regioregular poly(3-hexylthiophene) (P3HT) with number-average molecular weight $M_n \sim 64,000 \text{ g mol}^{-1}$ and fullerene (C₆₀) were purchased from Sigma–Aldrich and were used as received without further purification. The regioregularity of the P3HT material was specified as > 98.5 %. The active layer containing rr-P3HT (~5mg or a weight percentage of 50 %) and either C₆₀ or PCBM with concentration (~5 mg) was dissolved in 1 ml of 1,2 dichlorobenzene (DCB) solution to obtain a ratio of 1:1 by weight. DCB has a boiling point of 180 °C and a solubility of 28, 30 and >50 mg/ml in fullerene, P3HT and PCBM, respectively at room temperature [5.20, 5.21]. The solution was stirred overnight on a hotplate at 50 °C. No sonication or filtering is used in this process which

would adversely affect the polymer side chains and possibly lead to a decrease in the conjugation length of P3HT strands. The thin films were obtained by spin-coating the as-prepared solution onto a hot (annealed) silicon substrate. The spinning rate and time of spin-coating were 2500 rpm and 30 s. In order to control the evaporation rate of the solvent (DCB) from the P3HT films and blends the substrates were annealed at 70 and 110 °C on a hot plate for 15 min prior to spin-coating the photoactive layer. The hot substrate may accelerate the evaporation of DCB solvent during spin coating the P3HT films.

A Panalytical X'pert PRO PW 3040/60 x-ray diffractometer with a Cu K_α ($\lambda = 0.154$ nm) monochromated radiation source, operating at 45.0 kV and 40.0 mA was utilized in order to determine the crystallinity of the P3HT blended films. XRD data were collected in the 2θ ranging from 3 to 25° with a step size of 0.02°. The Raman spectroscopy measurements were conducted at room temperature with a 514nm excitation laser with a spectral resolution of 0.4 cm⁻¹. A Tecnai F20 field emission high-resolution transmission electron microscope (FE-HR-TEM), operated at 120 kV was employed to examine the internal structure and crystallinity of P3HT. Specimens for HR-TEM analysis were prepared by transferring a drop of the P3HT solution prepared above to a holey-carbon copper grid and dried at ambient conditions. To quantitatively relate the diffraction intensity in selected area electron diffraction (SAED) patterns to the crystallinity of the specimen investigated, all these SAED patterns were

performed by using a standard recording mode i.e. fixed magnification, field-limiting aperture of 100 μm and exposure time of 4.0 s for SAED acquisition.

The morphology of the P3HT blended films was investigated by LEO 1525 high resolution field emission scanning electron microscope (HR-FE-SEM) operating at an accelerating voltage of 5 kV. Atomic force microscopy (AFM) images of the top surface of the thin films of P3HT and its blends spin coated on Si (110) substrates in a tapping mode were analyzed using a Veeco AFM system (Digital Instruments) at ambient conditions. The conductivity and the mobility of the P3HT were extracted using a Hall Effect measurement system (ECOPIA, HMS-3000). The measurements were carried out at room temperature with a magnetic field of about 0.55 T. The optical properties of the films were characterized by UV–vis absorption measurements. The absorption spectra were obtained using a Perkin-Elmer Lambda 750 UV–vis spectrometer.

5.3. RESULTS AND DISCUSSION

5.3.1. Structural properties

Fig. 5.1 shows the XRD profiles of the as-prepared P3HT films and its blends spin coated on a Si (100) substrate at room temperature (RT) compared with the substrates annealed at different temperatures prior to active layer deposition. The corresponding structural evolution is depicted in Fig. 5.2. The P3HT film spin coated onto the un-annealed Si substrate exhibit a weak (100)

diffraction peak at $2\theta = 5.3^\circ$. This corresponds to an ordered self-organized lamellar structure with an interlayer spacing, which is formed by parallel stacks of P3HT main chains that are separated by regions that are filled with the alkyl side chains [5.24-5.26]. When the Si substrates are annealed at 70 and 110 °C a shift in the diffraction peak to higher 2θ angles ($2\theta = 5.42^\circ$) is observed, giving a significant decrease in d -spacing of the (100) plane as depicted in Fig. 5.1 and 5.2a.

This considerable decrease in the d -spacing with increasing substrate annealing temperature, hints that interdigitation or tilting of the side groups occurred during the formation of ordered aggregates in the solution and induced crystallization during film deposition. The full-width-at-half-maximum (FWHM) reduces, while the crystal size increases linearly with respect to substrate annealing temperature (Fig. 5.2b and c). Similar shifts in the diffraction peaks were also observed by Li *et al.* [5.27] by adding a few drops of n-hexane into *o*-dichlorobenzene solution. The as-prepared samples in the P3HT:C₆₀ (1:1 weight ratio) and P3HT: PCBM blends (Fig. 5.1b and c), shows no diffraction peaks. This is probably due to the presence of C₆₀ (or PCBM) molecules, which disturb the formation of P3HT crystallites at room temperatures. After depositing the blends on a hot substrate the crystallinity of the films drastically increased and a slight shift in the diffraction peaks to lower 2θ angles is observed, (Fig. 5.1b, c and 5.2b and c). This increase in crystallinity is probably due to the improved thermal diffusion of C₆₀ (or PCBM) molecules at elevated temperatures into larger C₆₀ (or PCBM) aggregates [5.28-5.31]. As a result of this motion, regions

with low C₆₀ or PCBM concentration occur, where the P3HT aggregates can convert into P3HT crystallites [5.25].

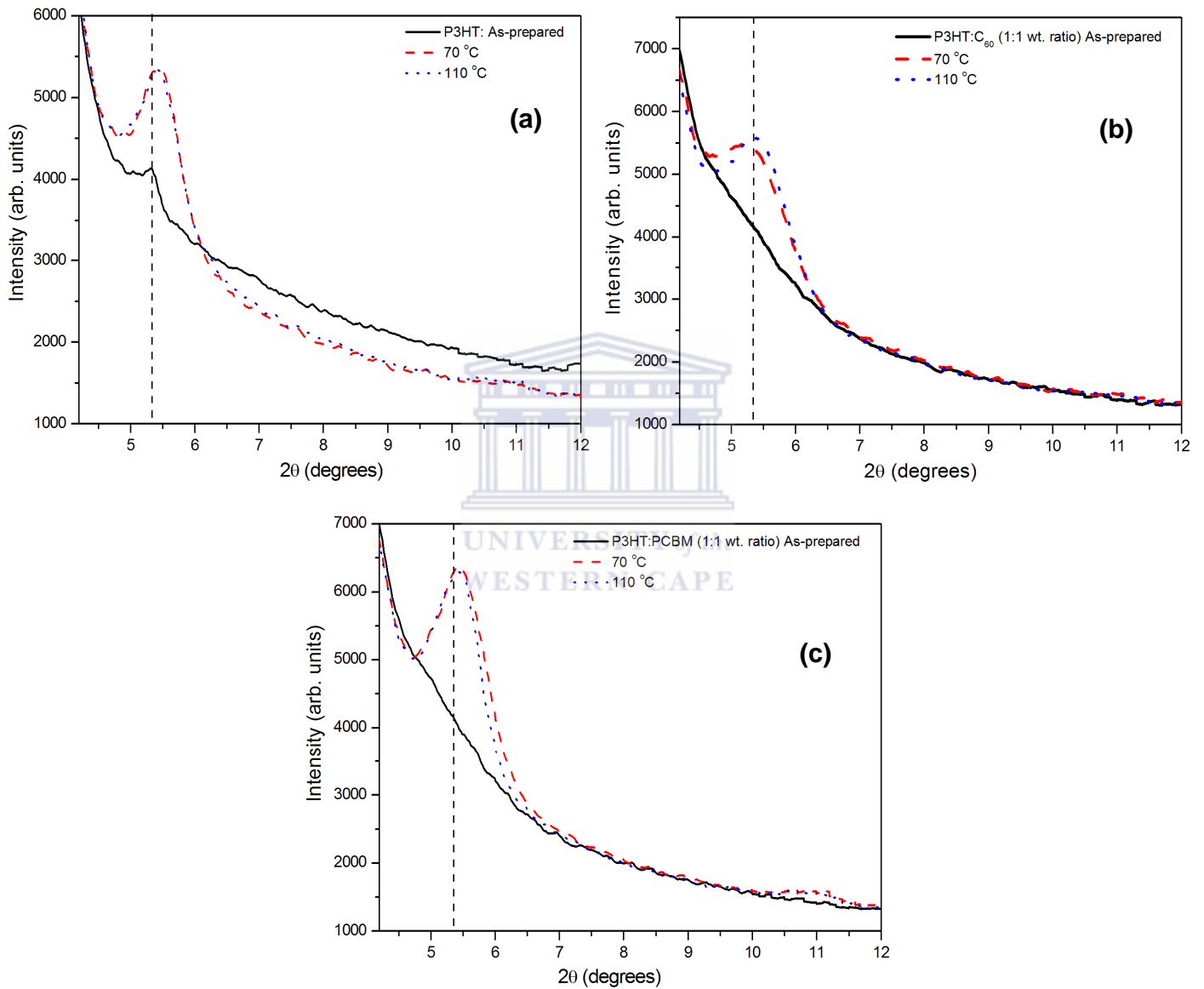


Figure 5. 1: XRD profiles of (a) P3HT and (b) P3HT:C₆₀ (c) P3HT:PCBM films spin-coated onto an un-annealed Si substrates and substrates annealed at 70 and 110 °C for 15 min.

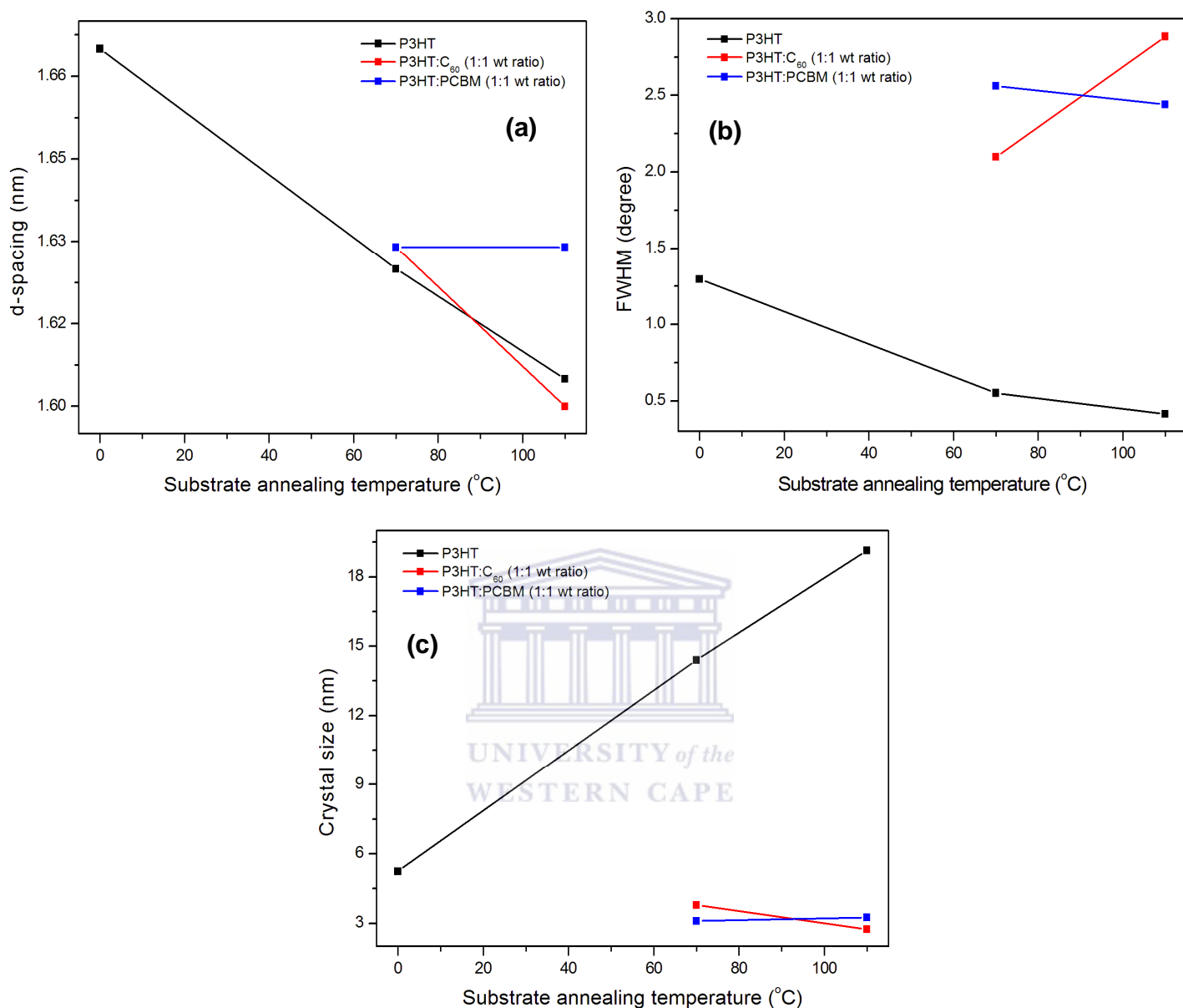


Figure 5. 2: Structural evolution of P3HT crystals in blends films during substrate annealing (a) d-spacing, (b) FWHM of the P3HT (100) peak and (c) the average P3HT (100) crystal size. Note: the line is used to guide the reader.

However, diffraction peaks caused by C₆₀ (or PCBM) were barely seen in the diffractogram of the blend films both with and without substrate annealing.

Thus, substrate annealing only promoted the crystallization of P3HT but had little influence on the crystallization of fullerenes. Therefore, the controlled evaporation rate of the high boiling point solvent (DCB), induced by prior substrate annealing, is an alternative strategy to induce highly ordered and crystalline P3HT in the blended films, which provides an alternative approach to produce organic PV devices with improved efficiencies.

To further demonstrate the alterations in the structure, Raman spectroscopy was employed. The intensive Raman bands of P3HT (Fig. 5.3) at 1445 and 1380 cm^{-1} are due to the C=C stretching vibrations of the thiophene ring and C-C skeletal stretching [5.32-5.34]. The Raman band of P3HT at 728 cm^{-1} is assigned to the deformation vibration of the C-S-C bond. No features attributed to C₆₀ (or PCBM) could be observed in the Raman spectra. It has been reported by Klimov *et al.* [5.32] that the Raman modes of P3HT in the blends are not influenced by the contributions of the C₆₀ fluorescence. It can be seen in Fig. 5.3a and b that the peak position corresponding to the C=C stretching vibrations exhibit a shift from 1455 to 1450 cm^{-1} after substrate annealing at 70 °C and higher temperatures. Such a downward shift in the wave-number is associated with an improvement in the crystallinity of the P3HT polymer and the extension of the effective conjugation length along the polymer backbone [5.35]. However, when the polymer is blended with PCBM in a 1:1 wt. ratio (Fig. 5.3c), an improvement in the polymer ordering is only observed after substrate annealing at 110 °C.

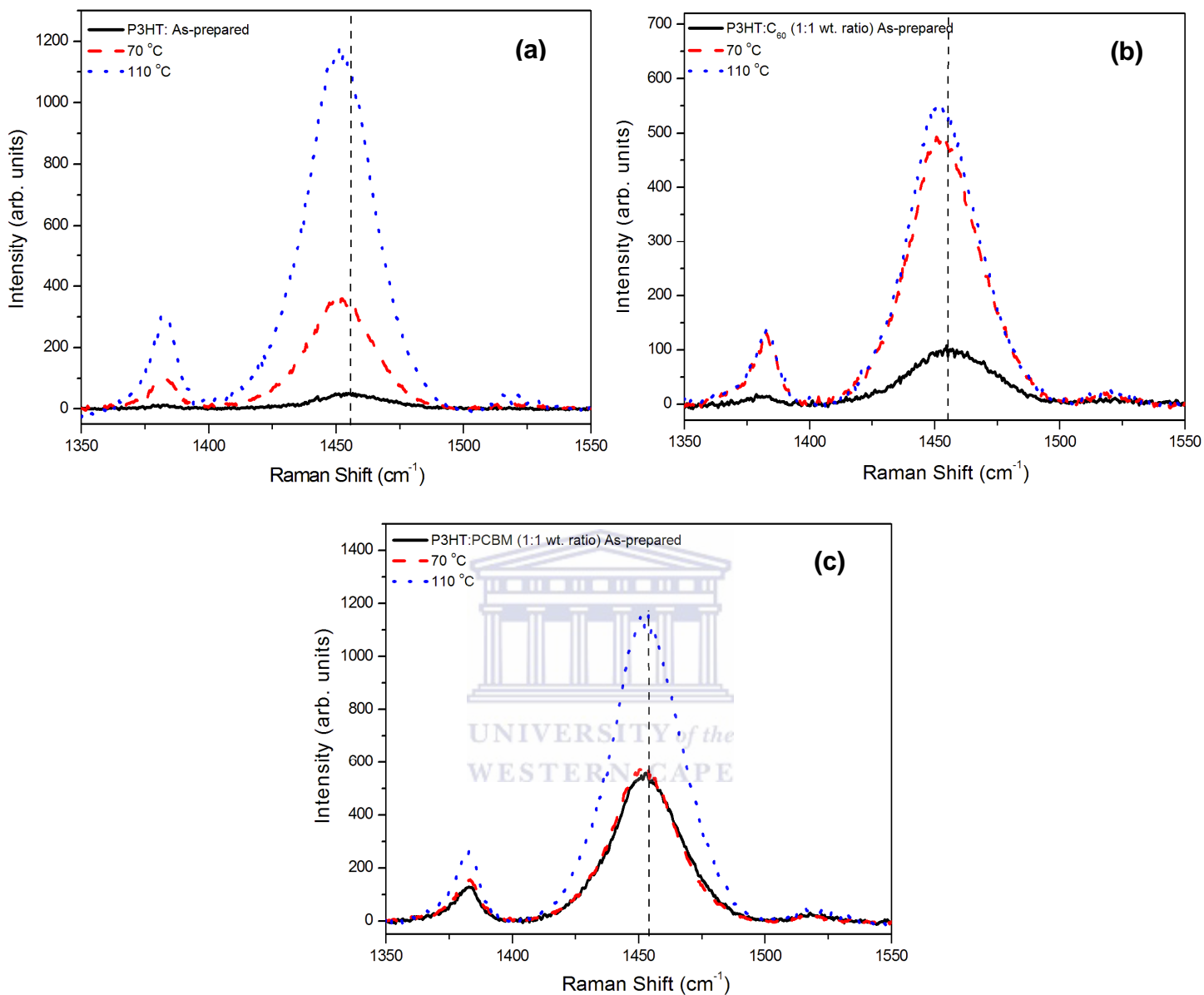


Figure 5. 3: Raman spectra of the as-prepared, substrate annealed films of (a) P3HT, (b) P3HT:C₆₀ (1:1 wt. ratio) and (c) P3HT:PCBM (1:1 wt. ratio) blends.

Fig. 5.4 shows a bright field TEM image of the P3HT:C₆₀ (1:1 wt ratio) blend prepared from DCB and the corresponding selected area electron diffraction (SAED) patterns. The SAED patterns in Fig. 5.4a, (spot 1-5) disclose different

crystalline ordering in the P3HT:C₆₀ blends. The SAED of the P3HT:C₆₀ blend (Fig. 5.4a) spot 1, shows a *d*-spacing of 0.39 and 0.23 nm associated to the reflections from crystallographic (020) planes of typical whisker-like P3HT crystals [5.36] and diffraction from C₆₀ nanocrystallites [5.19, 5.37]. However, spot 2 shows diffused Debye rings which results from C₆₀ nanocrystals that are randomly distributed in P3HT matrix. The SAED pattern in spot 3 reveals well-defined rings of high crystallinity as indicated by an arrow, with *d*-spacing of 0.248, 0.258 and 0.86 nm which are ascribed to C₆₀ nanocrystallites and P3HT. The 0.86 nm *d*-spacing corresponds to a reflection of (200) of P3HT.

As seen in the upper right (spot 4), the SAED pattern of the P3HT:C₆₀ blend indicates that the central region of sample comprises crystallites of different orientations, corresponding to *d*-spacing of 0.25, 0.28, 0.19, and 0.39 nm [5.19, 5.37]. Since the SAED pattern has been well established for semi-quantitative crystallinity analysis and proven to be a feasible and powerful tool in this field [5.19, 5.20, 5.38], we are able to draw a preliminary conclusion that the crystallization of P3HT blended with C₆₀ (spot 5, inset) has been substantially suppressed, as proven by the low electron diffraction intensity of crystallographic (020) planes of P3HT. The suppression of P3HT by C₆₀ was also observed in the XRD and Raman results.

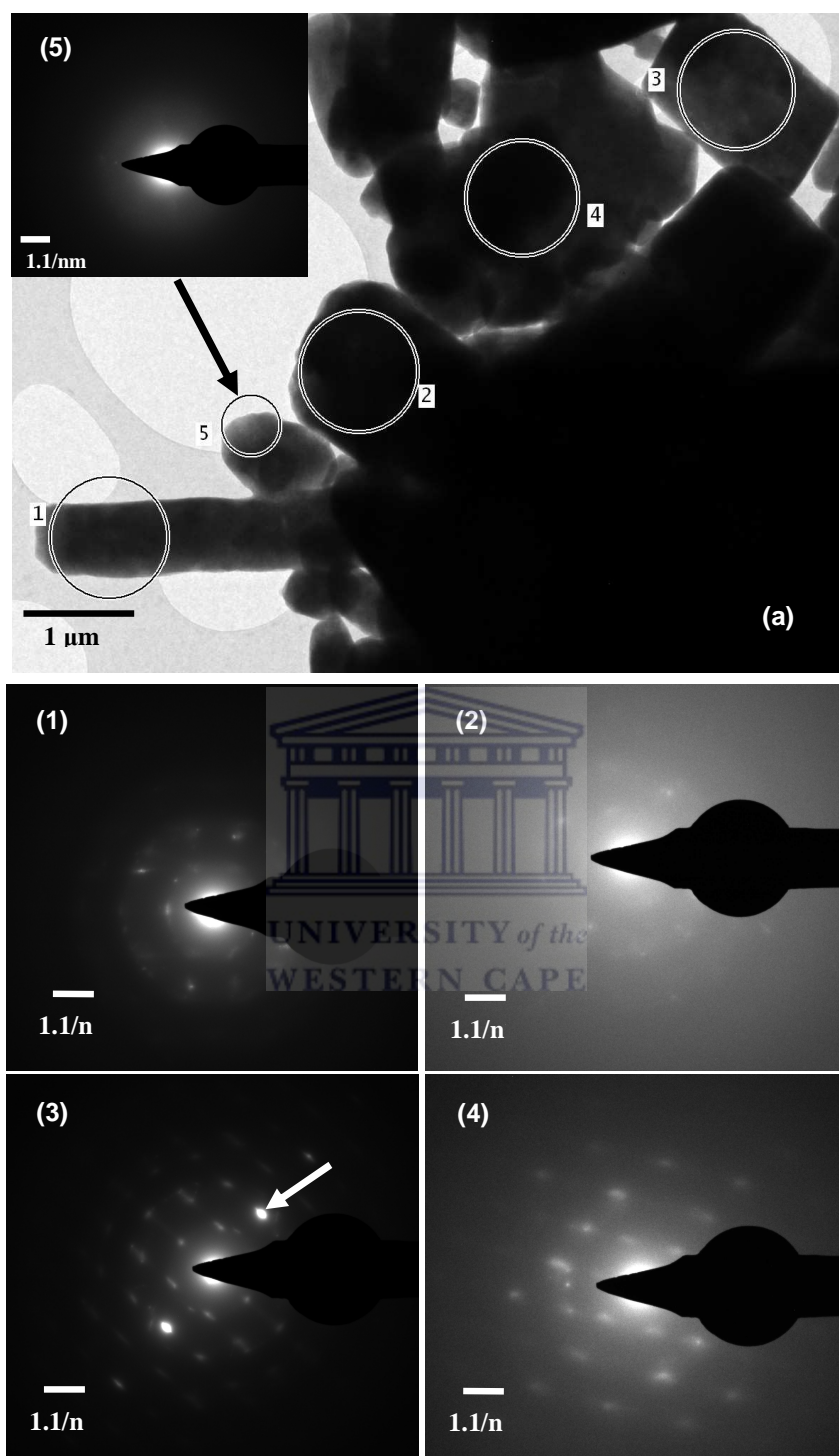


Figure 5. 4: Bright field-TEM images of (a) P3HT:C₆₀ dissolved in DCB solution and the corresponding SAED patterns obtained at different spots as denoted by circles in Fig. 4.4(a).

5.3.2. Surface Morphology

In order to understand the dependence of the photovoltaic performance on the morphology of the active layer, scanning electron microscopy (SEM) observations were carried out to provide images of the top surfaces of the P3HT and blends. Fig. 5.5 shows SEM micrographs of the as-prepared P3HT and blends compared with that spin coated on Si-substrates annealed at 110 °C. The as-prepared P3HT film has a smooth surface. When, the substrate is annealed at 110 °C, rod-like or fibrillar structures are uniformly distributed across the film. The formation of polymer fibrils and dopant islands adhered to the polymer fibrils on a pristine P3HT and doped P3HT films were observed by Singh *et al.* [5.39]. The SEM micrograph shows small C₆₀ aggregates on the surface of the as-prepared substrate of the P3HT:C₆₀ blended film.

Thermal annealing of the film shows that large C₆₀ clusters in the P3HT:C₆₀ blend diffused out of the polymer matrix. The blended film of P3HT and PCBM shows only a few small PCBM clusters (circles) embedded in the P3HT matrixes which are separated from each other, while the substrate annealed film at 110 °C shows fibres with different shapes. It is suggested that these fibres are induced due to a large free volume in the blended films after substrate annealing, allowing the P3HT to readily crystallize. Yang *et al.* [5.31] reported that the kinetics of crystal growth of PCBM in the blended films is controlled by both the long-range diffusion rate of PCBM molecules and the local incorporation rate of PCBM molecules.

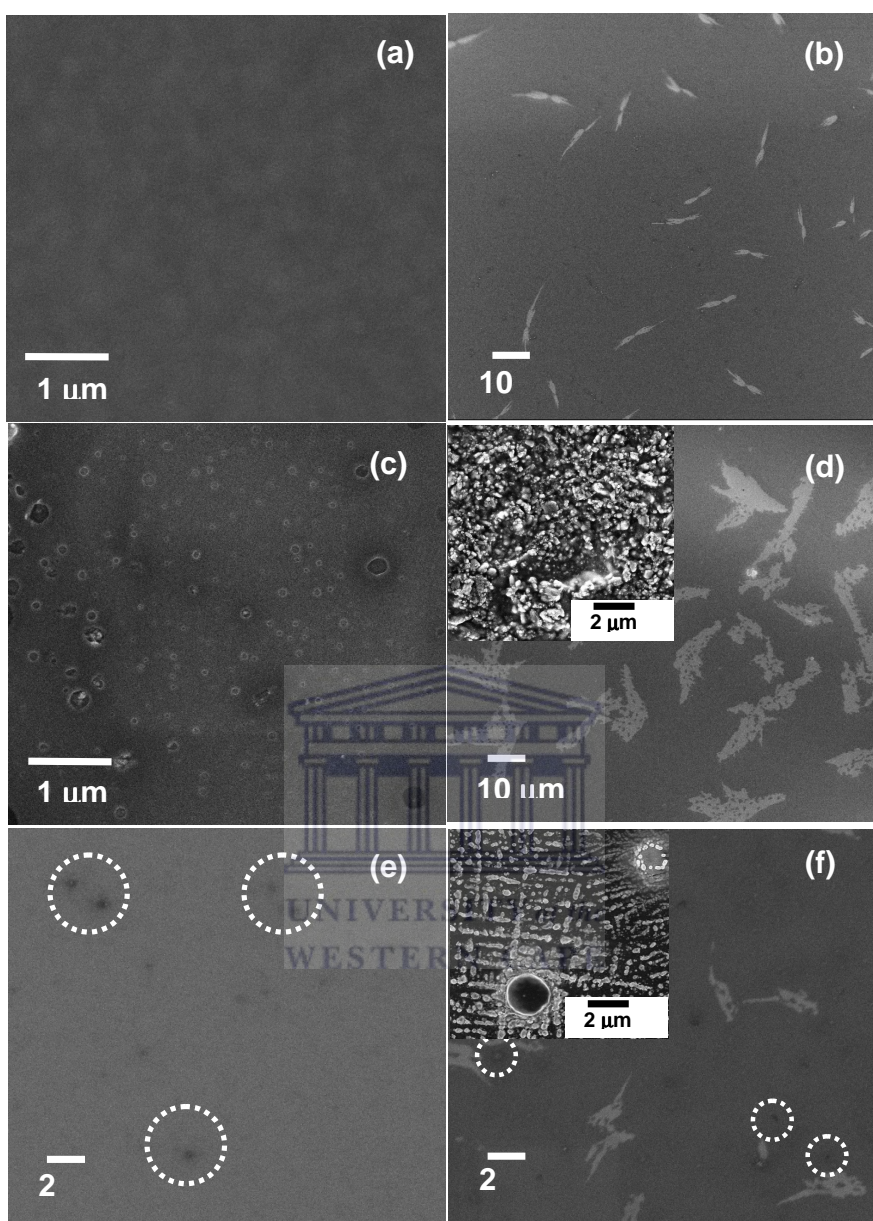


Figure 5. 5: FE-SEM micrographs of P3HT (a) un-annealed substrate, (b) substrate annealed at 110 °C, micrographs of P3HT:C₆₀ (c) un-annealed substrate, (d) substrate annealed at 110 °C, micrographs of P3HT:PCBM (e) un-annealed substrate and (f) substrate annealed at 110°C. The inset in (d) and (f) correspond to films thermally annealed at 110 °C.

In addition, they verified that crystal growth with a relatively low diffusion rate of molecules compared to the incorporation rate, that is, a diffusion-limited system, showed the size increment linearly proportional to the square root of growth time ($L \propto t^{1/2}$) rather than to growth time ($L \propto t$). Therefore, we could identify that the highly ordered P3HT crystals (or fibres) suppressed or retarded the diffusion of C₆₀ or PCBM molecules into the blend under the substrate annealing condition and subsequently limited the enlarged growth of the C₆₀ or PCBM clusters as depicted in Fig. 5.5e by circles. The micrograph in Fig. 5.5d and f (insets) shows that the surface has clusters/agglomerates of C₆₀ or PCBM with different sizes distributed across the surface.

This is due to the fact that under the thermal-annealing conditions (at 110 °C), C₆₀ or PCBM molecules could freely diffuse into the blend films and readily form large PCBM clusters based on three possible causes: (1) a sufficiently large driving force of the external treatment to quickly move C₆₀ (or PCBM) molecules, (2) a blend film with a too large free volume due to randomly distributed polymer chains and (3) the longer drying time obtained for “selectively extracted” C₆₀ molecules to crystallize when a solvent (DCB) with higher solubility of C₆₀ is used. Initially, high-temperature annealing treatments may force the fast diffusion of PCBM molecules into the blend films and then interrupt the evolution of the highly elongated P3HT crystals. In general, the diffusion is a temperature controlled process that increases with temperature [5.40].

In order to observe the morphology evolution much clearer, AFM was used to monitor the height images of P3HT and blended films as shown in Fig. 5.6 and Table 5.1. Control of the blend morphology at the nanoscale and high charge mobility is essential for polymer photovoltaic devices in terms of their power conversion efficiencies. Hence, it was reported that the donor/acceptor (D/A) blend morphology can be controlled by spin-coating the blend from a specific solvent preventing large-size phase separation or enhancing the polymer chain packing [5.41, 5.42].

The as-prepared P3HT film in Fig. 5.6a has a very smooth surface. After substrate annealing at 70 °C, (Fig. 5.6b) fibres with several micrometers in length are dominantly observed across the film. Moreover, an associated increase in the surface roughness is observed, Table 5.1. This increase in surface roughness is considered to be a signal of polymer self-organization and phase separation and is in good agreement with results obtained by Motaung *et al.* [5.28]. Furthermore, the pre-annealed substrate (110 °C) with the film deposited thereafter demonstrates more fibres that are locally ordered and appear to be better connected with neighbours. The better connectivity of neighbouring fibres would be expected to make inter-rod transport easier by increasing the electronic overlap between neighbouring fibres, and could explain the increased mobility if transport in films prepared at 70 °C is limited by the boundaries between the fibres. It is suggested that the P3HT formation of these fibres is due to the early crystallization from presided crystals on a hot substrate before spin-coating due to the controlled evaporation rate.

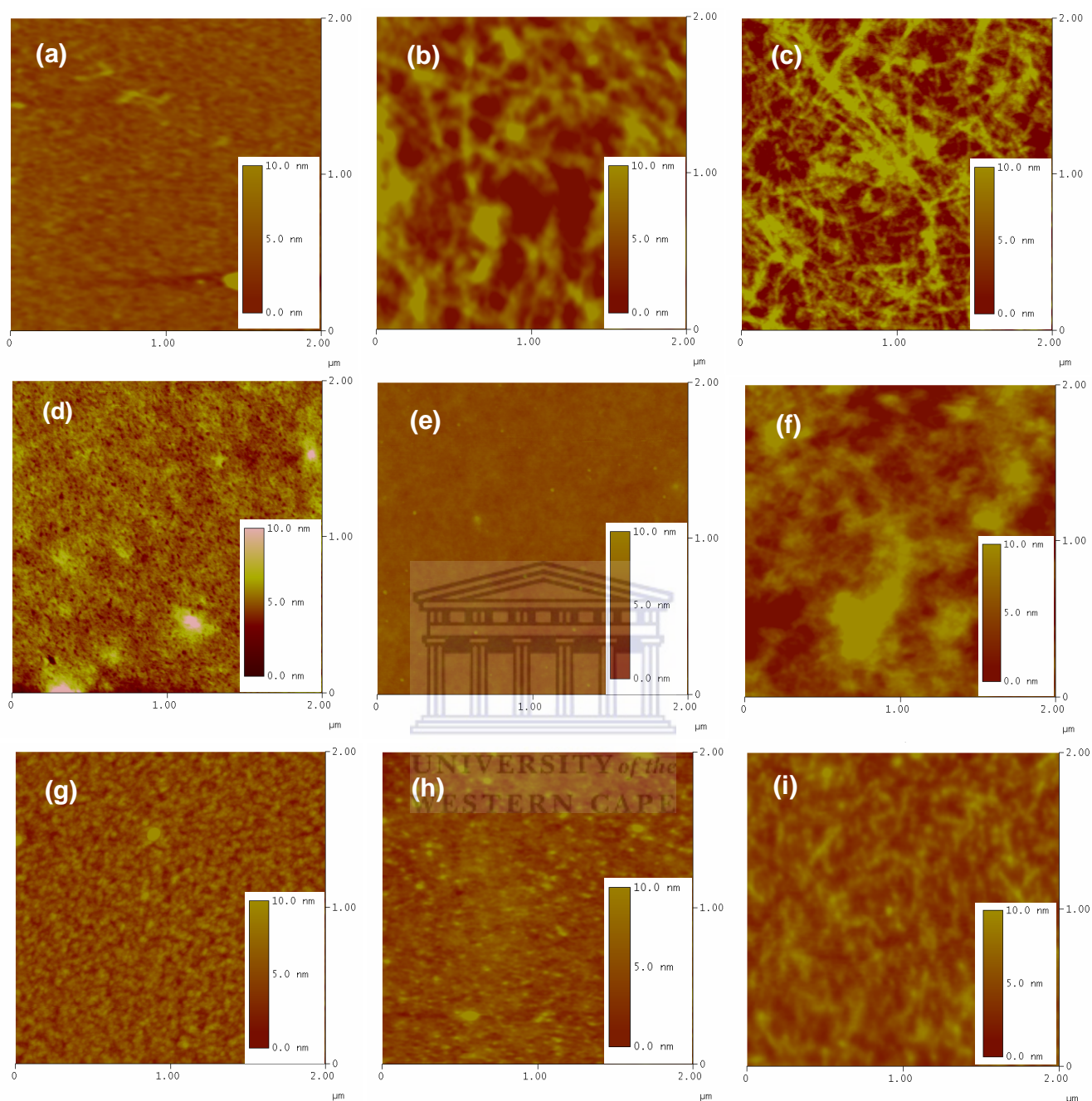


Figure 5. 6: AFM height images of P3HT (a) un-annealed substrate, (b) substrate annealed at 70 °C, (c) 110 °C; images of P3HT:C₆₀ (d) un-annealed substrate, (e) substrate annealed at 70 °C, (f) 110 °C; images of P3HT:PCBM (g) un-annealed substrate and (h) substrate annealed at 70°C and (i) 110 °C.

TABLE 5. 1: Root-mean-square roughness for different substrate annealing temperatures of P3HT and blended films.

Samples	Root-mean-square (rms) roughness (nm)		
	Un-annealed Si-Substrate	Substrate annealed at 70 °C	Substrate annealed at 110 °C
P3HT	0.74	2.56	2.75
P3HT:C ₆₀	0.81	1.02	4.42
P3HT:PCBM	1.07	0.89	1.13

Martens *et al.* [5.43] reported that the drying time is an important parameter for the size of the phase separated structures. They showed that by introducing a hot air flow over a drying film that the drying time could be decreased and consequently the extent of phase separation reduces. The as-prepared blended film of P3HT and C₆₀ in Fig. 5.6d exhibited a rather smooth surface, while the substrate annealed (70 °C) film displayed small C₆₀ clusters and a slight increase in roughness as shown in Fig. 5.6e, implying that the phase separation scale between C₆₀ and P3HT has been increased. However, the substrate annealed (110 °C) blended film of P3HT:PCBM (Fig. 5.6i) displayed short fibres, which might have been shortened by an inclusion of PCBM. We conclude that the formation of C₆₀ crystallites in combination with P3HT fibers contributes to an improved morphology in which not only large interface area for exciton dissociation is preserved but also bi-continuous pathways are constructed for

more efficient charge transport through the film. Therefore, better device performance can be anticipated.

5.3.3. Photo-physical properties

Mobility is a key factor for the efficient collection of photogenerated charges in solar cells [5.44-5.46]. As illustrated in Fig. 5.7 the mobility and conductivity of P3HT films substantially increases with the substrate annealing temperature. Since the mobility is a function of morphological variables such as the degree of crystallinity, crystallite size, phase domain size [5.44-5.46], it can be concluded that the enhancement of mobility is attributed to the improvement in the crystallinity and morphology as observed in the XRD, SEM and AFM analysis.

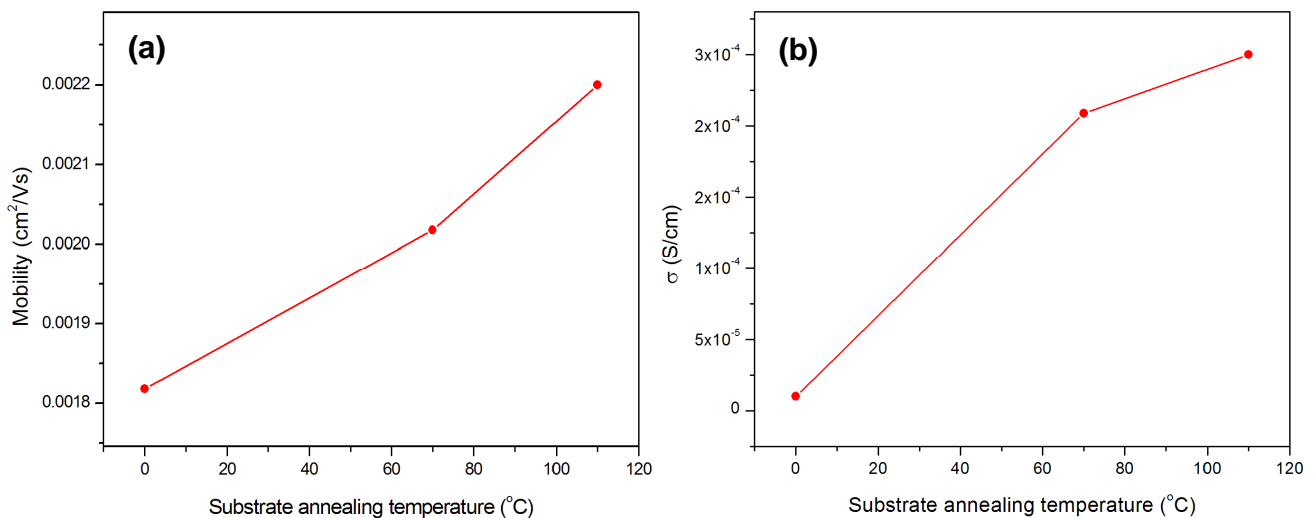


Figure 5. 7: Hall measurements on (a) the Mobility and (b) conductivity of P3HT films as a function of substrate annealing temperature annealing.

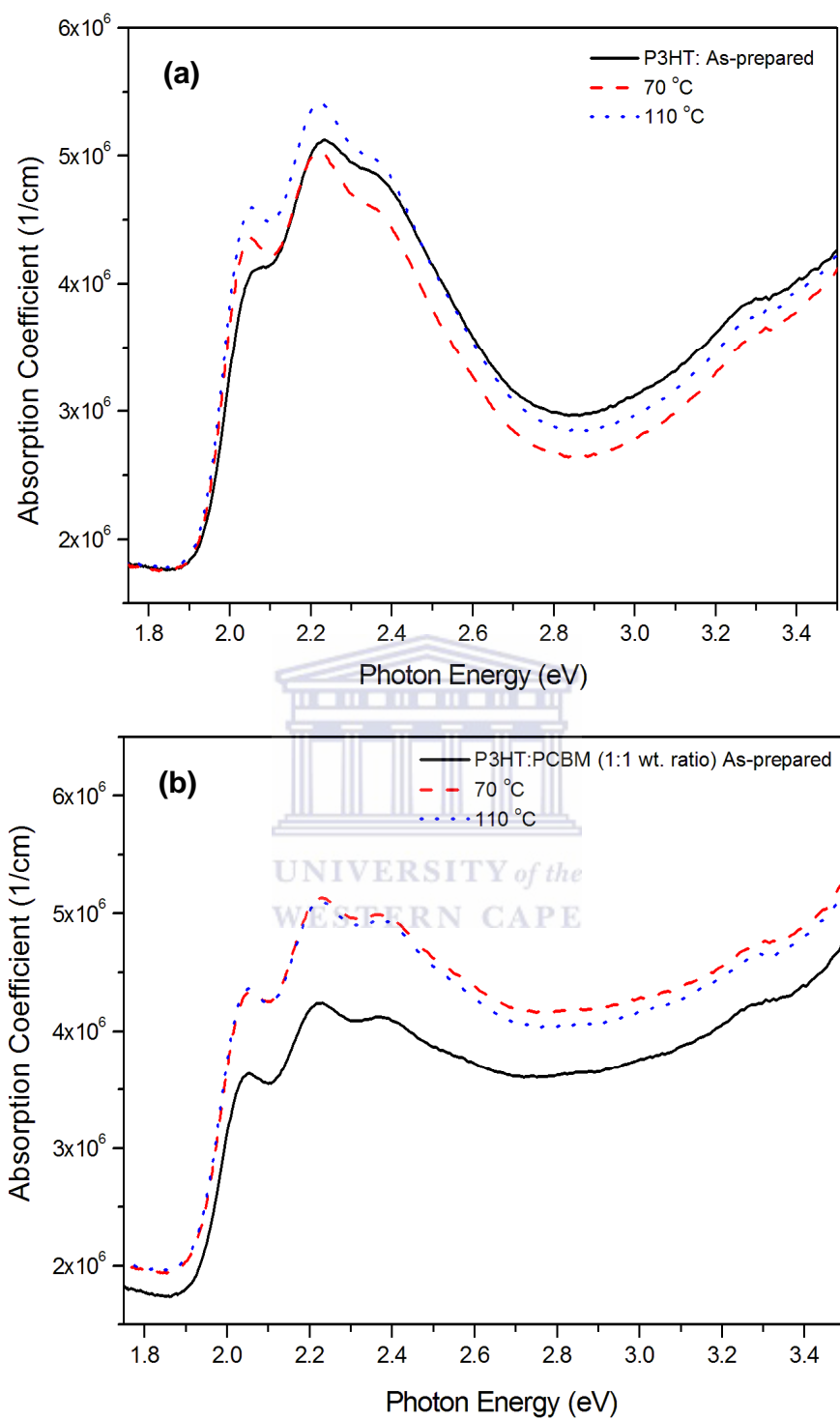
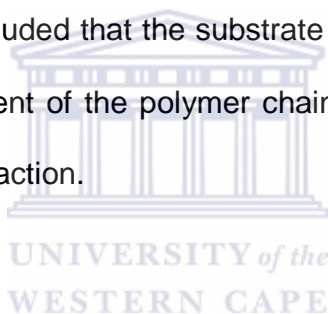


Figure 5. 8: UV-vis absorption spectra of the as-prepared and substrate annealed (a) P3HT films and (b) P3HT:PCBM (1:1 wt. ratio) blends.

This observation unambiguously confirms also that the increased P3HT crystallinity via the method introduced in this work plays a significant role in the improvement of conductivity of the thin film. This increase in conductivity may also be explained from the UV-vis spectra as shown in Fig. 5.8. The later shows a red shift of 0.02 eV, indicating that the band gap in the P3HT films decreases with the substrate annealing. This slight increase indicates a significant growth in the conjugation length of the polymer chains in the P3HT film, is induced by the controlled evaporation rate of the solvent during substrate annealing. Such shifts have been observed for conjugated polymers with a strong interchain interaction [5.15, 5.47]. It can be concluded that the substrate annealing treatment process enables spatial rearrangement of the polymer chains leading to a tight stacking and a strong interchain interaction.



5.4. CONCLUSION

The ability to control the film-drying rate via substrate annealing, opens a better route to obtain enhanced crystallinity and an optimal morphology. Pre-substrate annealing controls the crystallization of P3HT, the phase separation and diffusion of the acceptor material (C_{60} or PCBM) and also increases the electrical conductivity and Hall mobility of p-type P3HT. The SAED patterns revealed different crystallinity behaviours in P3HT: C_{60} blends which are mainly attributed to the relative solubility of C_{60} with respect to P3HT in DCB. The formation of self-assembled P3HT fibrillar structures that are locally ordered

contributes to an improved morphology in which inter-rod transport pathways are constructed for more efficient charge transport through the film and therefore, better device performance can be anticipated.



5.5. REFERENCES

- [5.1] C. W. Tang, Appl. Phys. Lett. 48 (1986) 183.
- [5.2] C. J. Brabec, N. S. Sariciftci, J. C. Hummelen, Adv. Funct. Mater. 11 (2001) 15.
- [5.3] S. E. Shaheen, D. S. Ginley, G. E. Jabbour, MRS Bull. 30 (2005) 10.
- [5.4] Z. Bao, A. Dodabalapur, A. J. Lovinger, Appl. Phys. Lett. 69 (26) (1996) 4108.
- [5.5] H. Sirringhaus, N. Tessler, R H. Friend, Science. 280 (5370) (1998) 1741.
- [5.6] J. F. Chang, B. Sun, D. W. Breiby, M. M. Nielsen, T I. Solling, H. Sirringhaus, Chem. Mater. 16 (2004) 4772.
- [5.7] D. H. Kim, Y D. Park, Y. Jang, H. Yang, Y H. Kim, K. Cho, et al. Adv. Funct. Mater. 15 (2005) 77.
- [5.8] G. Wang, J. Swensen, D. Moses, A. J. Heeger, J. Appl. Phys. 93 (10) (2003) 6137.
- [5.9] R. S. Loewe, S. M Khersonsky, R. D. McCullough, Adv. Mater. 11 (1999) 250.
- [5.10] M. C Iovu, E. E. Sheina, R. R. Gil, R. D. McCullough, Macromolecules 38 (21) (2005) 8649.
- [5.11] T. A. Chen, X. Wu, R. D. Rieke, J. Am Chem Soc. 117 (1995) 233.
- [5.12] A. Hayakawa, O. Yoshikawa, T. Fujieda, K. Uehara, S. Yoshikawa, Appl. Phys. Lett. 90 (2007) 163517
- [5.13] S.-I. Na, S.-H. Oh, S.-S. Kim, D.-Y. Kim, Org. Electron. 10 (2009) 496.

- [5.14] W. L. Ma, C. Yang, X. Gong, K. Lee, A. J. Heeger, *Adv. Funct. Mater.* 15 (2005) 1617.
- [5.15] G. Li, V. Shrotriya, J. Huang, Y. Yao, T. Moriarty, K. Emery, Y. Yang, *Nat. Mater.* 4 (2005) 864.
- [5.16] M. K. Riede, K. O. Sylvester-Hvid, M. Glatthaar, N. Keegan, T. Ziegler, B. Zimmermann, M. Niggenmann, A. W. Liehr, G. Willekr, A. Gombert, *Prog. Photovolt: Res. Appl.* 16 (2008) 561.
- [5.17] X. Yang, G. Lu, L. Li, E. Zhou, *Small* 3 (2007) 611.
- [5.18] X. Yang, J. Loos, S. C. Veenstra, W. J. H. Verhees, M. M. Wienk, J. M. Kroon, M. A. J. Michels, R. A. J. Janssen, *Nano Lett.* 5 (2005) 579.
- [5.19] L. H. Nguyen, H. Hoppe, T. Erb, S. Günes, G. Gobsch, N. S. Sariciftci, *Adv. Funct. Mater.* 17 (2007) 770.
- [5.20] R. S. Ruoff, D. S. Tse, R. Malhotra, D. C. Lorents, *J. Phys. Chem.* 97 (1993) 3379.
- [5.21] L. Li, H. Tang, H. Wu, G. Lu., X. Yang, *Organic Electronics* 10 (2009) 1334.
- [5.22] H.-G. Flesch, R. Resel, C. R. McNeill, *Org. Electron.* 10 (2009) 1549.
- [5.23] P. Vanlaeke, A. Swinnen, I. Haeldermans, G. Vanhoyland, T. Aernouts, D. Cheyns, C. Deibel, J. D' Haen, P. Heremans, J. Poortmans, J. V. Manca, *Sol. Energy Mater. Sol. Cells* 90 (2006) 2150.
- [5.24] H. Sirringhaus, P. J. Brown, R. H. Friend, M. M. Nielsen, K. Bechgaard, B. M. W. Langeveld-Voss, A. J. H. Spiering, R. A. J. Janssen, E. W. Meijer, P. Herwig, D. M. de Leeuw, *Nature* 401 (1999) 685.

- [5.25] T. Erb, U. Zhokhavets, G. Gobsch, S. Raleva, B. Stühn, P. Schilinsky, C. Waldauf, C.J. Brabec, *Adv. Funct. Mater.* 15 (2005) 1193.
- [5.26] U. Zhokhavets, T. Erb, H. Hoppe, G. Gobsch, N. S. Sariciftci, *Thin Solid Films.* 496 (2006) 679.
- [5.27] L. Li, G. L. and X. Yang, *J. Mater. Chem.* 18 (2008) 1984.
- [5.28] D. E. Motaung, G. F. Malgas, C. J. Arendse, S. E. Mavundla, C. J. Oliphant, D. Knoesen, *J. Mater. Sci.* 44 (2009) 3192.
- [5.29] H. Hoppe, M. Niggemann, C. Winder, J. Kraut, R. Hiesgen, A. Hinsch, D. Meissner, N. S. Sariciftci, *Adv. Funct. Mater.* 14 (2004) 1005.
- [5.30] D. Chirvase, J. Parisi, J. C. Hummelen, V. Dyakonov, *Nanotechnology* 15 (2004) 1317.
- [5.31] X. Yang, J. K. J. van Duren, R. A. J. Janssen, M. A. J. Michels, J. Loos, *Macromolecules* 37 (2004) 2151.
- [5.32] E. Klimov, W. Li, X. Yang, G. G. Hoffmann, J. Loos, *Macromolecules* 39 (2006) 4493.
- [5.33] D. E. Motaung, G. F. Malgas, C. J. Arendse, S. E. Mavundla, C. J. Oliphant, D. Knoesen, *Solar Energy Materials & Solar Cells* 93 (2009) 1674.
- [5.34] P. J. Brown, D. S.T homas, A. Kohler, J. S. Wilson, J.-S. Kim, C. M. Ramsdale, H. Sirringhaus, R. H. Friend, *Phys. Rev. B* 67 (2003) 064203.
- [5.35] C. Heller, G. Leising, G. Godon, S. Lefrant, W. Fischer, F. Stelzer, *Phys. Rev., B* 51 (1995) 8107.
- [5.36] K. Tashiro, M. Kobayashi, T. Kawai, K. Yoshino, *Polymer* 38 (1997) 2867.

- [5.37] C. Y. Yang, A. J. Heeger, *Synth. Met.* 83 (1996) 85.
- [5.38] J. X. Geng, T. Y. Zeng, *J. Am. Chem. Soc.* 128 (2006) 16827.
- [5.39] R. K. Singh, J. Kumar, R. Singh, R. Kant, S. Chand, V. Kumar, *Materials Chemistry and Physics* 104 (2007) 390.
- [5.40] W. D. Callister, Jr., *Materials Science and Engineering: An Introduction*, 5th ed., John Wiley, New York 2000.
- [5.41] S. E. Shaheen, C. J. Brabec, N. S. Sariciftci, F. Padinger, T. Fromerz, J. C. Hummelen, *Appl. Phys. Lett.* 78 (2001) 841.
- [5.42] J. K. J. van Duren, X. Yang, J. Loos, C. W. T. Bulle-Lieuwma, A. B. Sieval, J. C. Hummelen, R. A. J. Janssen, *Adv. Funct. Mater.* 14 (2004) 425.
- [5.43] T. Martens, Z. Beelen, J. D'Haen, T. Munters, L. Goris, J. Manca, *M. Proc. SPIE-Int. Soc. Opt. Eng.*, 40 (2003) 4801.
- [5.44] G. Tu, A. Bilge, S. Adamczyk, M. Forster, R. Heiderhoff, L. J. Balk, D. Muhlbacher, M. Morana, M. Koppe, M. C. Scharber, S. A. Choulis, C. J. Brabec, U. Scherf, *Macromol. Rapid Commun.* 28 (2007) 1781.
- [5.45] H. Xin, F. S. Kim, S. A. Jenekhe, *J. Am. Chem. Soc.* 130 (2008) 5424.
- [5.46] M. Dante, J. Peet, T. Q. Nguyen, *J. Phys. Chem. C* 112 (2008) 7241.
- [5.47] D. E. Motaung, G. F. Malgas, C. J. Arendse, S. E. Mavundla, D. Knoesen, *Materials Chemistry and Physics* 116 (2009) 279.

CHAPTER SIX

THE INFLUENCE OF THERMAL ANNEALING ON THE MORPHOLOGY AND STRUCTURAL PROPERTIES OF A CONJUGATED POLYMER IN BLENDS WITH AN ORGANIC ACCEPTOR MATERIAL

ABSTRACT

In this report, the influence of thermal annealing of thin P3HT films and P3HT:C₆₀ composites were studied regarding their morphology and structural properties. Atomic force microscope measurements on P3HT films and P3HT:C₆₀ composite disclose some variation in morphology during annealing due to the crystallization of C₆₀. The as-prepared P3HT:C₆₀ films have a higher surface roughness and larger cluster size compared to the as-prepared P3HT films. The thermal annealing effects on the optical microscopy indicate that the polymer shows improved capability to self-organize. Their structural properties were studied by X-ray diffraction analysis. It was found that the crystallinity of the investigated films is drastically increased upon annealing and a decrease in the grain sizes is observed.

The content of this chapter was published in: Journal of Material Science 44 (2009) 3192–

3197

6.1. INTRODUCTION

Plastic solar cells consisting of an interpenetrating network of fullerenes and conjugated polymers have gained wide spread scientific interest during the last decade due to their low production cost and easy solution processing, low specific weight mechanically flexibility [6.1-6.3]. Currently, the best devices consist of a single bulk-heterojunction (BHJ) active layer, where the polymer (donor) and fullerene (acceptor) are deposited from a common solvent. As the solvent dries the donor and acceptor components separate into domains. The eventual efficiency of the solar cell has shown to be extremely sensitive to the size, morphology, composition, and the crystallinity of the formed domains [6.4, 6.5].

Enhancement of the morphology in devices fabricated with a mixture of regio-regular poly(3-hexylthiophene) (P3HT) and [6,6]-phenyl C₆₁-butyric acid methyl ester (PCBM) has been observed with the use of heat-treatment methods, such as solvent annealing [6.6] and thermal annealing [6.3, 6.7–6.9] resulting in solar cells with higher power efficiencies (5%). The increase in solar cell efficiency can be explained by simultaneously increasing the optical absorption as well as the charge carrier mobility, which are correlated to the enhanced crystallization of P3HT during annealing [6.3]. Aasmundtveit *et al.* [6.10] reported that polythiophenes tend to crystallize in pristine P3HT films. Recently, it was shown by electron diffraction that P3HT is also capable of a crystalline organisation in blends with methanofullerenes [6.11].

Recently, power conversion efficiencies of up to 6.5% were reached for polymer tandem cells [6.12]. This progress has put polymer solar cells one step closer to commercialisation. In this article, the influence of thermal annealing on the morphology and structural changes of P3HT were investigated. The morphological changes of the active layers were monitored using various techniques. The d-spacing and size of polymer crystallites of as-prepared and annealed P3HT and its blends films were determined. The combination of XRD and AFM exhibited the difference between crystallization and the morphology of P3HT and C₆₀ during the annealing process.

6.2. EXPERIMENT DETAILS

6.2.1. Sample preparation

All the chemicals used in this experiment were purchased from Sigma Aldrich. Regio-regular poly(3-hexylthiophene) (rr-P3HT) was used as a light absorption and electron donating material; while fullerene (C₆₀) was used as an electron acceptor material. The molecular weight (M_n) of P3HT reported by Sigma Aldrich was ~64,000; with regularity that is greater than 98.5% for head-to-tail. These materials were used as received, without any further purification. Indium tin oxide (ITO) coated on a 1 mm glass substrate with a resistance between 8 and 12 Ω/square, and silicon (Si) (100) substrates were successfully cleaned with acetone and isopropyl alcohol and dried in dry nitrogen. A mixture of rr-P3HT (5 mg) and C₆₀ (5 mg) was dissolved in 1mL of chloroform solution. The solution was stirred over night at a temperature of 50 °C to maximize mixing

of P3HT:C₆₀ solution. The solubility of C₆₀ fullerene on a chloroform solution was reported to be about 0.16 mg/mL [6.13]. P3HT and its blends with a thickness of about 100 nm were spin coated onto the Si substrates. The samples were dried on a hot plate at a temperature of 50 °C for 15 min.

6.2.2. Characterization

A Tecnai F20 field emission high-resolution transmission electron microscope (HR-TEM), operated at 120 kV was employed to examine the internal structure and crystallinity of regio-regular P3HT. Specimens for HR-TEM analysis were prepared by dispersing the P3HT in chloroform, of which a drop was subsequently transferred to a holey-carbon copper grid and dried at ambient conditions. Atomic Force Microscopy (AFM) images of the top surface of thin films of regio-regular P3HT and its blends spin coated on Si (110) substrates in a tapping mode were analysed using a Veeco AFM system (Digital Instruments) at ambient conditions. A Polarised Optical Microscope (Carl Zeiss axiovisson) with a magnification of 100X was employed to study the optical morphology of the as-prepared P3HT films with that annealed at different temperatures for 30 min. Film thickness was measured using a Veeco DEKTAK 6M Stylus profilometer.

A Philips PW 1830 x-ray diffractometer with a Cu K_α ($\lambda = 0.154$ nm) monochromated radiation source, operating at 45.0 kV and 40.0 mA was utilized in order to determine the crystallinity of P3HT film and its blends spin coated onto a Si substrate. XRD data were collected in the 2 θ ranging from 3° to 40° with a

step size of 0.02° . The grain sizes of the films were calculated using the Scherrer formula.

6.3. RESULTS AND DISCUSSION

6.3.1. Atomic force microscopy measurements

The morphology of the polymer/acceptor composite or photoactive layers, that play a key role in the final solar cell performance, can be strongly modified and improved by thermal annealing. The surface topography obtained from an atomic force microscope (AFM) usually gives a good insight into the film formation ability and the tendency of the components to phase separate. Fig. 6.1 shows a series of AFM images of the P3HT and its blends obtained in tapping mode. The surface of the as-prepared P3HT on a Si substrate and P3HT:C₆₀ (1:1 wt. %) films is very smooth with a root mean square (rms) roughness (σ_{rms}) of 1.375 and 1.679 nm, respectively. The film does not show any coarse separation into different phases. The P3HT:C₆₀ (1:1 wt. %) film (Fig. 6.1d) shows a higher surface roughness, which is probably due to the addition of the fullerene (C₆₀) forming clusters around the film.

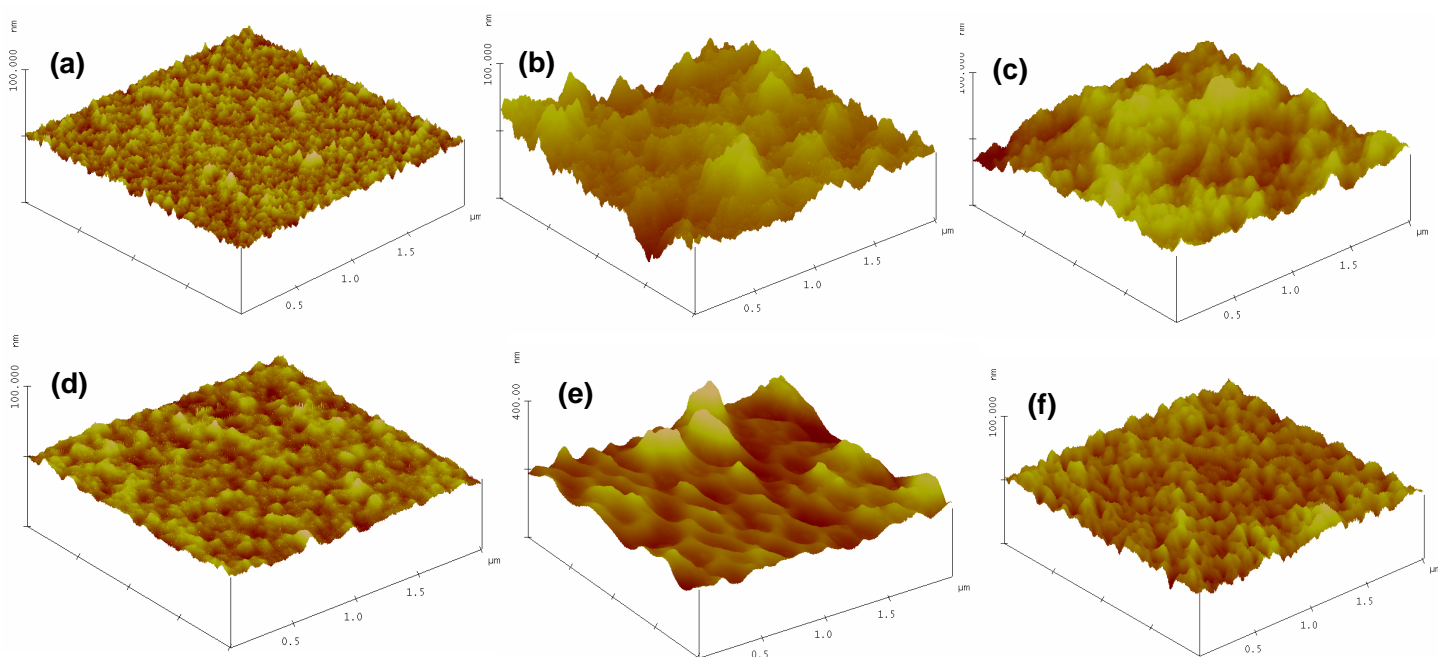


Figure 6. 1: AFM height images ($2\mu\text{m}\times 2\mu\text{m}$ size) of the surface of the active layer consisting of (a) as-prepared pure P3HT, (b) annealed at $110\text{ }^{\circ}\text{C}$, (c) annealed at $150\text{ }^{\circ}\text{C}$, (d) as-prepared P3HT:C₆₀ (1:1 wt. %), (e) P3HT:C₆₀ (1:1 wt. %) annealed at $110\text{ }^{\circ}\text{C}$, and (f) annealed at $150\text{ }^{\circ}\text{C}$. Note all the samples were annealed for 30 min.

However, upon annealing at $110\text{ }^{\circ}\text{C}$ for 30 min (Fig. 6.1b) the surface roughness of P3HT increases up to 7.89 nm, while P3HT:C₆₀ (1:1 wt. %) film (Fig. 6.1e) show a pronounced surface roughness of about 18.90 nm. When the samples were annealed at $150\text{ }^{\circ}\text{C}$, the surface roughness increased up to 8.25 and 19.31 nm for P3HT and the blend, respectively. It is evident in Fig. 6.1 that the annealed samples show a much coarser texture with broad “hill-like” features compared with the as-prepared samples. The rough surface is probably a

signature of polymer reorganization, which in turn enhances ordered structure formation in the thin film and also increases the carrier mobility which could produce a higher efficiency from the devices. This suggests that there is a thermodynamic driving force for the sample to reorganize towards a more stable equilibrium and thus to phase separate. However, excessive roughness makes phase segregation excessively comparable to the exciton diffusion length, which leads to the reduced charge segregation and device efficiencies. Similar results were also observed in the literature [6.14-6.16]. Recent morphological and structural studies [6.11] have shown that in P3HT: PCBM active layers the crystallization and the demixing are interdependent parameters.

6.3.2. Transmission electron microscopy measurements

The HR-TEM micrograph presented in Fig. 6.2 illustrates that the rr-P3HT are crystalline. The micrograph shows a homogeneous layer without any obvious phase separation. The inset in Fig. 6.2 corresponds to the fast Fourier transform (FFT) of the selected area. The FFT shows a very low crystallinity of P3HT indicating that P3HT material is composed of an amorphous polymer matrix with crystalline regions (circled in Fig. 6.2) which possess a spacing of $\sim 0.8 \pm 0.06$ nm, corresponding to the (200) planes. Drees *et al.* [6.17] also reported a bright field TEM image of P3HT showing a large and extended disordered (amorphous) zone between the crystalline lamellae.

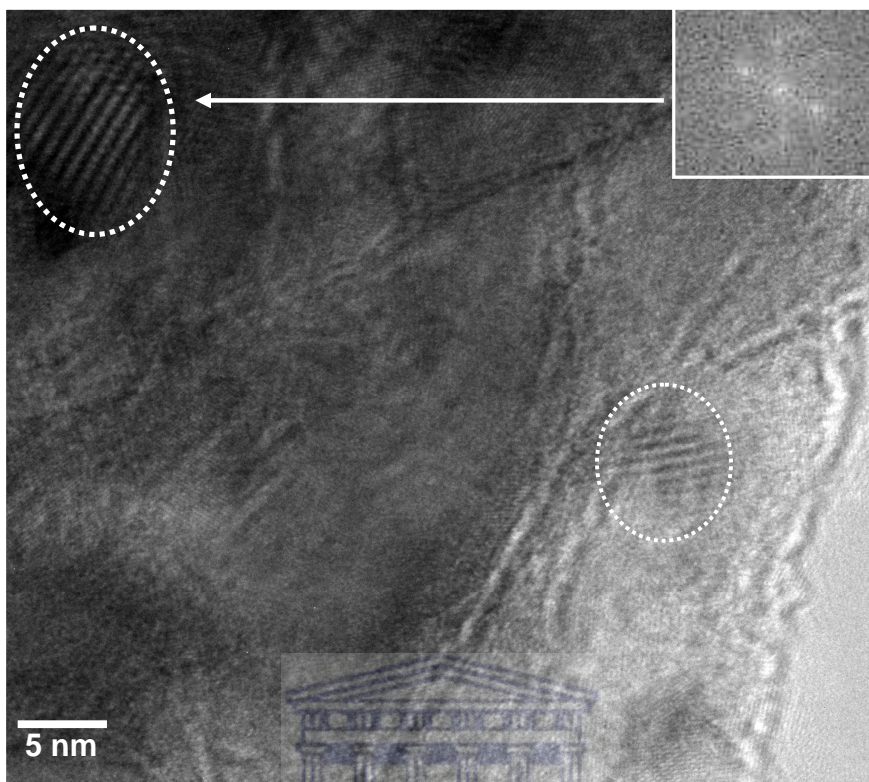


Figure 6. 2: HR-TEM micrograph of the rr-P3HT film and the corresponding fast Fourier transform (FFT) of the selected area (inset).

6.3.3. Optical microscopy measurements

Bright field optical microscopy micrographs of as-prepared P3HT films and P3HT:C₆₀ (1:1 wt. %) blends compared with that annealed at 110 °C and 150 °C for 30 min are shown in Fig. 6.3. It is evident in Fig. 6.3a that the as-prepared P3HT film is relatively smooth with tarnishes (small stains). When these films are annealed their optical contrast changes, the film becomes rougher and agglomerations of the films are observed. These changes in the optical micrographs are due to the annealing, indicating an enhancement in the crystallinity of the P3HT films.

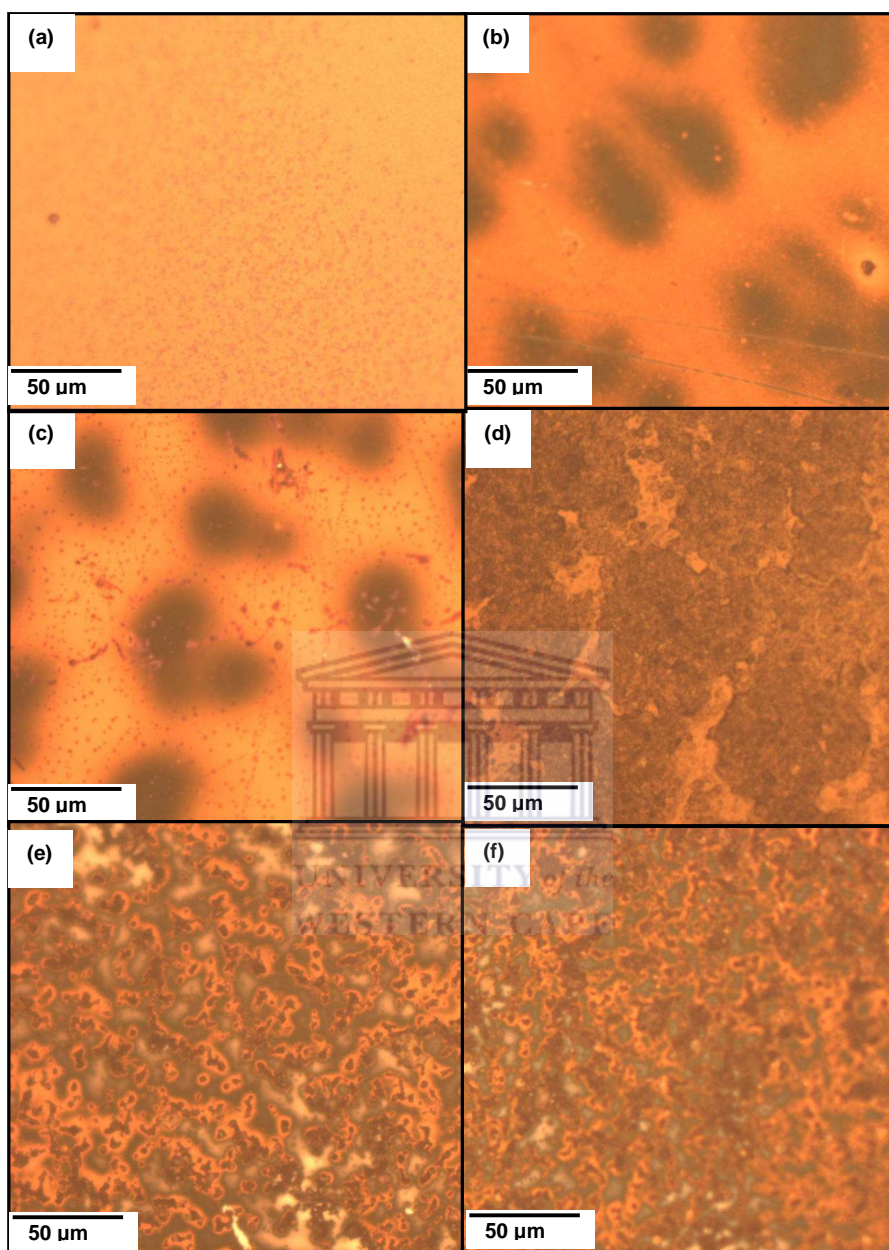
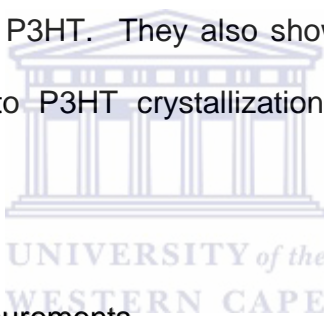


Figure 6. 3: Optical microscopy images of (a) as-prepared P3HT (b) P3HT film annealed at 110 °C, (c) P3HT film annealed at 150 °C, (d) as-prepared P3HT:C₆₀ (1:1 wt. %) blend, (e) annealed blend at 110 °C, and (f) annealed blend at 150 °C. Note all the samples were annealed for 30 min.

Moreover, when P3HT sample was blended with a C₆₀ fullerene, P3HT:C₆₀ (1:1 wt. %) (Fig. 6.3d), the as-prepared blend film showed an irregular behaviour and with larger agglomeration (spheres) as compared to as-prepared and annealed P3HT film. These agglomerations (or spheres) are related to C₆₀. However, when the blend is annealed, the spheres become bigger and show an increase in coarseness. The clustering of the spheres is probably due to a diffusion of C₆₀ into P3HT during annealing. This is in good agreement with results obtained by the AFM technique as well the results reported by Nguyen *et al.* [6.18]. Campoy-Quiles *et al.* [6.19] observed colour visible changes during a continuous heating cycle of P3HT. They also showed that these visible colour changes may correspond to P3HT crystallization which is then followed by melting of the material.



6.3.4. X-ray diffraction measurements

For a detailed study of the structural ordering of rr-P3HT, an XRD diffraction technique was used. Additionally, the changes upon thermal annealing of the films for 30 min at different temperatures were analyzed. Fig. 6.4 shows the XRD spectra of the as-prepared P3HT films and its blends P3HT: C₆₀ (1:1 wt. %) compared with that annealed at 110 and 150 °C for 30 min, respectively. The as-prepared sample shows a single diffraction peak before annealing at $2\theta = 5.4^\circ$ which is associated with the lamella structure of thiophene rings in P3HT [6.20]. Upon annealing, the sample shows a secondary peak (200) at 10.8° and tertiary peak (300) at 15.9° indicating that all pristine P3HT films show a well-organized

intraplane structure. The diffraction patterns of Fig. 6.4 correspond to as describe by the JCPDS {48-2040}. The peak indicated by the arrow at about 28.1° is associated with the Si substrate. However, the blend in Fig. 6.4b showed a (220), (311), (222) and (331) diffraction peaks at 17.7, 20.9, 21.7 and 27.4° upon annealing at 150 °C, which are associated with a C₆₀ fullerene as describe by the JCPDS {47-0787, 44-0558}. The corresponding lattice constant *d*, can be calculated using Bragg's law:

$$2d\sin(\theta) = n\lambda \quad (6.1)$$

where $\lambda = 0.154$ nm is the wavelength of incident beam, 2θ is the angle between incident and scattered X-ray wave vectors and *n* is the interference order. Therefore, using equation 6.1, we obtain $d = 1.64 \pm 0.05$ nm, 0.82 ± 0.05 nm and 0.56 ± 0.05 nm. The 0.82 nm spacing is similar to the *d*-spacing found in the TEM results. The detected peak originates from the P3HT crystallites with *a*-axis orientation (polymer backbone parallel and side chains perpendicular to the substrate) [6.21]. However, no diffraction peaks corresponding to the P3HT crystallites with other orientations such as polymer backbone and side chains parallel to the substrate were observed [6.22]. The mean sizes of the P3HT crystallites at (100) reflection L_{100} can be obtained using Scherrer's relation: [6.23, 6.24].

$$L = \frac{0.9\lambda}{B_{2\theta} \cos(\theta)} \quad (6.2)$$

where λ is the wavelength of the x-rays, $B_{2\theta}$ is the full width at half maximum intensity (FWHM) and θ is the diffraction angle. Therefore employing Scherer formula (6.2) we obtain the grain size of P3HT and P3HT:C₆₀ films at different annealing temperatures as shown in Table 6.1. As shown in Fig. 6.4 and Table 6.1, the emergence of a crystalline phase in the as-prepared samples is observed which is in good agreement with the HR-TEM results. This crystalline phase becomes more pronounced at a temperature of 150 °C. A minimum grain size of 12 nm is found in the as-prepared P3HT sample. At around 150 °C the grain size growth is well increased. This indicates an increase in the ordering of the alkyl chains within the main thiophene chains. However, when a P3HT is blended with C₆₀ fullerene (1:1 wt. %), the full width at half maximum (FWHM) of P3HT at 5.4° increases with the annealing temperature. The increase in a FWHM (reduction in grain sizes) as well a slight decrease in P3HT crystallites is due to a disordering of P3HT chains caused by an addition of C₆₀ fullerene. This can also be due to a diffusion of C₆₀ molecules out of the P3HT matrix forming larger clusters leading to a phase separation of P3HT and C₆₀.

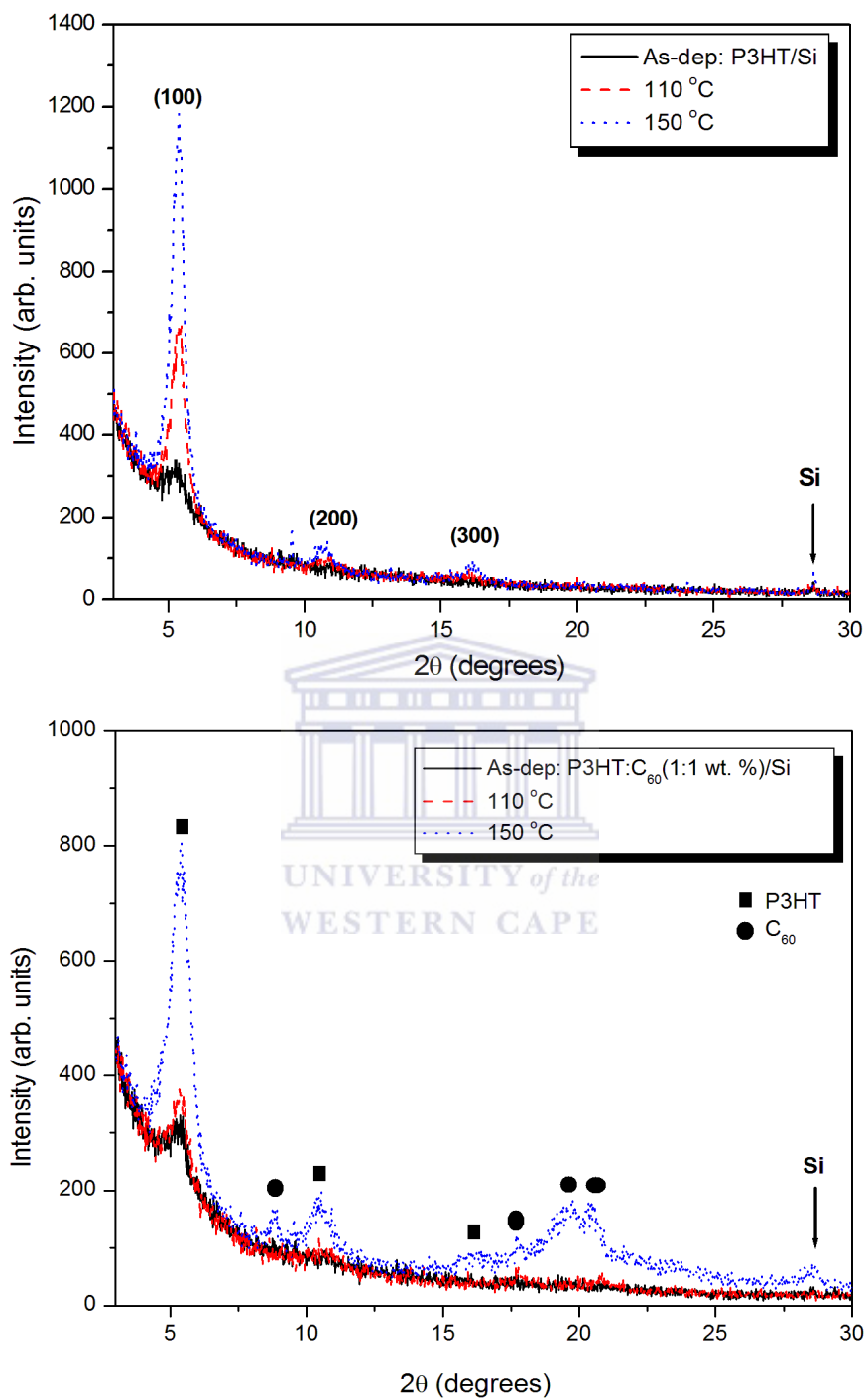


Figure 6. 4: XRD patterns of as-prepared and annealed (a) rr-P3HT film and its blend (b) P3HT: C₆₀ (1:1 wt. %) at 110 °C and 150 °C for 30 min. The P3HT peaks are indicated by a square and C₆₀ by a circle.

TABLE 6. 3: Grain size of P3HT and P3HT:C₆₀ (1:1 wt. %) films for different annealing temperatures.

	<i>P3HT Film</i>			<i>P3HT:C₆₀ Composite Film</i>		
	RT	110	150	RT	110	150
Temperature (°C)	RT	110	150	RT	110	150
Grain Size (nm)	12.2	13.4	15.9	17.2	14.7	12.1

Kline *et al.* [6.25] reported that films of higher molecular weight P3HT produces a broader XRD peak suggesting a more disordered film with smaller crystalline domains. The authors argue that the smaller π -stacked domains, connected by disordered polymer chains, would enable easier charge transport through the film and prevent charge trapping within crystalline domains or at grain boundaries. Chiu *et al.* [6.26] showed that when P3HT is blended with PCBM, the P3HT crystallite size reduces with an increase in annealing temperature and resulted in an increase in the short circuit current density (J_{sc}). They also showed that the particles of PCBM become larger and subsequently lead to better pathways for electron transport. Additionally, the C₆₀ clusters also enable better hole transport in the polymer phase. However, Huang *et al.* [6.27] demonstrated that longer annealing time (more than 60 min) exhibit too larger PCBM clusters, which leads to decrease in charge transport and device efficiency. It should be noted, that the obtained values correspond to the domain size along the a-axis and that no crystal with b- or c-axis orientation was

detected. Similar results on d-spacing were reported by Kim *et al.* [6.28] and Erb *et al.* [6.22].

6.4. CONCLUSION

In conclusion, we have studied the morphology and structural properties of P3HT films and P3HT:C₆₀ composite films both as-prepared and annealed at different temperatures. AFM measurements showed that the blends have a higher surface roughness compared to the pure P3HT films. After annealing, the surface roughness of pure P3HT and P3HT:C₆₀ (1:1 wt. %) film increased; this can be related to a signature of polymer reorganization, which in turn enhances ordered structure formation in the thin film. HR-TEM results showed a homogeneous layer of P3HT film without any obvious phase separation. The TEM studies also exhibited very low features of crystallization that indicates that it composed of an amorphous network with crystallites embedded in it. XRD studies have also demonstrated the crystalline nature of pure P3HT films. The as-prepared P3HT-films were found to be partially crystalline whereas the crystallinity increases as the temperature increases. In the case of the film annealed at 150 °C; a crystallite size of 15.9 nm was obtained from analysis of the X-ray diffraction pattern. A slight decrease in P3HT crystallites and an increase in grain sizes were observed when a P3HT:C₆₀ (1:1 wt. %), blended structure were prepared. This is due to a disordering of P3HT chains caused by the addition of fullerene. Upon annealing a reduction in the grain sizes was also

observed. This is probably due to a diffusion of C_{60} molecules out of P3HT matrix forming larger clusters leading to a phase separation of P3HT and C_{60} .



6.5. REFERENCES

- [6.1] S.-S. Sun and N. S. Sariciftci, Organic photovoltaics: mechanisms, materials, and devices, CRC Press, Boca Raton, FL, (2005).
- [6.2] C. J. Brabec, V. Dyakonov, J. Parisi and N. S. Sariciftci, Organic photovoltaics: concepts and realization, Springer, Berlin, Germany, (2003).
- [6.3] W. Ma, C. Yang, X. Gong, K. Lee, A. J. Heeger, Adv. Funct. Mater. 15, 1617 (2005).
- [6.4] H. Hoppe, N. S. Sariciftci, J. Mater. Chem. 16, 45 (2006).
- [6.5] J. J. M. Halls, A. C. Arias, J. D. MacKenzie, W. S. Wu, M. Inbasekaran, E. P. Woo, R. H. Friend, Adv. Mater. 12, 498 (2000).
- [6.6] G. Li, Y. Yao, H. Yang, V. Shrotriya, G. Yang, Y. Yang, Adv. Funct. Mater. 17 1636 (2007).
- [6.7] F. Padinger, R. S. Rittberger, N. S. Sariciftci, Adv. Funct. Mater. 13, 85 (2003).
- [6.8] X. N. Yang, J. K. J. Van Duren, M. T. Rispens, J. C. Hummelen, R. A. J. Janssen, M. A. J. Michels, J. Loos, Adv. Mater. 16 802 (2004).
- [6.9] N. Camaioni, G. Ridolfi, G. Casalbore-Miceli, G. Possamai, M. Maggini, Adv. Mater. 14 1735 (2002).
- [6.10] K. E. Aasmundtveit, E. J. Samuelsen, M. Guldstein, C. Steinsland, O. Flornes, C. Fagermo, T.M. Seeberg, L.A.A. Pettersson, O. Ingana's, R. Feidenhansl, S. Ferrer, Macromolecules. 33, 3120 (2000).
- [6.11] X. Yang, J. Loos, S.C. Veenstra, W.J.H. Verhees, M.M. Wienk, J.M. Kroon, M.A.J. Michels, R.A.J. Janssen, Nano-lett. 5, 579 (2005).

- [6.12] J. Y. Kim, K. Lee, N. E. Coates, D. Moses, Thuc-Quyen Nguyen, M. Dante, A. J. Heeger *Science* 317 222 (2007).
- [6.13] R. S. Ruoff, S. Doris. R. Tse, Malhotra, D. C. Lorents *J. Phys. Chem* 97 3379 (1993).
- [6.14] G. Li, V. Shrotriya, Y. Yao and Y. Yang, *J. Appl. Phys.* 98, 043704 (2005).
- [6.15] Y Kim, S. A. Choulis, J. J Nelson, D. D. C Bradley, J.. *Mat. Sci.* 40 (2005) 1371.
- [6.16] H-Z Yu, J-B Peng, *Chin. Phys. Lett.* 25, 1411 (2008)
- [6.17] M. Drees, H. Hoppe, C. Winder, H. Neugebauer, NS. Sariciftci, W. Schwinger, F. Schaffler, C. Topf, M. C. Scharber, Z. Zhud, *J. Mater. Chem.* 15 5158 (2005).
- [6.18] L. H. Nguyen, H. Hoppe, T. Erb, S. Günes, G. Gobsch, N. S. Sariciftci, *Adv. Funct. Mater.* 17 1071 (2007).
- [6.19] M. Campoy-Quiles, T. Ferenczi, T. Agostinelli, P. G. Etchegoin, Y. Kim, T. D. Anthopoulos, P. N. Stavrinou, D. D. C. Bradley, J. Nelson, *Nature Mat.* 7, 158 (2008).
- [6.20] J.Y. Kim, S.H. Kim, H.H. Lee, K. Lee, W. Ma, X. Gong, A.J. Heeger, *Adv. Mater.* 18, 572 (2006).
- [6.21] T. Erb, S. Raleva, U. Zhokhavets, G. Gobsch, B. Stuhn, M. Spode, O. Ambacher, *Thin Solid Films* 450, 97 (2004).
- [6.22] T. Erb, U. Zhokhavets, H. Hoppe, G. Gobsch, M. Al-Ibrahim, O. Ambacher, *Thin Solid Films* 511, 483 (2006).
- [6.23] B. E Warren, *X-Ray Diffraction* (New York: Dover) p. 251 (1990).

[6.24] B. D. Cullity, Elements of X-Ray Diffraction, Addison-Wesley, Reading, MA (1956).

[6.25] R. J. Kline, M. D. McGehee, E. N. Kadnikova, J. Liu, J. M. J. Frechet, Adv. Mater. 15, 1519 (2003).

[6.26] M.-Y. Chiu, U-S. Jeng, C-H. Su, Keng S. Liang, K. H. Wei, Adv. Mater. 20, 2573 (2008).

[6.27] Y.-C. Huang, et al., Sol. Energy Mater. Sol. Cells (2008), doi:10.1016/j.solmat.2008.10.027.

[6.28] Y. Kim, S. Cook, S. M. Tuladhar, S. A. Choulis, Nature Materials 5, 197 (2006).



CHAPTER SEVEN

THERMAL INDUCED CHANGES ON THE PROPERTIES OF SPIN-COATED P3HT:C₆₀ THIN FILMS FOR SOLAR CELL APPLICATIONS

ABSTRACT

The thermal transition behaviour, optical and structural properties of spin-coated P3HT:C₆₀ blended films with different C₆₀ ratios were investigated using differential scanning calorimetry (DSC), thermo-gravimetric analysis (TGA), ultraviolet-visible (UV-Vis) spectroscopy, photoluminescence (PL), Fourier transform infrared absorption (FT-IR) spectroscopy and Raman spectroscopy. DSC analysis showed that the P3HT:C₆₀ blends have quite different thermal characteristics. The absorption spectra of the annealed P3HT:C₆₀ (1:1 wt. %) films becomes enhanced and red shifted. This feature is evident in the photoluminescence measurements where the formation of polymer crystallites upon annealing is observed. Raman spectroscopy showed a substantial ordering in the polymer film during annealing. It was found that the performance of a P3HT:C₆₀ (1:1 wt. %) device was dramatically improved by annealing.

The content of this chapter was published in: Solar Energy Materials & Solar Cells 93

(2009) 1674–1680

7.1. INTRODUCTION

During the last decade, plastic solar cells have attracted substantial research interest because of their advantageous properties, such as low cost, light weight, large-area fabrication and mechanical flexibility [7.1-7.7]. The main focus in the organic solar cell research lies on increasing the power conversion efficiency under simulated sunlight [7.8]. It has been reported that by using high mobility donor polymers (e.g. poly(3-hexylthiophene) (P3HT)) and fullerene derivative, phenyl-C₆₁-butyric acid methyl ester (PCBM), as an electron acceptor yield a power conversion efficiencies (PCEs) of 5% [7.8-7.10]. Recently, PCE of up to 6.5% were reached for tandem cells [7.11]. Apart from the power conversion efficiency, there is however at least two other important factors that will put organic solar cells one step closer to commercialisation, such as processing into large area modules [7.5, 7.7, 7.12-7.13] and long-term stability of devices [7.13-7.22]. The production of very large area plastic solar cell modules up to 1000 cm² has been reported [7.5, 7.7, 7.13]. This has shown that it is highly feasible with existing technology to mass produce polymer solar cells at a very low cost.

Studies on the stability of organic photovoltaic cells have typically focussed on optimisation of the stability of encapsulated devices under continuous light illumination [7.13-7.15, 7.18-7.20]. Brabec *et al.* [7.20] reported lifetimes of up to 2000 h continuous operation for devices protected from oxygen and water ingress. However, lifetimes of up to 6000 h were achieved with an entirely flexible encapsulation technology [7.13]. Krebs *et al.* [7.14, 7.15] found a stable

polymer solar cell with a lifetime of up to 10000 h with the careful exclusion of water and oxygen. They also predicted an operational lifetime in excess of 20 000 h by using a thermal acceleration factor of 4 between 25 and 72 °C and an indoor illumination intensities of 50-100 W m⁻². It has been reported that ITO/ZnO/ZnO:poly-(3-carboxydithiophene) (P3CT)/PEDOT:PSS/Ag inverted type solar cells without sealing maintained 80 % of the initial performance for continuous illumination for 100 h in an ambient atmosphere [7.21]. In spite of tremendous advances in both the understanding and fabrication of organic solar cells, operational stability has reached a lifetime up to a year under outside conditions [7.17, 7.23]. These studies on the stability/degradation [7.13-7.22] issues showed that the topic is rather complicated and not fully understood.

Among conjugated polymers, poly(3-alkylthiophenes) (P3ATs) are one of the most promising conducting polymers because of their interesting electronic and optical properties and also because of their processability and chemical stability. Recently, semi crystalline regioregular poly(3-hexylthiophene) (P3HT) has attracted a lot of attention as a donor material, as it has the highest charge carrier mobility among the conjugated polymers and an absorption edge around 650 nm (band gap of 1.9 - 2.0 eV), combined with a high hole mobility exceeding 0.1 cm²/Vs [7.24]. These qualities make P3HT a good candidate for the polymer in polymer photovoltaic cells [7.8, 7.25–7.26]. In this paper, the thermal transition behaviour, structural and optical properties of P3HT:C₆₀ films with different blends are investigated at different annealing temperatures.

7.2. EXPERIMENT DETAILS

7.2.1. Sample preparation

All the chemicals used in this experiment were purchased from Sigma Aldrich. A regio-regular poly(3-hexylthiophene) (RR-P3HT) polymer was used as a light absorption and electron donating material; while a C₆₀ fullerene was used as an electron acceptor material. These materials were used as received, without further purification. Indium tin oxide (ITO) coated on a 1 mm glass substrate with a resistance between 8 and 12 Ω/square, was successively cleaned with solvents and dried in dry nitrogen. A mixture of rr-P3HT (5 mg) and C₆₀ with different ratios (2.5 mg, 5 mg, 20 mg) was dissolved in 1mL of chloroform solution. The solution was stirred over night at 50 °C in order to mix the P3HT:C₆₀ solution completely. A thin layer of poly(3,4-ethylenedioxythiophene):poly (styrenesulfonate) (PEDOT:PSS) solution was spin coated onto the ITO glass substrates and onto silicon (Si) substrates with the spin rate of 2500 rpm for 30 s. This was followed by thermal treatment of the substrates at 100 °C for 30 min.

The P3HT:C₆₀ blend with a thickness of about 100 nm was spin coated onto the PEDOT:PSS layer. The spinning rate and time of spin-coating were 2500 rpm and 30 s, respectively. However, for some samples no poly(3,4-ethylenedioxythiophene)-polystyrene sulphonic acid (PEDOT:PSS) layer was deposited onto the ITO/Glass and Si substrates. The samples were dried on a hot plate at a temperature of 50 °C for 15 min. The thermal annealing procedure

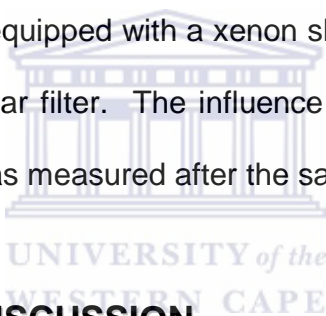
was accomplished by placing the P3HT:C₆₀/ITO/Glass or P3HT:C₆₀/Si structures in an oven at different temperatures ranging from 85 - 150 °C for a period of 30 min.

7.2.2. Characterization

The absorption spectra of the P3HT:C₆₀ organic layers with different ratios taken before and after the annealing procedure were measured by a Perkin Elmer UV/VIS spectrometer from 900 to 300 nm. The photoluminescence (PL) spectra were measured by exciting the samples with 350 nm line of deuterium lamp. It should be noted that for some photoluminescence and Raman measurements, that the blends deposited onto Si (100) substrates were used. The PEDOT:PSS/ITO glass substrates was not used in order to avoid masking of P3HT features which overlap with those of PEDOT. The emission was detected with Jobin Yvon PMT detector. The structure of pure P3HT with different concentrations of C₆₀ was characterized by Fourier transform infrared spectroscopy (FT-IR) using a Perkin Elmer FT-IR spectrometer and Raman spectroscopy using a Horiba Jobin Yvon HR800 micro-Raman spectrometer. The Raman spectroscopy measurements were conducted at room temperature with a 514 nm excitation laser. It should also be noted that for some FTIR and Raman spectroscopy measurements that the blends were spin-coated on a Si (100) substrate. The films thickness was measured using a Veeco DEKTAK 6M Stylus profilometer. Differential scanning calorimetry (DSC) curves for P3HT, C₆₀ and the two different P3HT:C₆₀ blends were obtained with a TA Q2000 DSC.

Approximately 7 mg of each sample was loaded in an aluminium pan. The analyses were conducted from -50 °C to 250 °C at heating and cooling rates of 10 °C /min and a nitrogen flow rate of 5 mL/min. Thermo-gravimetric analysis (TGA) (stability measurements) was performed on the two different P3HT:C₆₀ blends using a TA Q500 thermogravimetric analyser. Measurements were carried out in an oxygen atmosphere at a heating rate of 10 °C /min from room temperature to 950°C.

Solar cells were completed by evaporating 100 nm of Al on top of the active layer. The current–voltage (IV) characteristics were measured using a Keithley 2420 and a solar simulator equipped with a xenon short arc lamp with a power of 150 W and an AM 1.5G solar filter. The influence of thermal annealing on the photovoltaic performance was measured after the samples were annealed.



7.3. RESULTS AND DISCUSSION

7.3.1. Differential scanning calorimetry (DSC)

The thermal behaviour of P3HT and blends of P3HT:C₆₀ (1:1 wt. %) and P3HT:C₆₀ (1:4 wt. %) have been studied by DSC analysis. Fig. 7.1 shows the differential scanning calorimetry (DSC) measurements of P3HT and its blends heated from -50 °C to 250 °C in a nitrogen gas at a flow rate of 5 mL min⁻¹. It is evident from the cooling curves (Fig. 7.1a) that an endothermic transition is centred at 199.9 °C in regioregular P3HT and with a glass transition (T_g) \approx -4.7 °C. Zhao *et al.* [7.27] reported that during a non-isothermal experiment that at a

slower cooling rate, the crystallization of P3HT would start at higher temperatures, quite slowly and then continue over a wide temperature range. The transition shows the typical features of a melting/crystallization transition. The melting temperature depends on the crystallization conditions. A transition enthalpy value ($\Delta H=17.5$ J/g) was obtained during an exothermic transition from a crystalline to a liquid crystalline state around 229 °C. However, Chen *et al.* [7.28] determined a melting temperature of 240–245 °C for head-to-tail regioregular P3HT, while no indication for a glass transition temperature was given.

It is observed that DSC analysis of fullerene has two crystallizations peaks at around -16.6 °C and -15.2 °C (arrow) with a relaxation region at ~ 14.7 °C and an enthalpy of 8.9 J/g (Fig. 7.1b). When the polymer (P3HT) is blended with a C₆₀ (1:1 wt. %), as shown in Fig. 7.1c, they both exhibit endothermic and exothermic events which shifts to lower temperatures. The shifting of P3HT to lower temperatures is due to an addition of C₆₀. For the P3HT:C₆₀ (1:4 wt. %) blend (Fig. 7.1d), it can be seen that P3HT peaks become flat (or disappear), indicating that C₆₀ fullerene has an effect on the structure of P3HT. A similar behaviour was observed by Cugola *et al.* [7.29].

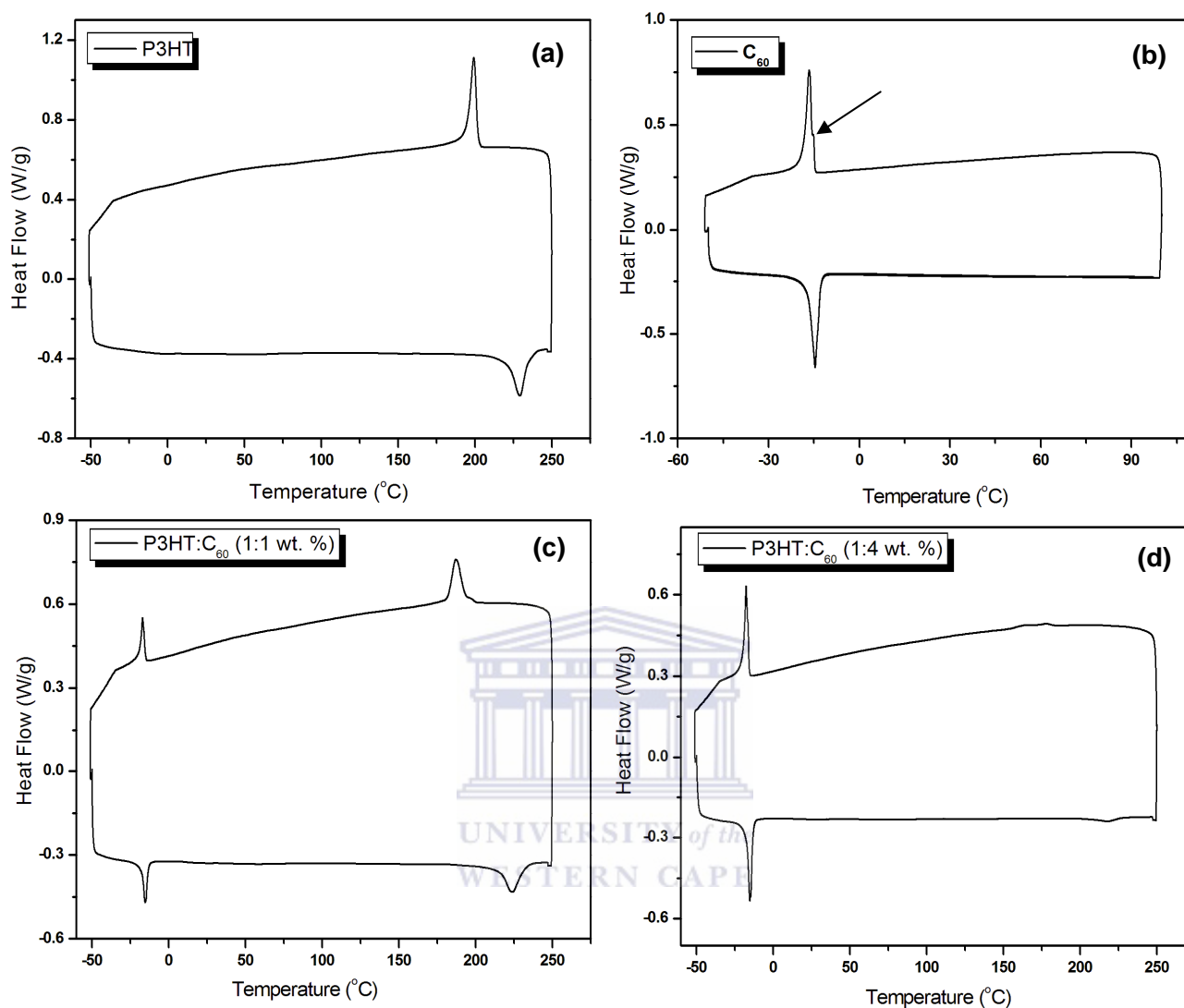


Figure 7. 1: DSC curves of (a) P3HT, (b) fullerene (C₆₀), (c) P3HT: C₆₀ (1:1 wt. %) and (d) P3HT: C₆₀ (1:4 wt. %), at heating rates of 10 °C min⁻¹ with a nitrogen flow rate of 5 mL min⁻¹.

7.3.2. Thermo-gravimetric analysis (TGA)

To estimate the thermal stability of P3HT:C₆₀ with different C₆₀ ratios, TGA analysis was performed in an O₂ atmosphere. Fig. 7.2 shows the TGA and

differential thermal analysis (DTA) of (a) P3HT:C₆₀ (1:1 wt. %) and (b) P3HT:C₆₀ (1:4 wt. %) blends. During sample preparation, nearly equal amounts (~7 mg) of the blends were loaded into a platinum pan. It is observed from Fig. 7.2a that the P3HT:C₆₀ (1:1 wt. %) mass loss takes place in a two-step mechanism, where the DTA consists of two maxima at temperatures around 454 and 614 °C. The first step of the mass loss began at about 430 °C and the second step began at about 526 °C. Such an oxidation at high temperature obviously cannot be due to physisorbed species [7.30].

The beginning of the mass loss is probably due to the loss of an alkyl side group attached to the aromatic thiophene backbone (hexyl group). As the temperature increases above 500 °C, the oxidation is accelerated and the pyrolysis of the aromatic backbone of polymer chains is ignited. It can be seen from Fig. 7.2b that the P3HT:C₆₀ (1:4 wt. %) composites exhibit slightly inferior thermal stability with increasing amount of fullerene contents as compared to the P3HT:C₆₀ (1:1 wt. %) blend. The first step of the mass loss began at about 420 °C and the second step began at about 518 °C. This may be due to low physico-chemical bonding states and microstructural features of the composites including the branching/percolating. Kumar *et al.* [7.31] showed that when P3HT is blended with a high amount of single walled carbon nanotubes (SWCNTs), the thermal stability decreases. Therefore, it can be concluded that the addition of fullerene C₆₀ to P3HT reduces the thermal stability of P3HT.

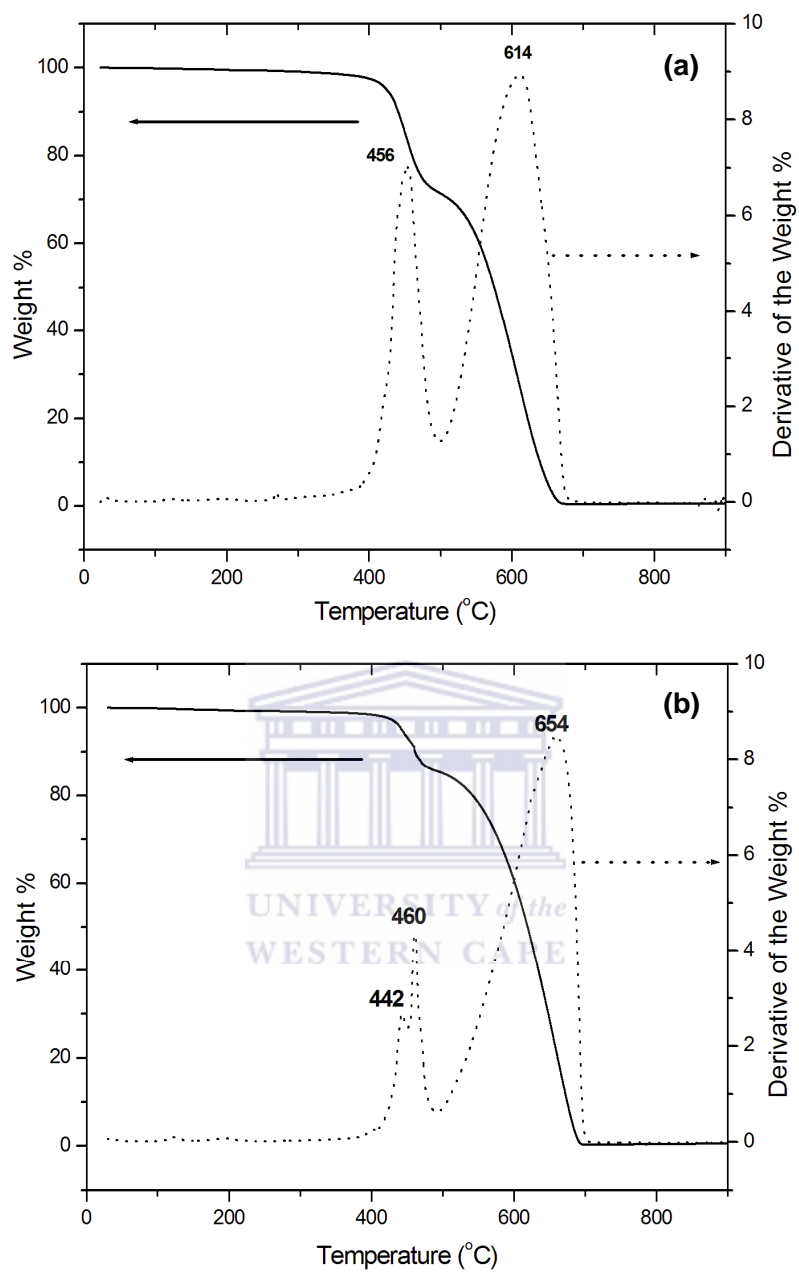
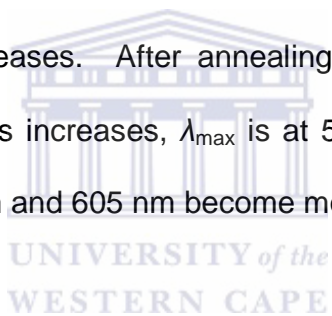


Figure 7. 2: TGA graphs of (a) P3HT:C₆₀ (1:1 wt. %), (b) 1:4 wt. % and its derivative plot showing the decomposition stages.

7.3.3. Ultraviolet-Visible Spectroscopy (UV-Vis)

Absorption spectra of mixtures of P3HT:C₆₀ with different ratios dissolved in chloroform solution were investigated before and after thermal annealing. Fig. 7.3 shows the UV–Vis spectra measured for as-prepared P3HT: C₆₀ (1:1 wt. %) films and that annealed at different temperatures. For the as-prepared film, the maximum peak absorption wavelength is at 502 nm with a shoulder at 600 nm and a barely visible shoulder at 544 nm. The effect of thermal annealing on the absorption spectra is apparent for the films treated at different temperatures. Broadening of the spectra towards longer wavelengths is observed when the annealing temperature increases. After annealing at 110 °C and above, the intensity of absorption peaks increases, λ_{max} is at 513 nm, showing a red shift, and the shoulders at 546 nm and 605 nm become more distinguishable.



The film annealed at 150 °C shows a similar behaviour as the one annealed 110 °C, this is clearly a superposition of the two spectra. Similar results were obtained for the P3HT:C₆₀ (1:4 wt. %) blend (results not shown). The absorption shift in the spectra suggests that annealing induced some ordering in the polymer chains. These changes may be attributed to an increasing interchain interaction among P3HT chains. It also indicates strong interchain–interlayer interactions among the P3HT chains as well as good polymer ordering in the blend films [7.28, 7.32-7.34]. The increasing interchain interaction among the P3HT chains because of thermal annealing results in more delocalized conjugated π electrons, the lowering of the band gap between π and π^* , and the

increase of the optical $\pi-\pi^*$ transition which results in the observed red shift in the peak absorption wavelength.

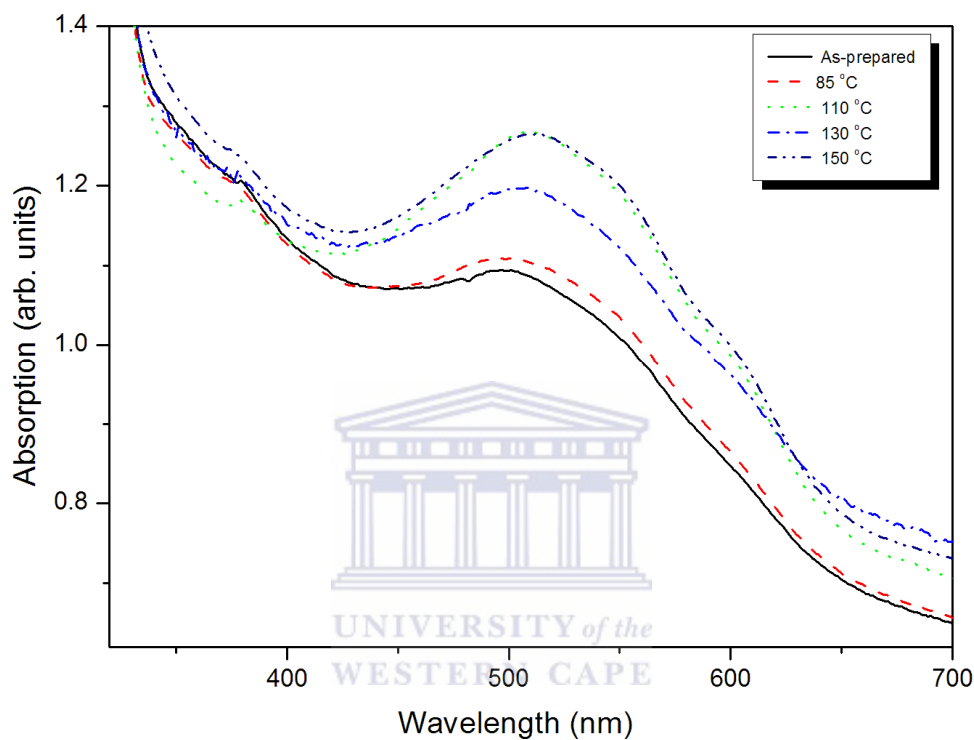


Figure 7. 3: Absorption spectra of an as-prepared P3HT:C₆₀ (1:1 wt. %) composite film compared with that annealed at different temperatures. The annealing time for all the films was 30 min.

7.3.4. Photoluminescence (PL)

Photoluminescence measurements on P3HT:C₆₀ thin films (Fig. 7.4) provide further evidence of the formation of polymer crystallites. The photoluminescence of the annealed sample is several times higher than that of the as-prepared ones. This indicates that the photo-induced electron transfer from the polythiophene

becomes less efficient upon annealing. However, Malgas *et al.* [7.30] showed that a complete quenching is observed for a P3HT:C₆₀ (1:1 wt. %) composite film without thermal annealing. The efficiency of electron transfer depends obviously on the mean distance between the conjugated polymer and fullerene molecules.

If the distance between the polymer and fullerene becomes comparable with the exciton diffusion length (~10 nm), some excitons cannot reach the neighbouring fullerene molecule and recombine radiatively, giving rise to the photoluminescence signal. Since the concentration of the C₆₀ in the film does not change upon annealing, we conclude that the change of the photoluminescence intensity originates from a phase separation and thus changes in the morphology of the active layer. Furthermore, in agreement with the crystallization process, a polymer aggregate formation is strongly indicated by the observation of a characteristic red shift in the PL spectrum of the annealed sample [7.35].

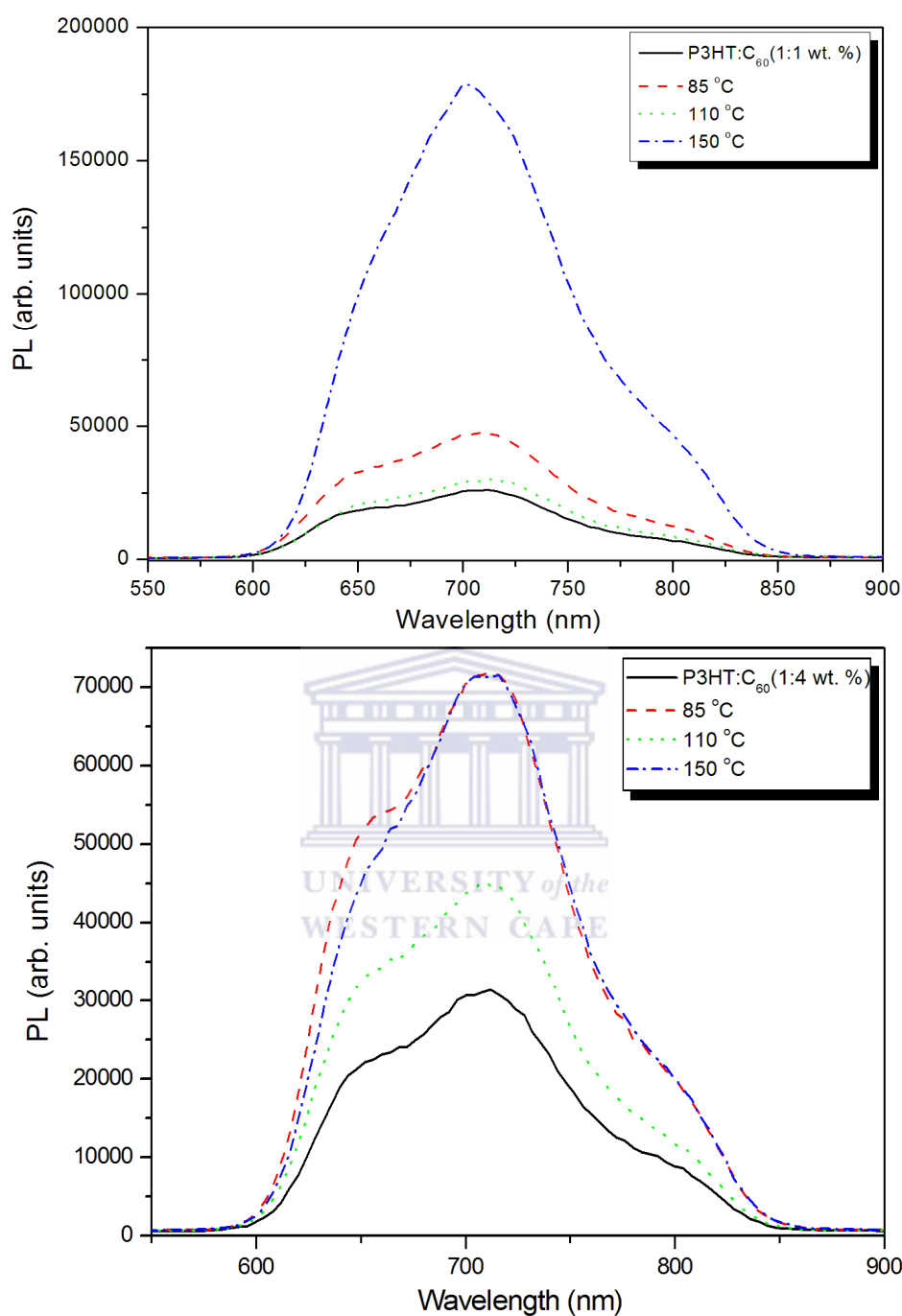
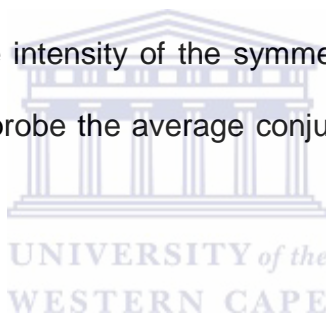


Figure 7. 4: Photoluminescence spectra of (a) P3HT:C₆₀ (1:1 wt. %) and (b) 1:4 wt. %. as-prepared and the annealed films. A considerable increase of the structure and some red-shift is observed, typical for crystalline ordering of the conjugated polymer.

7.3.5. Fourier Transform Infrared Spectroscopy (FT-IR)

The FTIR spectra of rr-P3HT films deposited on a Si substrate and compared with that annealed at different temperatures are shown in Fig. 7.5. The absorption band assignments of the FTIR absorption peaks for rr-P3HT are given in Table 7.1. The thiophene ring associated with P3HT shows an out of plane deformation of C-H, and the band at 819 cm^{-1} is assigned to this C-H deformation vibration of P3HT. The peak at 1509 and 1457 cm^{-1} represents the antisymmetric C=C stretching and symmetric stretching mode of P3HT, respectively. The ratio between the intensity of the antisymmetric stretching mode at 1509 cm^{-1} and the intensity of the symmetric stretching peak mode at 1456 cm^{-1} can be used to probe the average conjugation length of P3HT [7.36, 6.37].



When the P3HT films are annealed at different temperatures, little or no shifts to shorter or longer wavenumbers are observed for the aliphatic-C-H stretching vibrations and the C-H out of plane deformation. However, the intensity of the aliphatic-C-H stretching and aromatic-C-H out plane vibrations increases with an increase in annealing temperature, suggesting that the relative amount of twisting moiety in the crystalline state increases. Street *et al.* [7.38] reported that annealing induces the reorientation of lamellae and formation of high-mobility percolation paths with low-angle grain boundaries.

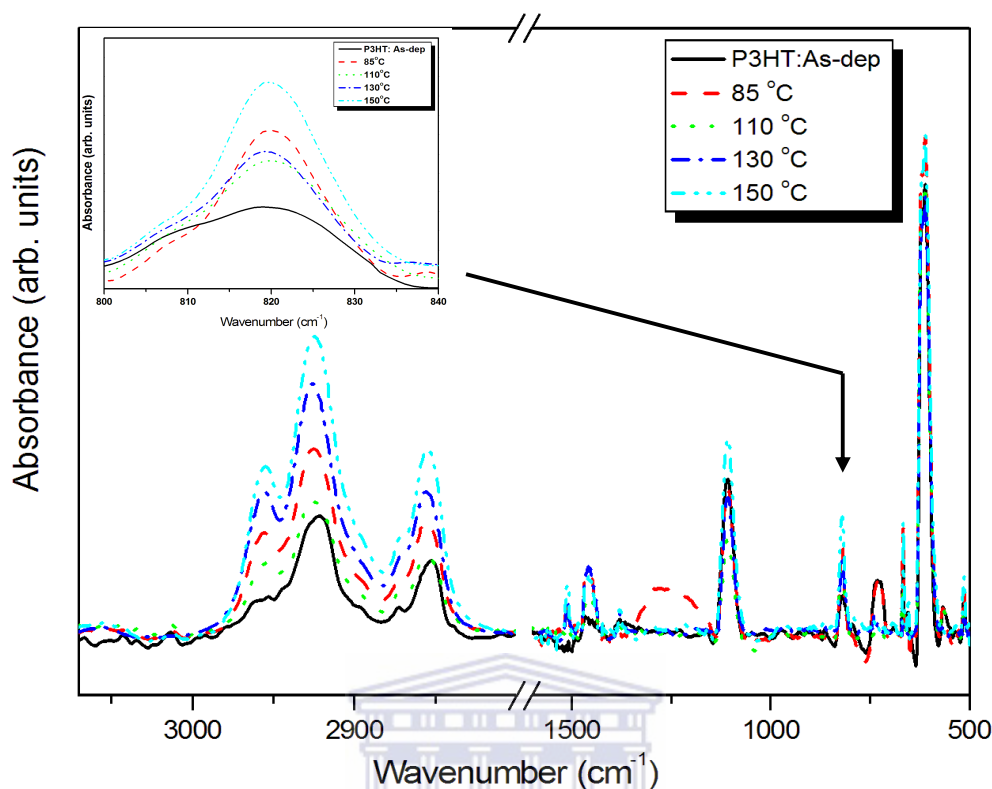


Figure 7. 5: FTIR absorbance spectra of as-prepared rr-P3HT films compared with that annealed at different temperatures for 30 min.

TABLE 7. 1: FTIR band positions (cm^{-1}) of P3HT films and their assignments annealed at different temperatures.

Sample (P3HT)	C-H out of Plane mode	Anti symmetric C=C stretching mode	symmetric C-C stretching mode	Aliphatic C-H stretching mode
[6.24, 6.25]	819	1509	1456	2850, 2921, 2954
(85 °C)	820	1507	1457	2856, 2925, 2955
(110 °C)	820	1507	1457	2856, 2925, 2955
(130 °C)	820	1507	1457	2856, 2925, 2955
(150 °C)	820	1507	1457	2856, 2925, 2955

7.3.6. Raman Spectroscopy

Fig. 7.6 compares the Raman spectra of the rr-P3HT films deposited on a Si substrate with that annealed at different temperatures for 30 min. The spectrum of the rr-P3HT film deposited on Si features all the vibrational frequencies expected for the conjugated polymer [7.39]. The peak at 1450 cm^{-1} can be attributed to the symmetric C=C stretching deformation, while the medium intensity band at 1375 cm^{-1} is associated with C–C stretching deformations in the aromatic thiophene ring [7.35, 7.40]. In order to extract additional information from the Raman spectra, we compared the $1350\text{--}1500\text{ cm}^{-1}$ region of P3HT film before and after thermal annealing (insert Fig. 7.6).

It is observed that the intensity in the Raman shift of the symmetric C=C mode and C–C mode in the aromatic thiophene ring increases with annealing temperature suggesting a substantial ordering in the polymer film during heating. This is in good agreement with the photoluminescence data. No peak shift are observed in the C=C signal after annealing. A downward shift in the wavenumber generally indicates an increase in the crystallinity of P3HT polymer and the extension of the effective conjugation length along the polymer backbone [7.41].

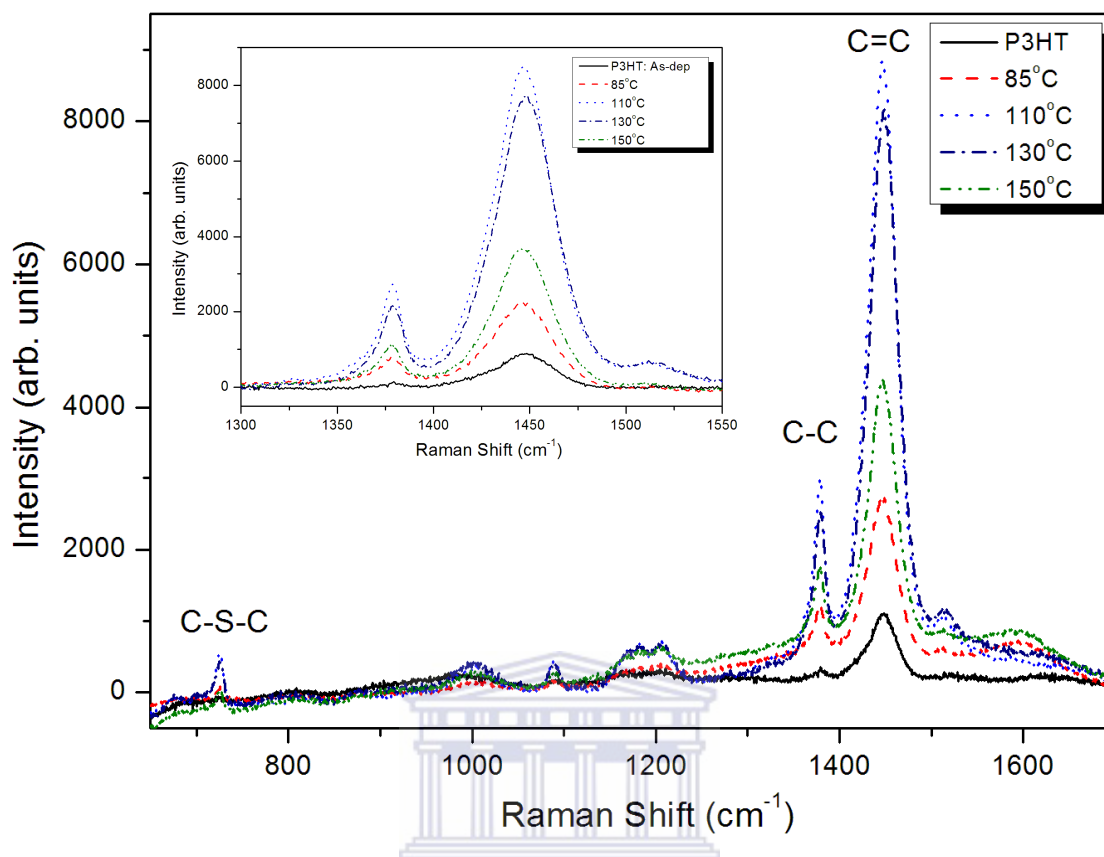


Figure 7. 6: Raman spectra of rr-P3HT film spin-coated on a Si substrate compared with that annealed at different temperatures for 30 min.

7.3.7. Photovoltaic measurements

A popular strategy to improve the power conversion efficiency with a fixed material system is by post-production annealing. We have carried out the thermal treatment of the devices before the metal (Al) electrode deposition. The dark $J-V$ curves of the P3HT devices with different C_{60} ratios are shown in Fig. 7.7a. The conductivities of the P3HT: C_{60} were increased by blending C_{60} . The higher the concentration of C_{60} , the higher the conductivity of P3HT: C_{60} devices. The device performance for as-prepared and annealed photovoltaic devices of the type

ITO/P3HT:C₆₀ (1:1 wt. %)/Al under AM1.5 conditions with light intensity of 1000W/m² at room temperature are shown in Fig. 7.7b. Improvements of the photovoltaic characteristics are observed during annealing in Fig. 7.7 and Table 7.2.

The short-circuit current density and fill factor increased for the higher temperature annealed (150 °C) device, leading to an improvement of power conversion efficiency going from $\eta = 0.009\%$ for the as-prepared device to $\eta = 0.029\%$ for the 150°C annealed sample; suggesting that the carrier transport network in the cells was promoted. However, the open-circuit voltage decreases upon annealing. It has been demonstrated that in polyalkylthiophenes the improvement of three dimensional ordering/conjugation is leading to lower oxidation potentials [7.42]. Therefore the increase of polymer ordering by thermal annealing (also observed by UV-vis and Raman spectroscopy), may account for the drop-off of V_{oc} .

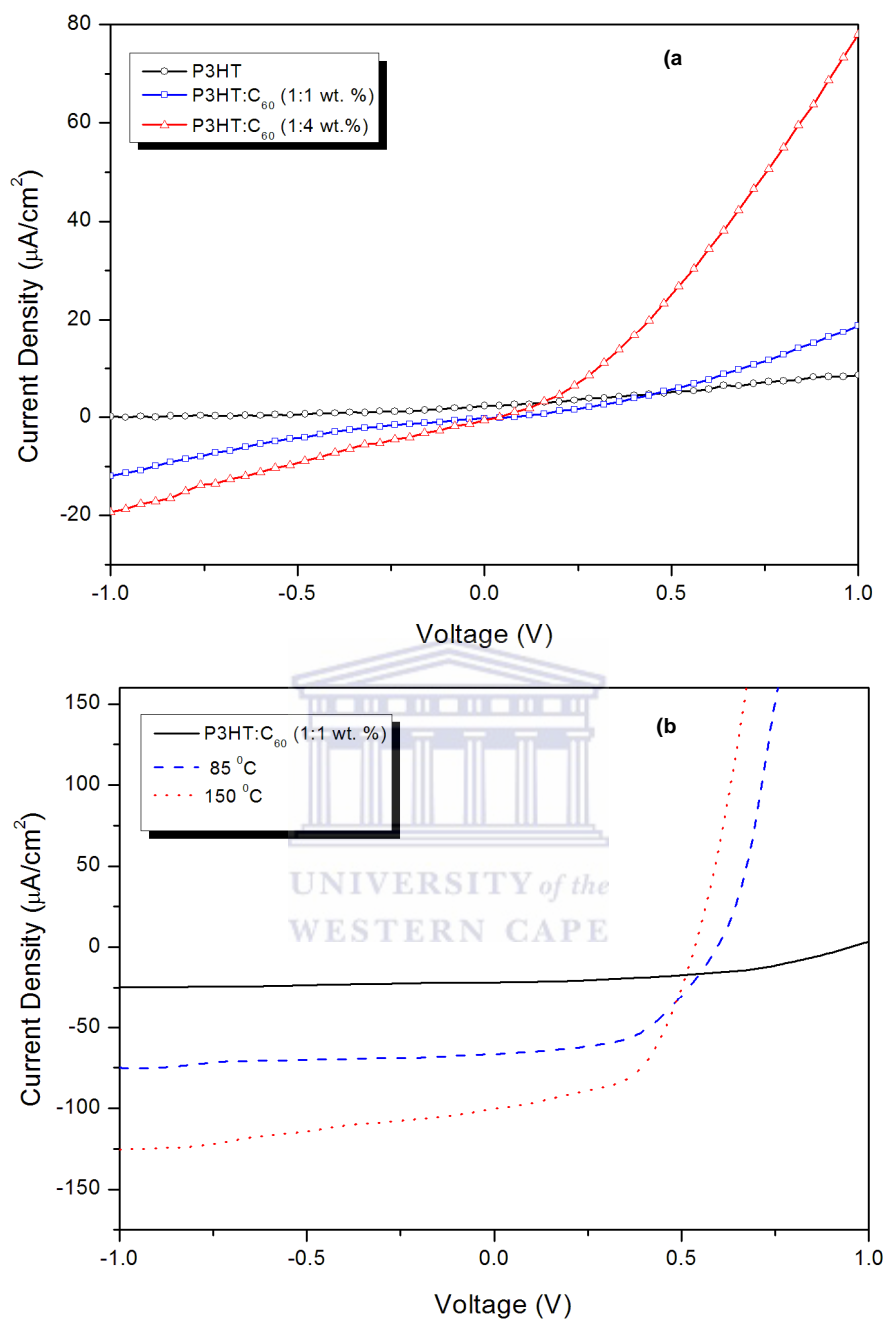


Figure 7. 7: Current density–voltage (J–V) characteristics of the (a) P3HT:C₆₀ solar cells with different C₆₀ ratios in dark and (b) as-prepared and annealed P3HT:C₆₀ (1:1 wt. %) devices under white light illumination.

TABLE 7. 2: Photovoltaic devices performance of P3HT:C₆₀ (1:1 wt. %) structures before and after annealing.

<i>Device Architecture</i>	<i>J_{sc} (μA/cm²)</i>	<i>V_{oc} (V)</i>	<i>FF</i>	<i>η (%)</i>
Glass/ITO/P3HT:C ₆₀ (50 wt. %)/Al As-prepared	21.87	0.96	0.43	0.009
Glass/ITO/P3HT:C ₆₀ (50 wt. %)/Al 85 °C	66.95	0.59	0.52	0.021
Glass/ITO/ P3HT:C ₆₀ (50 wt. %)/Al 150 °C	100.1	0.54	0.54	0.029

7.4. CONCLUSION

We have studied the structural and optical properties of both as-prepared and annealed P3HT:C₆₀ blended films using, DSC, TGA, UV–Vis absorption, photoluminescence, FT-IR, and Raman spectroscopy. DSC analysis showed that the blends have quite different thermal properties. TGA thermographs showed that the P3HT:C₆₀ composites exhibit a slightly inferior thermal stability with an increased amount of fullerene. A red shift of the absorption was found for annealed P3HT:C₆₀ (1:1 wt. %) films. These changes were explained in terms of the formation of polymer crystallites upon annealing. The photoluminescence measurements confirmed the formation of the polymer crystallites upon annealing and also showed that the photo-induced electron transfer becomes less effective upon annealing. This concludes that the degree of order in the polymer films has a drastic effect on both the absorption properties and the

electron charge transport. It was found that the performance of a P3HT:C₆₀ device improved by annealing.



7.5. REFERENCES

- [7.1] C. J. Brabec, N. S. Sariciftci, J. C. Hummelen, Plastic solar cells, *Adv. Funct. Mater.* 11 (2001) 15.
- [7.2] H. Spanggaard, F. C. Krebs, *Sol. Energy Mater. Sol. Cells* 83 (2004) 125.
- [7.3] C. Winder, N. S. Sariciftci, *J. Mater. Chem.* 14 (2004) 1077.
- [7.4] E. Bundgaard, F. C. Krebs, *Sol. Energy Mater. Sol. Cells* 91 (2007) 954.
- [7.5] F. C. Krebs, J. Alstrup, H. Spanggaard, K. Larsen, E. Kold, *Sol. Energy Mater. Sol. Cells* 83 (2004) 293.
- [7.6] S. Günes, H. Neugebauer, N. S. Sariciftci, *Chem. Rev.* 107 (2007) 1324
- [7.7] F. C. Krebs, H. Spanggaard, T. Kjaer, M. Biancardo, J. Alstrup, *Mater. Sci. Eng. B* 138 (2007) 106.
- [7.8] F. Padinger, R. S. Rittberger, N. S. Sariciftci, *Adv. Funct. Mater.* 13 (2003) 85.
- [7.9] W. Ma, C. Yang, X. Gong, K. Lee, A. J. Heeger, *Adv. Funct. Mater.* 15 (2005) 1617.
- [7.10] G. Li, V. Shrotriya, J. Huang, Y. Yao, T. Moriarty, K. Emery, Y. Yang, *Nat. Mater.* 4 (2005) 864.
- [7.11] J. Y. Kim, K. Lee, N. E. Coates, D. Moses, T. Q. Nguyen, M. Dante, A. J. Heeger, *Science*, 317 (2007) 222.
- [7.12] G. Dennler, C. Lungenschmied, H. Neugebauer, N. S. Sariciftci, A. Labouret, *J. Mater. Res.* 20 (2005) 3224.

- [6.13] C. Lungenschmied, G. Dennler, H. Neugebauer, N. S. Sariciftci, M. Glatthaar, T. Meyer, A. Meyer, Sol. Energy Mater. Sol. Cells 91 (2007) 379.
- [7.14] F. C. Krebs, H. Spanggaard, Chem. Mater. 17 (2005) 5235.
- [7.15] F. C. Krebs, K. Norrman, Prog. Photovolt.: Res. Appl. 15 (2007) 697.
- [7.16] X. Yang, J. Loos, S. C. Veenstra, W. J. H. Verhees, M. M. Wienk, J. M. Kroon, M. A. J. Michels, R. A. J. Janssen, Nano Lett. 5 (2005) 579.
- [7.17] E. A. Katz, S. Gevorgyan, M. S. Orynbayev, F. C. Krebs, Eur. Phys. J. Appl. Phys. 36 (2007) 307.
- [7.18] H. Neugebauer, C. J. Brabec, J. C. Hummelen, N. S. Sariciftci, Sol. Energy Mater. Sol. Cells 61 (2000) 35.
- [7.19] F. Padinger, T. Fromherz, P. Denk, C. J. Brabec, J. Zettner, T. Hierl, N. S. Sariciftci, Synth. Met. 121 (2001) 1605.
- [7.20] C. J. Brabec, J. A. Hauch, P. Schilinsky, C. Waldauf, MRS Bull. 30 (2005) 50.
- [7.21] F. C. Krebs, Sol. Energy Mater. Sol. Cells 92 (2008) 715.
- [7.22] M. Jørgensen, K. Norrman, F. C. Krebs, Sol. Energy Mater. Sol. Cells 92 (2008) 686.
- [7.23] J. A. Hauch, P. Schilinsky, S. A. Choulis, R. Childers, M. Biele, C. J. Brabec, Sol. Energy Mater. Sol. Cells 92 (2008) 727.
- [7.24] D. H. Kim, Y. D. Park, Y. S. Jang, H. C. Yang, Y. H. Kim, J. I. Han, D. G. Moon, S. J. Park, T. Y. Chang, C. W. Chang, M. K. Joo, C. Y. Ryu, K. W. Cho, Adv. Func. Mat. 15 (2005) 77.

- [7.25] N. Camaioni, G. Ridolfi, G. C. Miceli, G. Possamai, M. Maggini, *Adv. Mater.* 14 (2002) 1735.
- [7.26] I. Riedel, V. Dyakonov, *Phys. Stat. Sol. (a)* 201 (2004) 1332.
- [7.27] Y. Zhao, G. Yuan, P. Roche, M. Leclerc, *Polymer*, 36 (1995) 2211.
- [7.28] T-A. Chen, X. Wu, D. Rieke, *J. Amer. Chem. Soc.* 117 (1995) 233.
- [7.29] R. Cugola, U. Giovanella, P. Di Gianvincenzo, F. Bertini, M. Catellani, S. Luzzati, *Thin Solid Films* 511-512 (2006) 489.
- [7.30] G. F. Malgas, C. J. Arendse, S. Mavundla, F. R. Cummings, *J. Mater. Sci.* 43 (2008) 5599.
- [7.31] J. Kumar, R. K. Singh, V. Kumar, R.C. Rastogi, R. Singh, *Diamond & Rel. Mater.* 16 (2007) 446.
- [7.32] R. D. McCullough, S. Tristram-Nagle, S. P. Williams, R. D. Lowe, M. Jayaraman, *J. Amer. Chem. Soc.* 115 (1993) 4910.
- [7.33] H. Sirringhaus, N. Tessler, R.H. Friend, *Science* 280 (1998) 1741.
- [34] H. Sirringhaus, P.J. Brown, R.H. Friend, M.M. Nielsen, K. Bechgaard, B.M.W. Langeveld-Voss, A.J.H. Spiering, R.A.J. Janssen, E.W. Meijer, P. Herwig, D.M. de Leeuw, *Nature* 401 (1999) 685.
- [7.35] P. J. Brown, D. S. Thomas, A. Kohler, J.S. Wilson, J.-S. Kim, C.M. Ramsdale, H. Sirringhaus, R. H. Friend, *Phys. Rev. B* 67 (2003) 064203.
- [7.36] Y. Furukawa, M. Akimoto, I. Harada, *Syn. Met.* 18 (1987) 151.
- [7.37] R. A. Street, J. E. Northrup, A. Salleo, *Phys. Rev. B* 71 (2005) 165202.
- [7.38] M. Trznadel, A. Pron, M. Zagorska, R. Chrzaszcz, J. Pielichowski, *Macromolecules* 31 (1998) 5051.

- [7.39] R. Osterbacka, C. P. An, X. M. Jiang, Z. V. Vardeny, *Synth. Metal* 116 (2001) 317.
- [7.40] G. Louarn, M. Trznadel, J. P. Buisson, J. Laska, A. Pron, M. Lapkowski, S.J. Lefrant, *J. Phys. Chem.* 100 (1996) 12532.
- [7.41] C. Heller, G. Leising, G. Godon, S. Lefrant, W. Fischer, F. Stelzer, *Phys. Rev. B* 51 (1995) 8107.
- [7.42] M. Catellani, C. Arbizzani, M. Mastragostino, A. Zanelli, *Synth. Met.* 69 (1995) 373.



CHAPTER EIGHT

INSIGHTS INTO THE STABILITY AND THERMAL-DEGRADATION OF P3HT:C₆₀ BLENDED FILMS FOR SOLAR CELLS

ABSTRACT

This paper demonstrates the changes in the nanoscale morphology of the blended films induced by a diffusion of C₆₀ molecules and degradation during longer thermal treatment above the glass transition temperature (130 °C). The results showed that the film morphology including the size and population of poly(3-hexylthiophene) (P3HT) crystallites rapidly reduced with annealing time. A large scale (>1µm) C₆₀ aggregations demonstrating a bulky phase separation between the polymer and C₆₀ was identified after 5 hrs annealing, which resulted in a degradation of charge carrier mobility and conductivity. X-ray diffraction verifies that the interchain packing of P3HT within the crystallized phase improved with an increasing in annealing time, but the volume fraction of the P3HT (100) phase normal to substrate increased up to 3 hrs and decreased at longer annealing times resulting in the ageing of the films. Changes in the infrared spectra of the extended annealed samples were recorded, and the oxidation products were identified. A degradation mechanism that accounted for the modifications in the infrared spectra and a detachment of the hexyl chain

from P3HT was demonstrated resulting to chain cutting, conjugation loss and a reduction in the UV–vis absorbance. The morphology change with the annealing time resulted in an abrupt decrease in the PCE of P3HT:C₆₀ solar cells. These findings signify that the stability of P3HT:C₆₀ solar cells cannot be secured for longer annealing period owing to the unsettled morphology.



The content of this chapter was published in: Journal of Materials Science (2011) DOI:

10.1007/s10853-011-5408-9

8.1. INTRODUCTION

Polymer solar cells based on conjugated polymers have been intensively investigated as a potential source of renewable electrical energy, since photo-induced electron transfer from conjugated polymer to fullerene was first reported in 1992 by Sariciftci *et al.* [8.1]. An exceptional improvement in the device performance of polymer solar cells has been made, as the architecture of the polymer solar cell has been changed from the Schottky barrier single layer [8.2] to the donor/acceptor bilayer and bulk heterojunction (BHJ) [8.3–8.5]. From a material point of view, blends of poly(3-hexylthiophene) (P3HT) and [6,6]-phenyl-C₆₁-butyric acid methyl ester (PCBM) are most widely used as an active layer. Various studies showed that the device performance based on these materials is strongly related to the nano-morphology of the blends, where van der Waals crystal packing of the molecules and the formation of nanoscale domains of the two phases are strongly dependent on the processing conditions, solvents used and finally on post-production treatment [8.5-8.8].

Power conversion efficiencies (PCEs) ranging between 5 and 6.5% have been reported for simple BHJ cells [8.4, 8.5] and for tandem cells [8.9], respectively, while the predictions of the theoretically and practically accessible PCEs are indicated to be around 10% [8.10, 8.11].]. As an area of focus, the PCE is of course very important in order to compete with the more mature silicon technology and justify research in an inferior technology. However, significant improvement of stability and increase of lifetimes up to scales that could comply

with industrial standards are essential requirements for further progress and commercialization of organic solar cell devices [8.12-8.18].

To date, some of these criteria have been achieved individually, but they have not all been combined for the same material or material technology. Krebs *et al.* [8.14] reported stable solar cells with a lifetime in excess of 10 000 hours under full sun (AM1.5), high temperature and with exclusion of oxygen and moisture. They also predicted an operational lifetime in excess of 20 000 hours by using a thermal acceleration factor of 4 between 25 and 72 °C and an indoor illumination intensities of 50 – 100 Wm⁻² [8.13, 8.14]. Katz *et al.* [8.15] reported a most stable PV cell of P3CT-C₆₀ in outdoor testing. Krebs [8.17] reported a reasonable storability of a PV cell in ambient air without any form of encapsulation and continuous operation in air at 1000Wm⁻², AM1.5, 72 ± 2 °C, 35 ± 5% relative humidity for 100 h to 80% of the initial performance. So far there have been few studies in the accelerated studies where the devices are subjected to extra stress in the form of high temperatures, high incident light intensities and continuous illumination [8.19-8.21]. However, the thermal stability on morphology, structure and electrical properties, such as charge carrier mobility and conductivity, of P3HT blended with C₆₀ has not been fully addressed. In this paper, we investigate the thermal ageing of P3HT:C₆₀ blended films and correlate this with the chemical structure, morphological opto-electronic properties and photovoltaic device changes induced during the long annealing time.

8.2. EXPERIMENTAL DETAILS

8.2.1. Sample preparation

Regioregular poly(3-hexylthiophene) (rr-P3HT) was used as a light absorption and electron donating material; while C₆₀ fullerene was used as an electron acceptor material. The molecular weight (M_n) of P3HT reported by Sigma Aldrich was ~64,000 g mol⁻¹; with regularity that is greater than 98.5% for head-to-tail. These materials were used as received, without any further purification. Sample preparations were done according to the following procedure. Indium tin oxide (ITO)-coated glass (surface resistivity of 8-12 Ω/sq⁻¹, transmittance >83%) and silicon (Si) (100) substrates were ultrasonically cleaned with organic solvents and detergents, and then rinsed in de-ionized water. Photoactive layers were prepared by mixing P3HT:C₆₀ in a 1:1 weight ratio and dissolving the constituents in either chloroform (CF) or dichlorobenzene (DCB). CF has a boiling point of 132.0 °C and a solubility of 0.16 mg mL⁻¹ in C₆₀ fullerene, at room temperature [8.22]. To attain a complete dissolution between the polymer and blends, the solutions were stirred overnight at 50 °C. It is worthy to mention that no sonication or filtering was used in this process, since it would adversely affect the polymer side chains and possibly lead to a decrease in the conjugation length of P3HT strands. The active layer consisting of the polymer and the blends was spin-coated on top of the ITO-glass and Si substrates and dried at 50 °C for 15 min, to evaporate the excess solvent. To observe the thermal ageing (stability) of P3HT and the blended films, they were subjected to

extra stress in the form of high temperature annealing (130 °C) and times (0-30 hrs). For device fabrication a thin layer of poly(3,4-ethylenedioxythiophene):poly(styrenesulfonate) (PEDOT:PSS) solution was spin coated onto the ITO glass substrates. This was followed by thermal treatment of the PEDOT:PSS/ITO substrates at 100 °C for 30 min. The active layer consisting of the polymer blends was spin-coated on top of the PEDOT:PSS/ITO glass substrates and dried at 50 °C for 15 min.

8.2.2. Characterization

Atomic force microscopy (AFM) images of the top surface of the thin films of in a tapping mode were analyzed before and after the thermal degradation, using a Veeco AFM system (Digital Instruments). The microstructures of thermal degradation of the blended films (ageing blended films) were studied using a Carl Zeiss Imager Z1M polarised optical microscope (POM). The films thickness (~ 90 nm) was measured using α -stepper Veeco DEKTAK® 6M Stylus profilimeter instrument. The degree of ordering of the P3HT domains were characterized by Panalytical X'pert PRO PW 3040/60 x-ray diffractometer equipped with a Cu K_{α} ($\lambda = 0.154$ nm) monochromated radiation source. The measurements were extracted at 45.0 kV and 40.0 mA. Data were obtained from $2\theta = 1$ to 35° with a step size of 0.02° .

The Raman spectroscopy measurements were conducted at room temperature with a 514nm excitation laser with a spectral resolution of 0.4 cm^{-1} . The structure of pure P3HT with different concentrations of C_{60} prepared from CF

and DCB solvents was characterized by Fourier transform infrared spectroscopy (FT-IR) using a Perkin Elmer FT-IR spectrometer. The conductivity and the mobility of the P3HT and blended films were extracted using a Hall Effect measurement system (ECOPIA, HMS-3000). All measurements were performed at room temperature in air. The absorption spectra of the blended films were measured using a Varian Cary 1E ultra violet–visible (UV–vis) spectrometer.

Solar cells were completed by laminating a Platinum top electrode on top of an ITO glass substrate. This glass/Pt substrate was placed on top of the ITO/PEDOT:PSS/P3HT:C₆₀ (inset Fig. 11) substrate with an appropriate displacement and laminated together by applying a certain pressure at a controlled temperature using a hydrostatic pressurizer with hot plates (AH-1TC, ASONE, Japan). The current–voltage (IV) characteristics were measured using a Keithley 4200 Semiconductor Characterization System. The devices were irradiated at 100 mW cm⁻² using a xenon short arc lamp xenon lamp-based Sciencetech SF150 solar simulator with a power of 150 W. The optical power at the sample was 100 mW cm⁻², detected using a daystar meter. All the photovoltaic properties were evaluated in ambient air conditions at room temperature.

8.3. RESULTS AND DISCUSSION

Polymer-based organic solar cells are known to display a poor stability in real use conditions, and the photo and thermal degradation of the active organic layer play an important role in the reduced lifetime of the devices. To examine how the annealing sequence of the polymer photoactive layer is affecting the stability, we carried out AFM studies to characterize the phase separation and the microstructure of as-prepared and long-time annealed P3HT:C₆₀ films on the Si substrate at 130 °C, which are below the melting point (T_m) of P3HT (229 °C) [8.23]. Fig. 8.1 shows the height and phase images of the as-prepared P3HT:C₆₀ (1:1 wt. ratio) blended film spin-coated from chloroform solution and those annealed at long times. The as-prepared film is smooth with an atomically flat surface, Fig. 8.1a and b.

The surface roughens significantly increase with thermal annealing up to 30 hrs, Fig. 8.1c-f and Fig. 8.2, which are induced by overgrown large-scale C₆₀ clusters (or domains). The size of these domains varies from 200 nm up to tens of micrometres [8.24-8.26]. The roughening of the surface could be due to macro-scaled phase separation resulting from polymer self-organization into a disordered structure with fewer P3HT crystallites. Although the crystallites grew upon annealing, they flowed with the amorphous P3HT domains and increase the propagation of the P3HT:C₆₀ phase separation. The large phase separation may deteriorate the device performance.

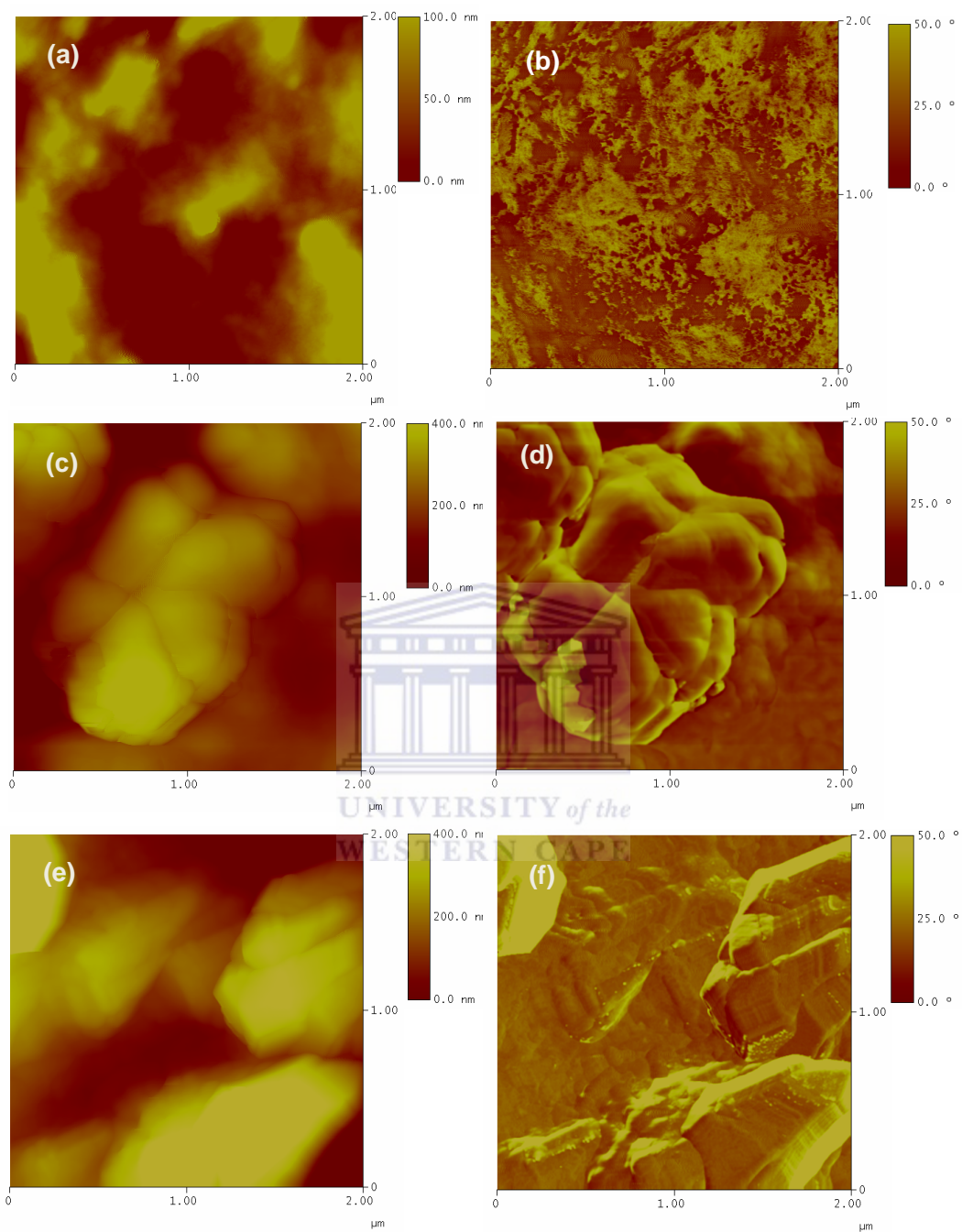


Figure 8. 1: AFM height and phase images ($2\mu\text{m}\times 2\mu\text{m}$) of as-prepared P3HT:C₆₀ (1:1 wt. ratio) films dissolved in CF (a) as-prepared height, (b) phase images, (c) 5hr annealed height, (d) phase images, (e) 30 hr annealed height and (f) phase images,

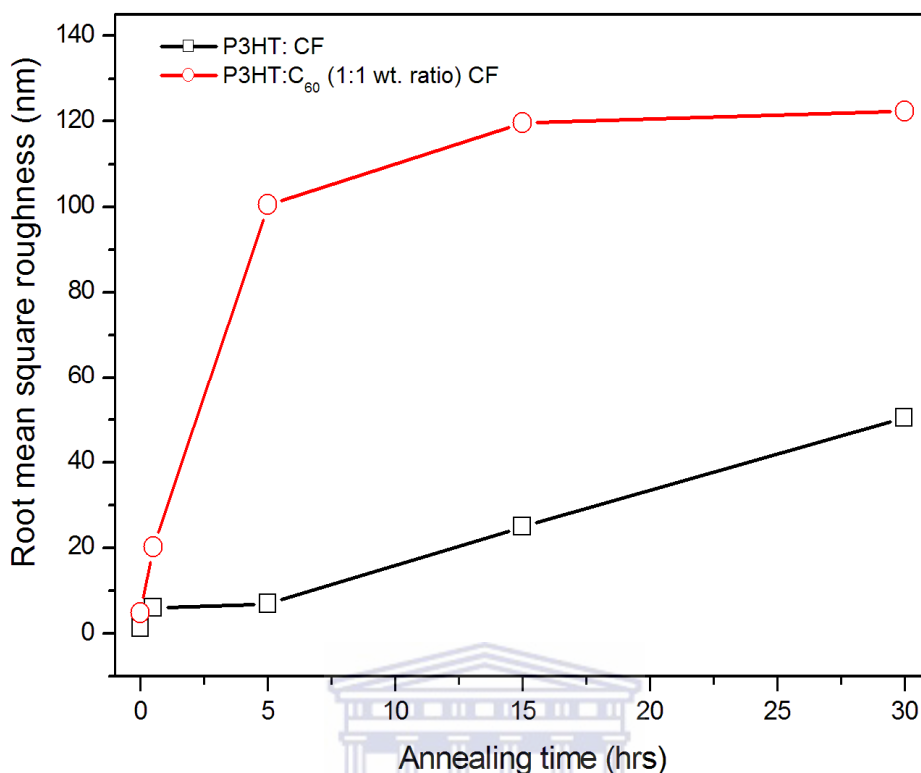


Figure 8. 2: Root mean square roughness values of the films as a function of annealing time.

Phase contrast optical microscopy on both blends prepared from either CF or DCB demonstrated that tiny clusters related to fullerene molecules diffuse out of the upper part of the blend film towards the nanoscopic C₆₀ domains that are already present both in the lower regions of the spin-coated film and near the air surface after 10 hrs of annealing (Fig. 8.3b and e). After 30 hrs of exposure, tiny clusters surrounded the larger aggregates, and a further depletion or degradation (see circles) in the C₆₀ content within the upper, subsurface, part of the blend layer was observed (Fig. 8.3f). Swinnen *et al.* [8.27] demonstrated that large PCBM clusters in blend films can rapidly grow up to a few hundred micrometers

in length under a condition that accelerates PCBM diffusion, such as high-temperature annealing.

These results suggests that, although nanometer-scale phase separation of the donor/acceptor blend can be attained in the laboratory through device optimization, prolonged exposure to elevated temperatures will induce macrophase separation with micrometer scale and large surface roughness (Fig. 8.2). This could be due to the fact that the nanometer-scale phase separation in the blends of the conjugated polymer and the fullerene derivatives is not thermodynamically stable [8.28]. It is suggested that the macrophase separation may limit charge separation, which occurs at the donor–acceptor interface and thus lower the PCE in the photovoltaic device. The macrophase-separated domain size ($>1 \mu\text{m}$ scale) observed for longer annealing time is much larger than the exciton diffusion length in conjugated polymers.

It should be noted that the stability of P3HT and blended films at $130 \text{ }^\circ\text{C}$ (in this study) can be related to the long-term stability at low temperature (e.g. $25 \text{ }^\circ\text{C}$, operating conditions of a solar cell) by an acceleration model based on the Arrhenius equation [8.19]: an increase in temperature accelerates molecular and segmental motions, bringing the system more rapidly to equilibrium (or apparent equilibrium), and therefore short-time annealing at high temperature corresponds to long time annealing at low temperature.

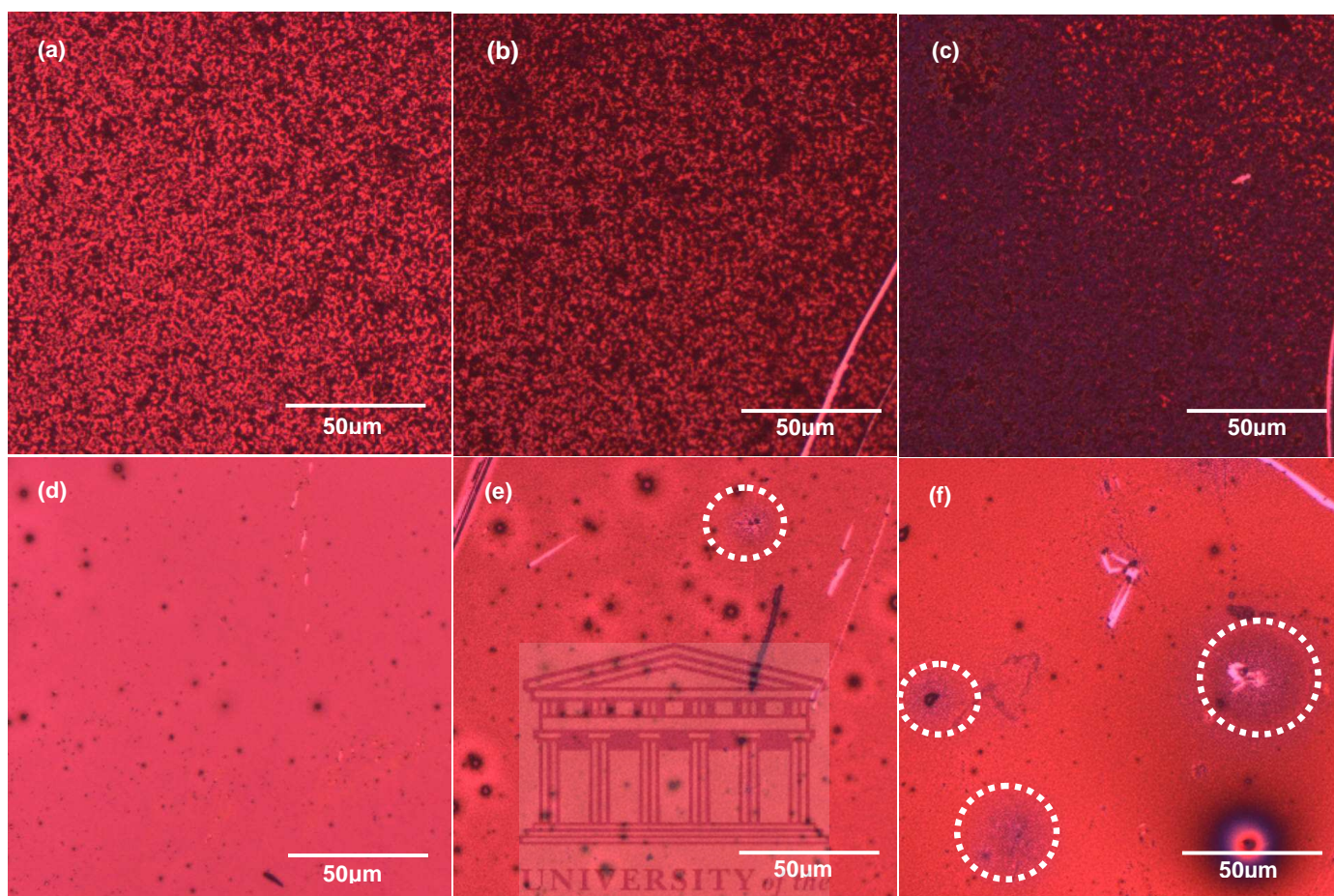


Figure 8. 3: Polarized optical micrographs of the surface of a P3HT:C₆₀ (1:1 wt. ratio) films prepared from CF, (a) as-prepared, 0hrs (b) 10 hrs, (c) 30 hrs while the images in d-f corresponds to as-prepared, 10 hrs, 30 hrs films prepared using DCB.

To investigate the effect of long time annealing on the ageing and chain packing of P3HT in the blend films, the XRD patterns of P3HT and the P3HT:C₆₀ blended films annealed at different times are shown in Fig. 8.4. Before annealing, the films show the (100) diffraction peak at $2\theta = 5.4^\circ$, corresponding to

an ordered lamellar structure with an interlayer spacing, which was formed by parallel stacks of P3HT main chains that were separated by the alkyl side chains, as shown in the inset of Fig. 8.4a [8.29]. The (100) peak intensity of the annealed films up to 5hrs is much stronger than the as-prepared sample, while the diffraction peaks shifted to higher 2θ angles and a reduction in the full-width-at-half-maximum (FWHM) is observed. This result to a momentous decrease in the d-spacing and an increase in the grain sizes of the (100) plane, as depicted in Fig. 8.5.

The decrease in the d-spacing with shorter annealing time suggests that inter-digitation or tilting of the side groups transpired during the formation of ordered aggregates in the solution and induced crystallization during film deposition. Motaung *et al.* [8.30] showed a decrease in the d-spacing with pre-annealed substrates prior to the active layer deposition. During longer annealing times (5 – 30 hrs) the peak intensity reduces and the diffraction peaks shift to lower angles presenting an increase in d-spacing and FWHM (Fig. 8.5b) and as well as decrease in grain size (Fig. 8.5c), which demonstrated a complete breakage of lamellar staking of polythiophene induced by thermal stress. It is suggested that the volume fraction of the π -conjugated planes of P3HT (100) with lamella; are oriented normal to the substrate [8.6, 8.31].

Therefore, the interchain packing of P3HT within the crystallized phase improved with an increasing in annealing time, but the volume fraction of the P3HT (100) phase normal to substrate increased up to 3hrs and decreased at longer annealing time resulting to the ageing of the films

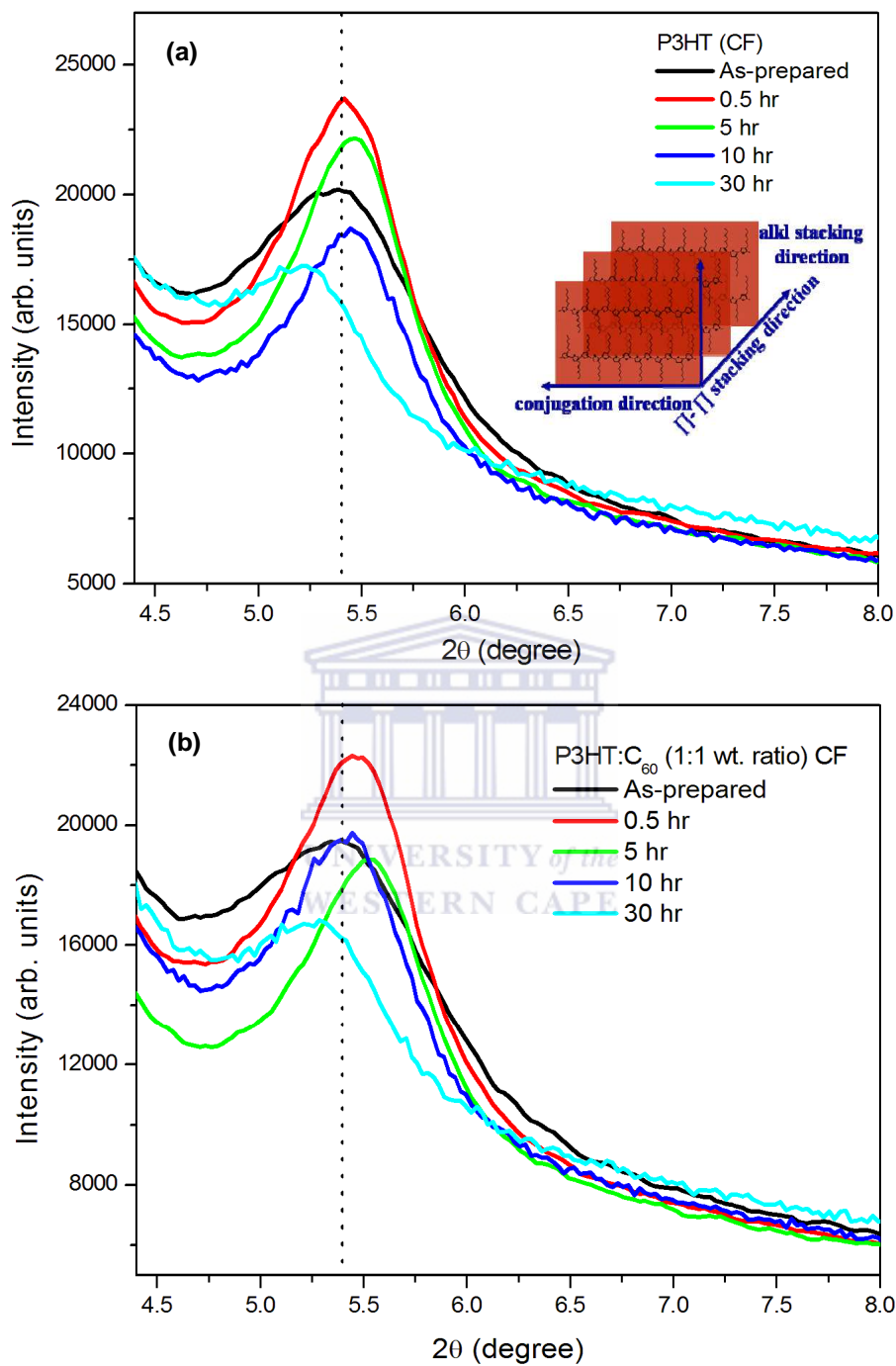


Figure 8. 4: Diffraction patterns of (a) rr-P3HT (CF) and (b) P3HT:C₆₀ (1:1 wt. ratio) (CF). The inset depicts the orientation of the P3HT crystalline domains with respect to the substrate (Fig 5a).

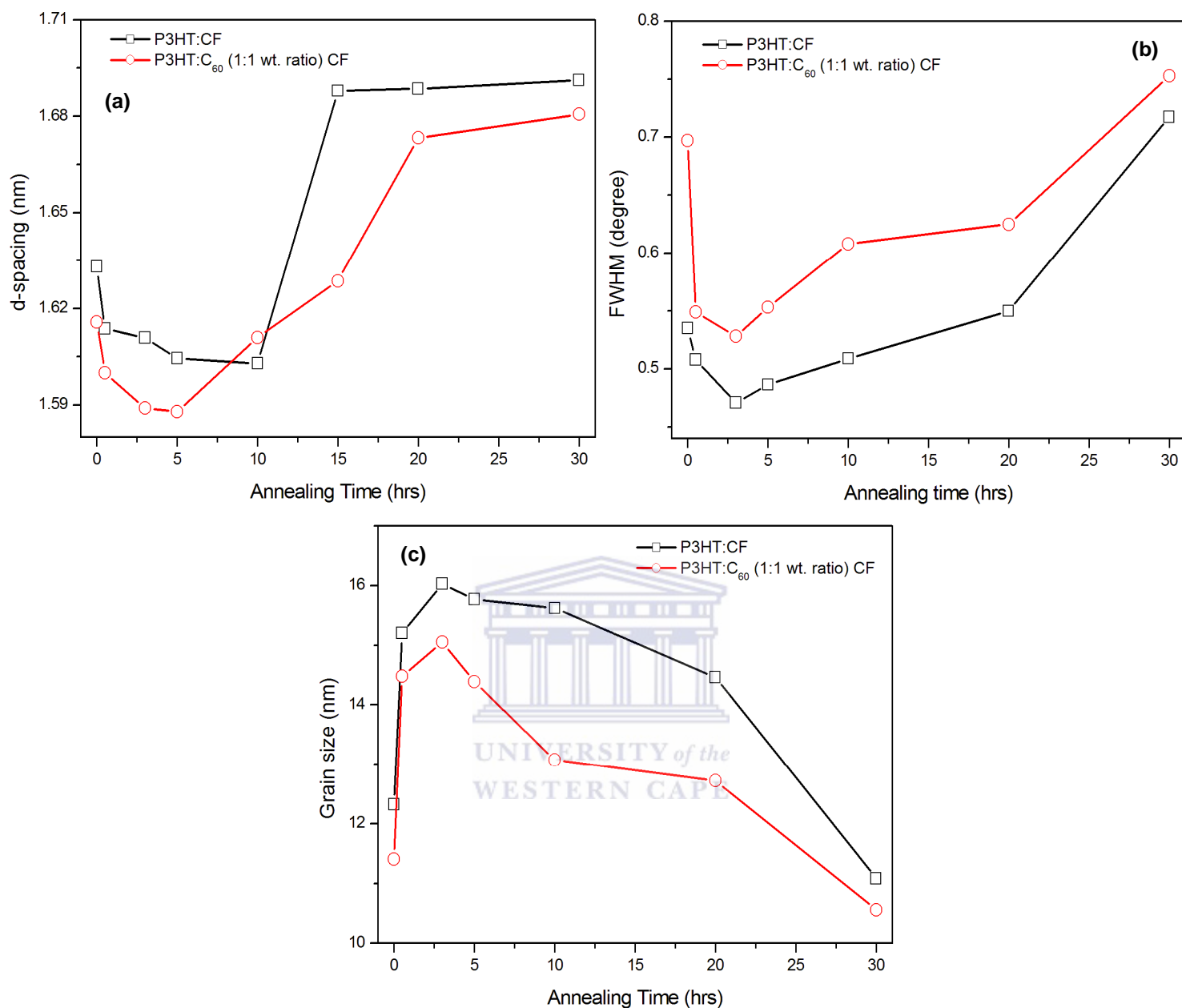


Figure 8. 5: Structural ageing of P3HT crystals during extended annealing (a) d-spacing, (b) FWHM of the P3HT (100) peak and (c) the average P3HT (100) crystal size.

It is concluded that the P3HT crystallites turns out to be unstable due to enhanced thermal motion of the P3HT molecules at longer annealing times,

which results in the “melting” of the P3HT crystallites and thus a reduction of the P3HT crystallinity as confirmed by the XRD and Raman analysis (Fig. 8.6). A reduction in the C=C stretching vibrations of the thiophene ring, C–C skeletal stretching and C-S-C ring deformation at 1440, 1380 and 720 cm^{-1} wavenumber [8.23, 8.32, 8.33] is observed with longer annealing times. This indicates the formation of disordered/less crystalline material; with a slight reduction in the conjugation length as the annealing time increases. Simultaneously, broadening of the FWHM of these peaks from 29.36 cm^{-1} (as-prepared) to 50.41 cm^{-1} (30 hrs annealed) also supports the reduction in the chain length.

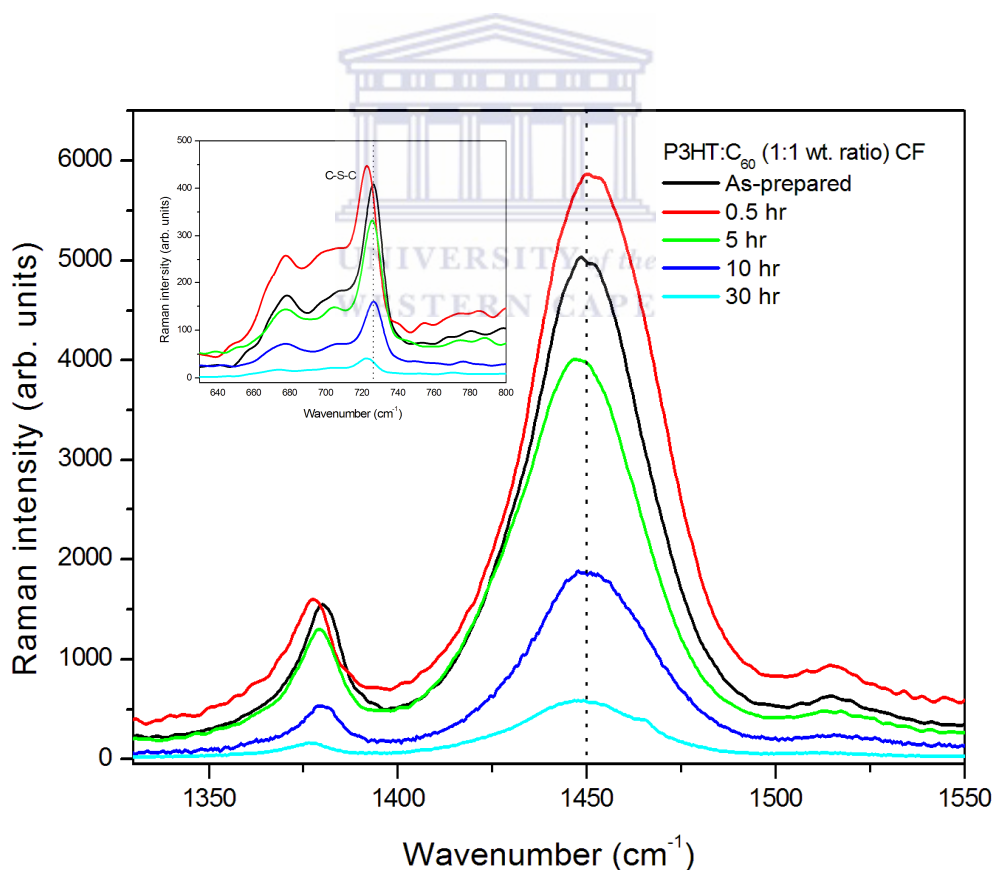


Figure 8. 6: Raman spectra of as-prepared and annealed films of P3HT:C₆₀ (1:1 wt. ratio).

Fig. 8.7 shows the FTIR spectra of the thermal degradation of P3HT and the blended film prepared from a chloroform solution. The peak at 2690 cm^{-1} , assigned to methyl asymmetric stretching vibration of the hexyl side chain gradually reduces in intensity with an increase in annealing time, which involves the detachment of the side chain from the P3HT backbone (Fig. 8.7a). Two other peaks at 2923 cm^{-1} and 2855 cm^{-1} , corresponding to methylene in phase and out phase vibrations also decrease in intensity with an increase in annealing time. After 5 hours of annealing; a new shoulder arise around 2956 cm^{-1} , and disappears with extended annealing time.

At the same time, a new band (or shoulder) at 2870 cm^{-1} progressively developed with longer annealing exposure. Furthermore, a small shift in frequency and a total disappearance of the symmetric ring stretching mode peaks at 1457 cm^{-1} and the anti-symmetric C=C stretching peak 1510 cm^{-1} (circle) are observed with longer annealing times. Since the ratio between the intensity of the anti-symmetric C=C stretching peak and the intensity of the symmetric stretching peak can be used to probe the average conjugation length of P3HT [8.34-8.36], the results indicates that the conjugation length of P3HT chains is disrupted during longer annealing times (Fig. 8.7b and c). The signals at 1115 and 620 cm^{-1} , which corresponds to the S=O and S-O stretching frequencies of a sulfonic acid or ester according to the literature data, arise during the 5- 10 hrs annealing time (result not shown).

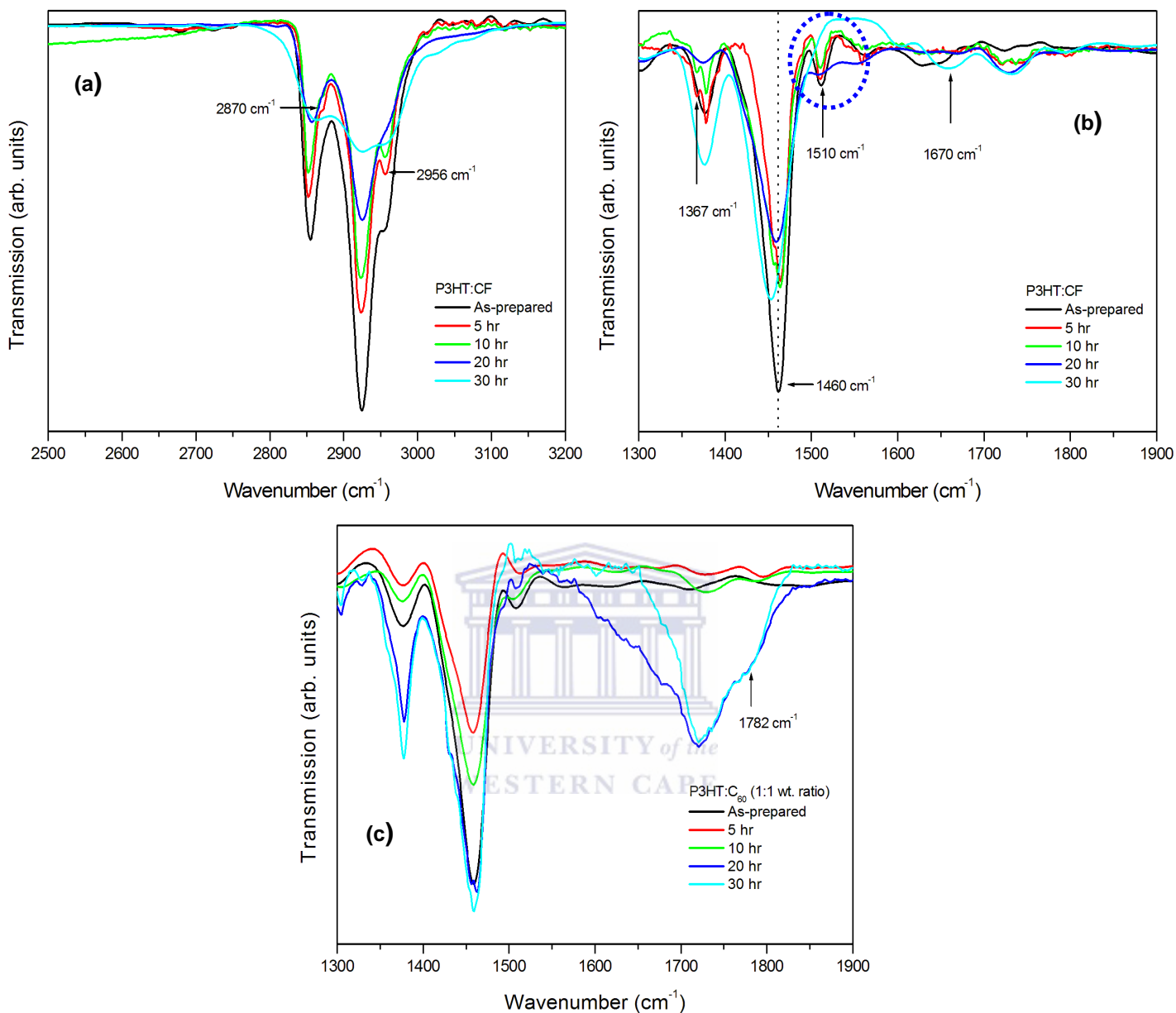


Figure 8. 7: FTIR spectra of as-prepared P3HT and P3HT:C₆₀ (1:1 wt. ratio) films compared with that annealed at 130 °C for different times.

The peak at 668 cm⁻¹ assigned to the C–S stretching in pre-treated P3HT and blended films disappears during longer annealing time indicating the loss of the C-S units. A similar degradation on the P3HT structure (alkyl groups and

thiophene rings) was observed by Manceau *et al.* [8.37, 8.38], when exposing the polymer under UV-visible light and thermal ageing. Moreover, one can observe the formation of thermal products in the carbonyl region (Fig. 8.7c). A band is detected at 1782 cm^{-1} and a broadening appears near the region $1700\text{--}1710\text{ cm}^{-1}$, which is attributed to C_{60} moiety [8.39]. This conclusion is confirmed by the fact that the degradation of C_{60} also provokes the development of a band at 1782 cm^{-1} accompanied by another one at 1745 cm^{-1} . It can be concluded that a gradual decrease in intensities of the FTIR peaks in the finger print region indicates a thermal degradation of P3HT with increasing in annealing exposure [8.40].

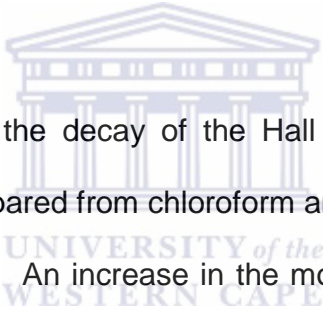


Fig. 8.8 demonstrates the decay of the Hall mobility and conductivity of P3HT and blended films prepared from chloroform and dichlorobenzene solutions during long annealing times. An increase in the mobility and conductivity of the P3HT and the blended films is observed after a short anneals. Such an increase, especially in the case of the blends, may be attributed to enhanced polymer ordering, since C_{60} crystallizes out of the polymer matrix under optimized annealing conditions [8.41-8.43] leaving the polymer chains behind that will endeavour to reorganize and obtain an optimized morphology. It is clear that films spin-coated from CF disclose a higher mobility and conductivity compared to films spin-coated from DCB.

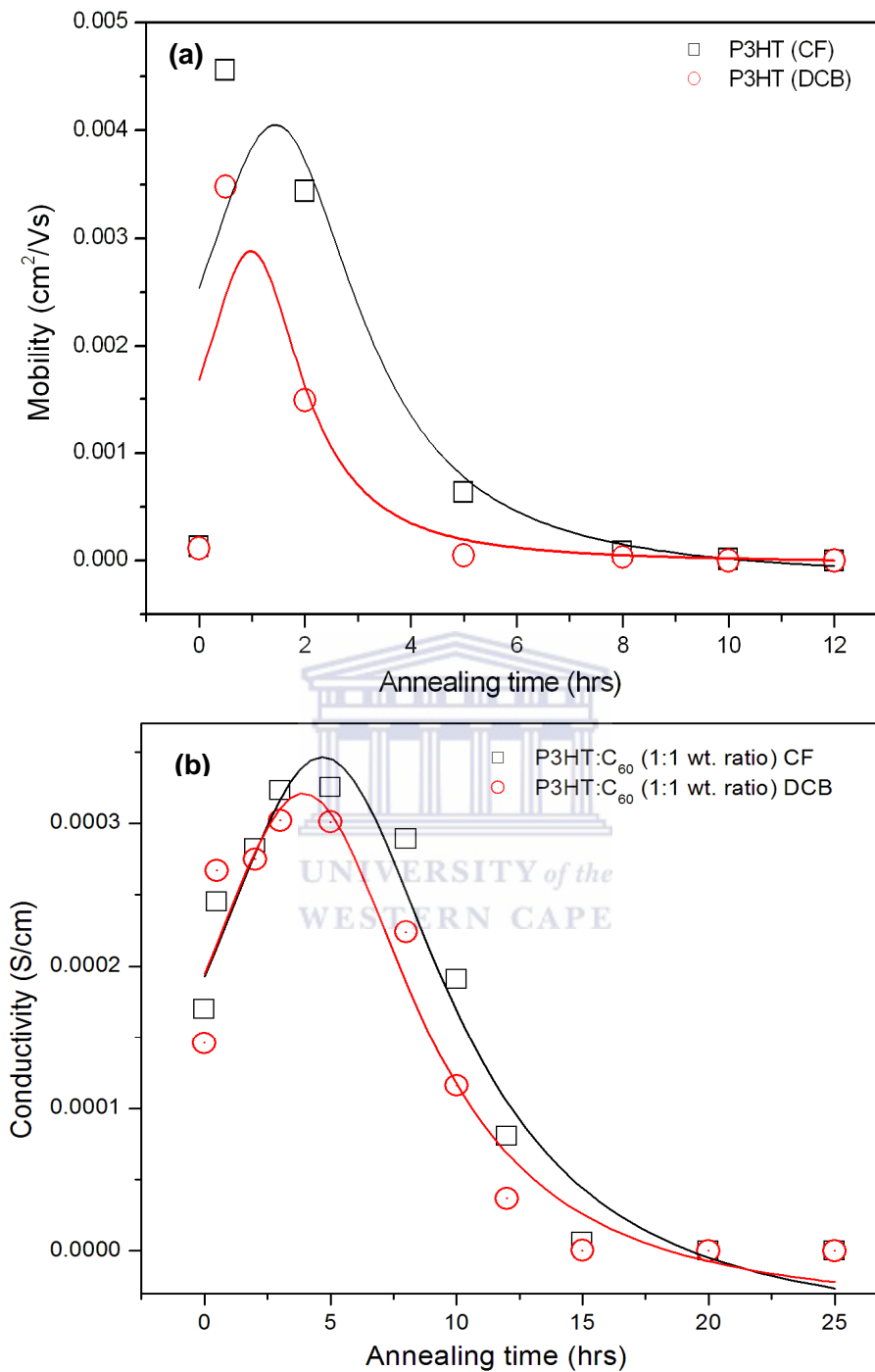


Figure 8. 8: Hall Effect (a) mobility of as-prepared and annealed films of P3HT and (b) electrical conductivity extracted from blended films. Solid lines are a visual guide of the behaviour.

It is assumed that the improved electrical properties of films spin-coated from CF are induced by smaller polymer and fullerene clusters formed during spin-coating, which lead to the development of continuous pathways for charge carriers and an increase in the interfacial area that enhances the exciton dissociation [8.44]. It is interesting to note that, during longer annealing times (5-25 hrs), a considerable decrease in both the mobility and conductivity were observed. It is suggested that the changes in the mobility and conductivity could be due to a depletion of P3HT and C₆₀. Furthermore, it can be concluded that the decrease in mobility is attributed to the formation of large clusters during longer annealing times as observed in the POM, XRD and AFM analysis.

The UV-vis absorbance spectra (Fig. 8.9) show a blue-shift and a complete reduction in the absorbance with an increase in annealing time, indicating that the thermal degradation aggravates the modification of the chemical structure of chromophore groups and reduces the conjugation length of P3HT. This is in good agreement with the FTIR results obtained and discussed in Fig. 8.7. Thermal degradation also altered the degree of inter-chain order in the microcrystalline domains of P3HT, as shown by the disappearance of the shoulder at 600 nm for the P3HT films dissolved using dichlorobenzene. This could be due to the higher solubility of P3HT and C₆₀ in DCB, thereby inducing a finer phase separation and smaller grain size [8.45].

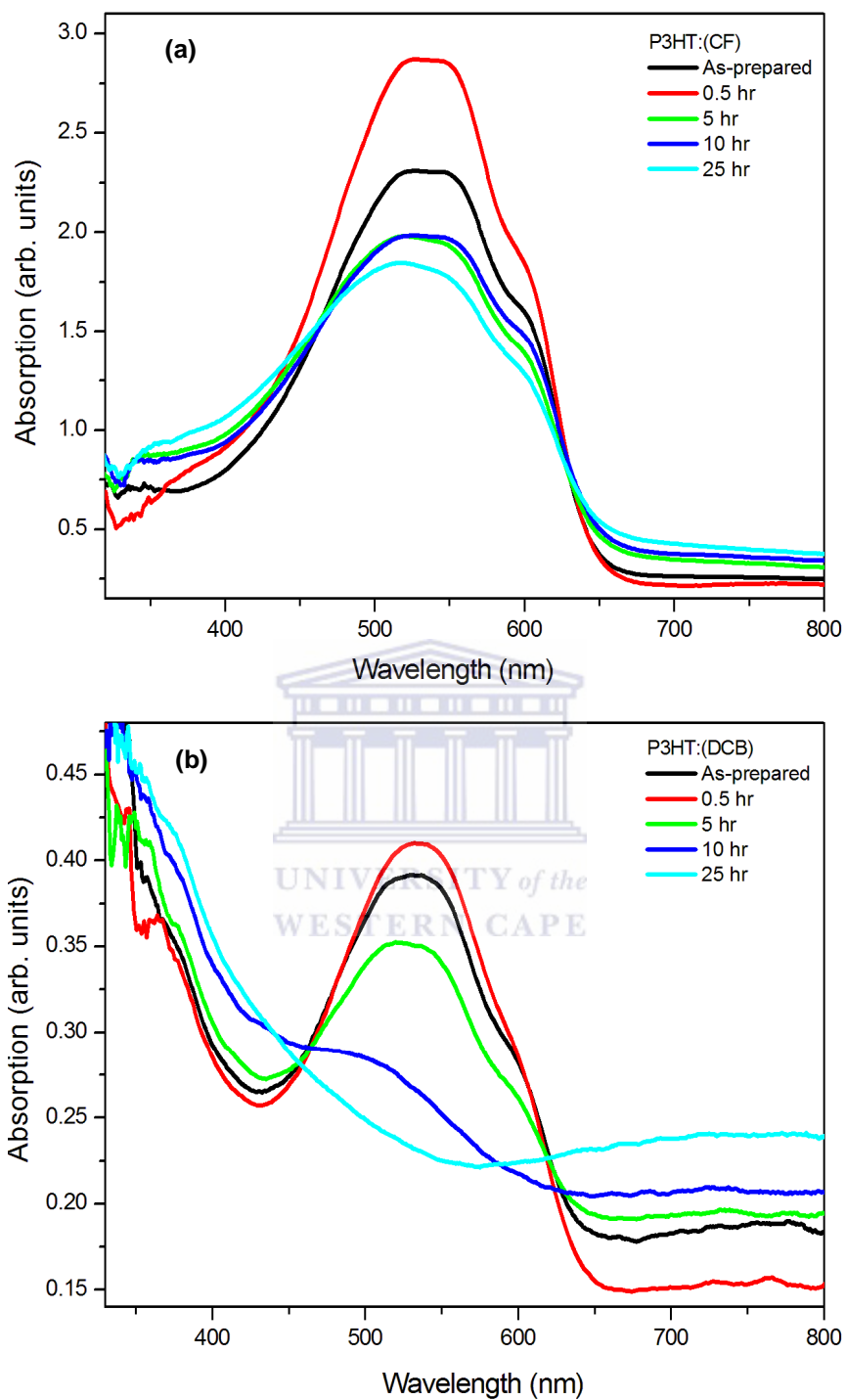


Figure 8. 9: UV–visible absorption spectra of the as-prepared and annealed films of (a) P3HT (CF), (b) P3HT (DCB), (c) P3HT: C₆₀, 1:1 wt. ratio (DCB) and (d) (1:4 wt. ratio) (DCB).

Through analysis of the P3HT:C₆₀ film degradation process, the obtained data allowed us to propose a degradation mechanism that accounted for the formation of the different oxidative species due to the impact of thermal annealing on the polymer blends. Fig. 8.10 shows a two step pathway for the degradation of the blends. In step 1 (scheme 1), thermal degradation of P3HT as observed in Raman and FTIR analyses starts approximately after an annealing time of 5 hrs. The results establish that P3HT starts to degrade with the detachments of lighter fragments like C-S units, as confirmed by the Raman and UV-vis analyses, with the modification of the chemical structure of chromophore groups which results in a reduction of the conjugation length of P3HT. A thermal decomposition of the C-S units of polythiophene on pyrolysis mass photometry at a very low temperature (~ 50 °C) has also been reported by Vatansever *et al.* [8.46]. The degradation after 30 hrs is due to the subsequent loss of C₆H₁₃ detached from the polymer backbone. POM results showed that after 30 hrs of exposure, tiny clusters that surrounded the larger polymer and C₆₀ aggregates, depletes or degrades. Reddy *et al.* [8.47] demonstrated that the final products of C₂H₂ units after CS and C₆H₁₃ detached from the polymer backbone resulted in amorphous carbon and a mixture of fullerenes.

Degradation products of FTIR stretching frequencies (1115 and 620 cm⁻¹) have also been identified after 10 hrs of annealing as shown in Fig. 8.10 (scheme 2). Rivaton *et al.* [8.48] indicated sulphinate moieties can be formed by sulphone degradation, as observed in the case of polysulphone. It is also known that

sulphur atoms can be readily oxidized by hydroxyl radicals (OH^\bullet) to form sulfoxides and sulphones [8.49]. The characteristic IR vibrations of sulfoxides (1045 cm^{-1}) have been detected. Therefore, it is possible that the sulphur atom of the thiophene ring is initially oxidized into sulfoxides, then into sulphones that are later decomposed into sulphinate esters.

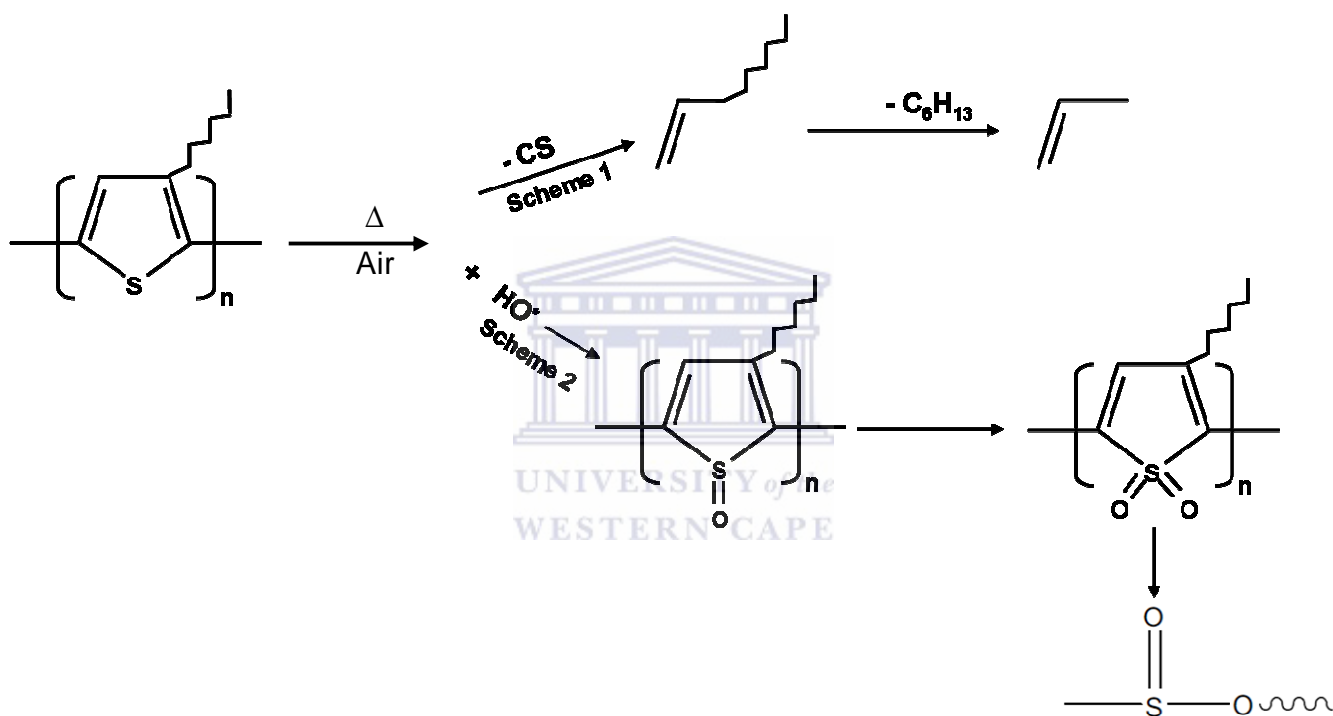


Figure 8. 10: The probable pathway followed by the thermal degradation of a P3HT polymer.

To understand the degradation mechanism on the photovoltaic device performance, the current density voltage ($I-V$) curves of the devices annealed for different times are shown in Fig. 8.11. It is evident from Fig. 8.11 and Table 8.1 that the as-prepared device exhibits a low PV performance with a short circuit

current density (I_{sc}) of $29.67 \mu\text{A}/\text{cm}^2$, fill factor (FF) of 0.15, open circuit voltage (V_{oc}) of 0.32 V, and PCE of 0.014%. After annealing for 30 min, the I_{sc} , and FF increased remarkably resulting to a PCE 0.048%. This increase in the PCE is due to the improved absorption of the incident light (Fig. 8.9) and the charge transportation property (Fig. 8.8) of the highly ordered P3HT:C₆₀ structure. The C₆₀-rich region reduces the recombination losses and increases the current density [8.50-8.51]; thus, increasing the performance of the solar cell after annealing.

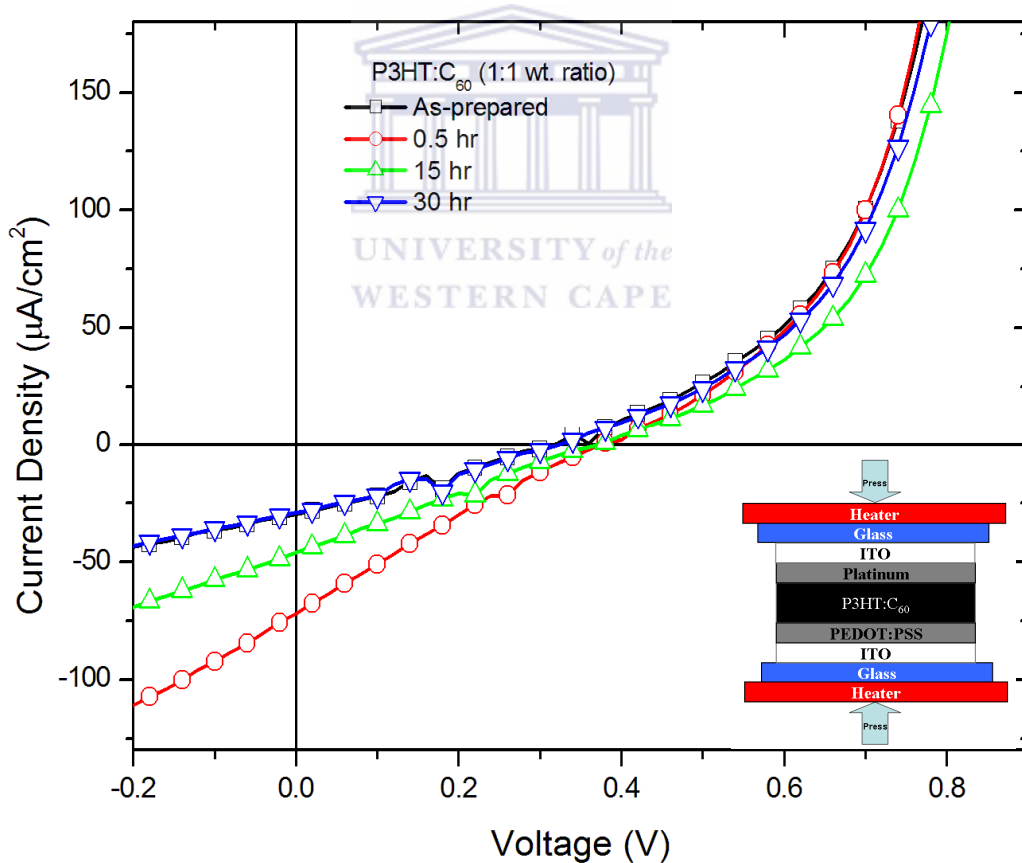


Figure 8. 11: I–V curves for devices processed from P3HT:C₆₀ and annealed at 130 °C for different times.

Upon annealing for longer times the performance of the solar cell reduced considerably (Table 8.1). This is due to a degradation ordering of P3HT, the deficient C₆₀ molecules that accepted the generated electrons, and the deteriorated phase separation resulting from the formation of the large C₆₀ aggregates/clusters (Fig. 8.1) through the high temperature annealing. The larger C₆₀ cluster does not only induce a large-scale phase separation between P3HT and C₆₀, but also a rough P3HT:C₆₀ (1:1 wt ratio) blend film as depicted in Fig. 8.1. The rough P3HT:C₆₀ layer may form some shunt paths after the top electrode deposition, resulting in a low open circuit voltage [8.52].

TABLE 8. 1: Photovoltaic devices performance of blended structures

<i>Annealing time (hrs)</i>	<i>I_{sc} (μA/cm²)</i>	<i>V_{oc} (V)</i>	<i>FF</i>	<i>PCE (%)</i>
As-prepared	29.67	0.32	0.15	0.014
0.5	72.84	0.35	0.19	0.048
15	47.84	0.35	0.16	0.027
30	28.73	0.36	0.14	0.015

8.4. CONCLUSION

Alterations in the nanoscale morphology of the blend films of P3HT and blended films induced by a diffusion of C₆₀ molecules and degradation during longer thermal treatment above glass transition temperature was observed.

Distinct degradation kinetics and morphological changes that indicate the occurrence of different underlying physico-chemical mechanisms were observed. A large scale ($>1\mu\text{m}$) C_{60} aggregations denoting large phase separation between the donor and acceptor was identified, which arose after 5hrs annealing. Alterations on the micro-structure resulted on the degradation of grain sizes, charge carrier mobility and electrical conductivity. FTIR indicated that under extended thermal annealing the alkyl groups and thiophene rings vanish. The results establish that P3HT starts to degrade at early annealing stages (5 hrs) with detachments of lighter fragments like C-S units, and then followed abstraction of hydrogen attached to a carbon atom that is adjacent to a double bond, leading to backbone, side chain and sulphur oxidations. Chain scissions, conjugation loss and a decrease in the UV-visible absorbance arise from these reactions. The presence of C_{60} was observed to mainly reduce the rate of P3HT degradation, which can be ascribed to scavenging effect of C_{60} . The morphology change with the annealing time is closely related to the change of the PCE of solar cells: the PCE of P3HT: C_{60} significantly decreases with increasing annealing time. Considering all the experimental observations, it can be suggested that the stability of P3HT: C_{60} solar cells cannot be secured for longer annealing period owing to the unsettled morphology and structure.

8.5. REFERENCES

- [8.1] N S. Sariciftci, L. B. Smilowitz, A J. Heeger and F. Wudl, *Science* 258 (1992) 1474.
- [8.2] H. Antoniadis, B. R. Hsieh, M. A. Abkowitz, S. A. Jenekhe, M. Stolka, *Synth. Met.* 62 (1994) 265
- [8.3] C. W. Tang, *Appl. Phys. Lett.* 48 (1986) 183.
- [8.4] G. Li, V. Shrotriya, J. Huang, Y. Yao, T. Moriarty, K. Emery, Y. Yang, *Nat. Mater.* 4 (2005) 864
- [8.5] W. Ma, C. Yang, X. Gong, K. H. Lee, A. J. Heeger, *Adv. Funct. Mater.* 15 (2005) 1617.
- [8.6] Y. Kim, S. Cook, S.M. Tuladhar, S.A. Choulis, J. Nelson, J.R. Durrant, D.D.C. Bradley, M. Giles, I. Mcculloch, C.-S. Ha, M. Ree, *Nat. Mater.* 5 (2006) 197.
- [8.7] H. Hoppe, N.S. Sariciftci, *J. Mater. Chem.* 16 (2006) 45.
- [8.8] X. Yang, J. Loos, S.C. Veenstra, W.J.H. Verhees, M.M. Wienk, J.M. Kroon, M.A.J. Michels, R.A.J. Janssen, *Nano. Lett.* 5 (4) (2005) 579.
- [8.9] J.Y. Kim, K. Lee, N.E. Coates, D. Moses, T.-Q. Nguyen, M. Dante, A.J. Heeger, *Science* 317 (2007) 222.
- [8.10] L.J.A. Koster, V.D. Mihailetschi, P.W.M. Blom, *Appl. Phys. Lett.* 88 (2006) 093511.
- [8.11] M.C. Scharber, D. Mu hlbacher, M. Koppe, P. Denk, C. Waldauf, A.J. Heeger, C.J. Brabec, *Adv. Mater.* 18 (2006) 789.

- [8.12] C. Lungenschmied, G. Dennler, H. Neugebauer, N. S. Sariciftci, M. Glatthaar, T. Meyer, A. Meyer, *Sol. Energy Mater. Sol. Cells* 91 (2007) 379.
- [8.13] F. C. Krebs, H. Spanggaard, *Chem. Mater.* 17 (2005) 5235.
- [8.14] F. C. Krebs, K. Norrman, *Prog. Photovolt. Res. Appl.* 15 (2007) 697.
- [8.15] E. A. Katz, S. Gevorgyan, M. S. Orynbayev, F. C. Krebs, *Eur. Phys. J. Appl. Phys.* 36 (2007) 307.
- [8.16] F. Padinger, T. Fromherz, P. Denk, C. J. Brabec, J. Zettner, T. Hierl, N. S. Sariciftci, *Synth. Met.* 121 (2001) 1605.
- [8.17] F. C. Krebs, *Sol. Energy Mater. Sol. Cells* 92 (2008) 715.
- [8.18] M. Jørgensen, K. Norrman, F. C. Krebs, *Sol. Energy Mater. Sol. Cells* 92 (2008) 686.
- [8.19] S. Schuller, P. Schilinsky, J. Hauch, C.J. Brabec, *Appl. Phys. A* 79 (2004) 37.
- [8.20] R. De Bettignies, F. Leroy, M. Firon, C. Sentein, *Synth. Met.* 156 (2006) 510.
- [8.21] S. Bertho, G Janssen, T. J. Cleij, B. Conings, W. Moons, A. Gadisa, J. D'Haena, E. Goovaerts, L. Lutsen, J. Manca, D. Vanderzande, *Solar Energy Materials & Solar Cells* 92 (2008) 753–760.
- [8.22] R. S Ruoff, D. S Tse, R. Malhotra, D. C. Lorents, *J. Phys. Chem.* 97 (1993) 3379.
- [8.23] D. E. Motaung, G. F. Malgas, C. J. Arendse, S. E. Mavundla, C. J. Oliphant, D. Knoesen, *Sol. Energy Mater. Sol. Cells* 93 (2009) 1674.

- [8.24] D. Chirvase, J. Parisi, J.C. Hummelen, V. Dyakonov, *Nanotechnology* 15, (2004) 1317–1323.
- [8.25] E. Klimov, W. Li, X. Yang, G.G. Hoffmann, J. Loos, *Macromolecules* 39, (2006) 4493–4496.
- [8.26] T. J. Savenije, J. E. Kroeze, X. Yang, J. Loos, *Adv. Funct. Mater.* 15, (2005) 1260–1266.
- [8.27] A. Swinnen, I. Haeldermans, M. van de Ven, J. D’Haen, G. Vanhoyland, S. Aresu, M. D’Olieslaeger, J. Manca, *Adv. Funct. Mater.* 16 (2006) 760.
- [8.28] S. Miyanishi, K. Tajima, K. Hashimoto, *Macromolecules* 42 (2009) 1610.
- [8.29] Erb T, Zhokhavets U, Gobsch G, Raleva S, Stuhn B, Schilinsky P, Waldauf C and Brabec C J 2005 *Adv. Funct. Mater.* **15** 1193
- [8.30] D. E. Motaung, et al., *Materials chemistry and physics*, (2010) doi:10.1016/j.matchemphys.2010.06.021.
- [8.31] G. Li, Y. Yao, H. Yang, V. Shirotriya, G. Yang, Y. Yang, *Adv. Funct. Mater.* 17 (2007) 1636.
- [8.32] P.J. Brown, D.S. Thomas, A. Kohler, J.S. Wilson, J.-S. Kim, C.M. Ramsdale, H. Sirringhaus, R.H. Friend, *Phys. Rev. B* 67 (2003) 064203–064218.
- [8.33] G. F. Malgas, C. J. Arendse S. E. Mavundla, F. R. Cummings, *J. Mater. Sci.* 43 (2008) 5599.
- [8.34] Y. Furukawa, M. Akimoto, I. Harada, *Synthetic Metals* 18 (1987) 151.
- [8.35] M. Trznadel, A. Pron, M. Zagorska, R. Chrzaszcz, J. Pielichowski, *Macromolecules* 31 (1998) 5051.

- [8.36] D. E. Motaung, G. F. Malgas, C. J. Arendse, S. E. Mavundla, D. Knoesen, *Mater. Chem. Phys.* 116 (2009) 279.
- [8.37] M. Manceau, A. Rivaton, J-L. Gardette, S. Guillerez, N. Lemaitre, *Polymer Degradation and Stability* 94 (2009) 898–907
- [8.38] M. Manceau, et al., *Sol. Energy Mater. Sol. Cells* (2010), doi:10.1016/j.solmat.2010.03.012
- [8.39] S. Chambon, A. Rivaton, J-L. Gardette, M. Firon, *Sol. Energy Mater. Sol. Cells* 91 (2007) 394–398
- [8.40] G. Gustafsson, O. Inganas, J. O. Nilsson, *Synth. Met.* 28 (1989) 427–34.
- [8.41] D. E. Motaung, G. F. Malgas, C. J. Arendse S. E. Mavundla, C. J. Oliphant, D. Knoesen, *J. Mater. Sci.* 44 (2009) 3192
- [8.42] L.M. Andersson, F.L. Zhang, O. Inganas, *Appl. Phys. Lett.* 89 (2006) 142111.
- [8.43] A. Kumar, G. Li, Z. Hong, Y. Yang, *Nanotechnology* 20 (2009) 165202.
- [8.44] C.Y. Kwong, A.B. Djuricic, P.C. Chui, K.W. Cheng, W.K. Chan. *Chem Phys Lett* 384 (2004) 372–5.
- [8.45] D. E. Motaung, G. F. Malgas, C. J. Arendse, *Synthetic Metals* 160 (2010) 876–882
- [8.46] F. Vatansever, U. Akbulut, L. Toppare, J. Hacaloglu, *Polymer* 37 (7) (1996) 1103-1107
- [8.47] P. K. Reddy, P. J. Goutam, D. K. Singh, A. K. Ghoshal, P. K. Iyer, *Polymer Degradation and Stability* 94 (2009) 1839–1848

- [8.48] A. Rivaton, J. L. Gardette, *Polymer Degradation and Stability* 66 (1999) 385-403.
- [8.49] I. Barnes, J. Hjorth, N. Mihalopoulos, *Chem Rev.* 106 (3) (2006) 940–75.
- [8.50] M. Reyes-Reyes, K. Kim, D. J. Carroll, *Appl. Phys. Lett.* 87 (2005) 083506.
- [8.51] R. Shilkler, M. Chiesa, R. H. Friend, *Macromolecules* 39 (2006) 5393
- [8.52] D. E. Motaung, G. F. Malgas, C. J. Arendse, *J Mater Sci* 45 (2010) 3276.



SUMMARY

Polymer based photovoltaic (PV) devices have been stimulating ever increasing interest as a promising alternative for renewable resource of energy. These devices as opposed to conventional silicon solar cells have increasing attention because of their potentials for the production of flexible and large areas solar cell at a remarkable low cost.

In this thesis, the effect of solvents on the crystallization and interchain interaction of P3HT and C₆₀ fullerene films were studied using XRD, UV-vis, PL, Raman and FTIR spectroscopy. The polymer blends formed with non-aromatic solvents exhibited an improved crystallinity and polymer morphology than that formed with aromatic solvents. An improved ordering was demonstrated in the polymer films spin coated from non-aromatic solvents. This indicates that the limited solubility of rr P3HT in a marginal solvent such as non-aromatic solvents can offer a strategy to obtain highly ordered crystal structures and lead directly to optimal morphologies on the films.

The interaction between P3HT and C₆₀ in solid-state thin films was studied by UV-vis absorption, photoluminescence, FTIR and Raman spectroscopy analysis. The spectroscopic investigations showed that the films of P3HT and blends with different ratios of P3HT:C₆₀ exhibit an efficient photo-induced charge transfer. The blended P3HT:C₆₀ film with a 1:4 wt. ratio showed incompletely quenching while the blended P3HT:C₆₀ film (1:1 wt. ratio) revealed a completely quenching. This was evidenced by electron spin resonance (ESR). The ESR

measurements allowed us to quantify the charge transfer between P3HT and C₆₀, which resulted in positive P3HT polarons. Therefore, such changes of the photoluminescence intensity originates from a phase separation and thus changes in the morphology of the active layer. The fullerene surplus at higher concentrations (P3HT:C₆₀ film with a 1:4 wt. ratio) is not homogeneously dispersed within the polymer matrix, but diffuses away and creates phase separated clusters, agglomerates or C₆₀ islands. The complete quenching of the P3HT:C₆₀ film with a 1:1 wt. ratio indicates that due to the finer phase separation in the chloroform blend, all of the C₆₀ is in close enough contact with the polymer to undergo a charge transfer.

In order to control the formation of microscopic morphology and evaporation rate of the solvent (DCB) from the P3HT films and blends the substrates were annealed prior to deposition of an active layer. It was demonstrated that the pre-substrate annealing controls the crystallization of P3HT, the phase separation and diffusion of the acceptor material (C₆₀ or PCBM) and also increases the electrical conductivity and Hall mobility of p-type P3HT. The formation of self-assembled P3HT fibrillar structures that are locally ordered were observed induced by the suppressed growth of fullerenes clusters and therefore, better device performance can be anticipated.

Besides, substrate annealing, thermal annealing on the photovoltaics parameters on P3HT:C₆₀ cells (1:1 wt. ratio) were investigated at different annealing temperatures under the air mass (AM) 1.5 illumination (100 mWcm⁻²). It was found that the performance of a P3HT:C₆₀ device was dramatically

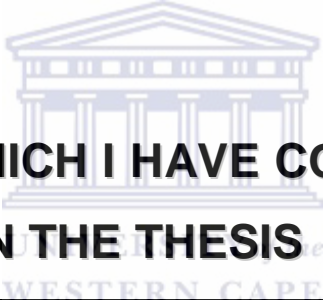
improved by annealing at 150 °C due to the on-going thermal transition of P3HT molecules in the presence of C₆₀ transition and the substantial ordering in the polymer film during annealing.

Finally, alterations in the nanoscale morphology of the blend films of P3HT and blended films induced by a diffusion of C₆₀ molecules and degradation during longer thermal treatment above glass transition temperature was demonstrated. Distinct degradation kinetics and morphological changes that indicate the occurrence of different underlying physico-chemical mechanisms were observed. Alterations on the micro-structure resulted on the degradation of grain sizes, charge carrier mobility and electrical conductivity, as well as a degradation on the power conversion efficiency of P3HT:C₆₀ solar cells. The results demonstrated that under extended thermal annealing the alkyl groups and thiophene rings fade away. P3HT starts to degrade at early annealing stages with detachments of lighter fragments like C-S units, and then followed abstraction of hydrogen attached to a carbon atom that is adjacent to a double bond, leading to backbone, side chain and sulphur oxidations. These results suggests that, although nanometer-scale phase separation of the donor/acceptor blend can be attained in the laboratory through device optimization, prolonged exposure to elevated temperatures will induce macro-phase separation with micrometer scale and large surface roughness. Therefore, these signify that the stability of P3HT:C₆₀ solar cells cannot be secured for longer annealing period owing to the unstable morphology.

LIST OF ARTICLES INCLUDED IN THIS THESIS

- [1] **David E. Motaung**, Gerald F. Malgas, Christopher J. Arendse, Thomas Malwela, "*Investigation of the effects of substrate annealing on the properties of polymer blends*", *Materials Chemistry and Physics* 124 (2010) 208–216
- [2] **David E. Motaung**, Gerald F. Malgas, Christopher J. Arendse, "*Comparative study: The effects of solvent on the morphology, optical and structural features of regioregular poly(3-hexylthiophene):fullerene thin films*", *Synthetic Metals* 160 (2010) 876–882.
- [3] **David E. Motaung**, Gerald F. Malgas, Christopher J. Arendse "*Correlation between the morphology and photo-physical properties of poly(3-hexylthiophene: fullerenes*", *Journal of Material Science* 45 (2010) 3276–3283
- [4] **David E. Motaung**, Gerald F. Malgas, Christopher J. Arendse, "*Insights into the stability and thermal-degradation of P3HT:C₆₀ blended films for solar cells*", *Journal of Materials Science* (2010) DOI: 10.1007/s10853-011-5408-9
- [5] **David E. Motaung**, Gerald F. Malgas, Christopher J. Arendse, Siphon, E. Mavundla and D. Knoesen, "*Structural and photo-physical properties of spin-coated P3HT thin films*", *Material Chemistry and Physics* 116 (2009) 279-283

- [6] **David E. Motaung**, Gerald F. Malgas, Christopher J. Arendse, Siphon E. Mavundla, Clive J. Oliphant and Dirk Knoesen, "*The influence of thermal annealing on the morphology and structural properties of a conjugated polymer in blends with an organic acceptor material*", Journal of Material Science 44 (2009) 3192-3197
- [7] **David E. Motaung**, Gerald F. Malgas, Christopher J. Arendse, Siphon E. Mavundla, Clive J. Oliphant and Dirk Knoesen, "*Thermal induced changes on the properties of spin-coated P3HT:C₆₀ thin films for solar cell applications*", Solar Energy Materials and Solar Cells 93 (2009) 1674-1680



ARTICLES TO WHICH I HAVE CONTRIBUTED BUT NOT INCLUDED IN THE THESIS

- [1] **David E. Motaung**, E Manikandan, Neil Coville, Mathew Moodley, "*In-situ optical emission study on the role of C₂ in the synthesis of single-walled carbon nanotubes*", Journal of Applied Physics 107 (2010) 044308.
- [2] **David E. Motaung**, Gerald F. Malgas, Christopher J. Arendse, Jayita Bandyopadhyay, "*A detailed structural characterization and analysis of poly(3-hexylthiophene) and blends: Joint DSC and SWAXS measurements*"
In preparation

- [3] A.S. Bolokang, M.J. Phasha, C. Oliphant, **D Motaung**, “*XRD analysis and Microstructure of milled and sintered V, W, C, Co powders*”, International Journal of Refractory Metals and Hard Materials 29 (2011) 108–111.
- [4] Sipho E. Mavundla, Gerald F. Malgas, **David E. Motaung**, Emmanuel. I. Iwuoha, “*Physicochemical and morphological properties of poly aniline-pyrrole copolymers*”, Journal of Material Science 45 (2010) 3325–3330.
- [5] C. J. Oliphant, C. J. Arendse, G. F. Malgas, **D. E. Motaung**, T. F. G. Muller and D. Knoesen, “*Dual Catalytic Purpose of the Tungsten Filament During the Synthesis of Single-Helix Carbon Microcoils by Hot-Wire CVD*”, Journal of Nanoscience and Nanotechnology 9 (2009) 5870-5873.
- [6] C. J. Arendse, G. F. Malgas, T. F. G. Muller, D. Knoesen, C. J. Oliphant, **D. E. Motaung** and B. W. Mwakikunga, “*Thermally induced nano-structural and optical changes of nc-Si:H deposited by hot-wire CVD*”, Nanoscale Research Letters 4 (2009) 307–312.
- [7] C. J. Oliphant, C. J. Arendse, G. F. Malgas, **D. E. Motaung**, T. F. G. Muller and D. Knoesen, “*Filament poisoning at typical carbon nanotube deposition conditions by hot-filament CVD*”, Journal of Material Science 44 (2009) 2610–2616.